EPITAXIAL GROWTH OF SiC BY CHEMICAL VAPOR DEPOSITION AND APPLICATION TO ELECTRONIC DEVICES

by

KENTARO SHIBAHARA

December 1987

Department of Electrical Engineering
Kyoto University

EPITAXIAL GROWTH OF SiC BY CHEMICAL VAPOR DEPOSITION AND APPLICATION TO ELECTRONIC DEVICES

by

KENTARO SHIBAHARA

December 1987

Department of Electrical Engineering
Kyoto University

PREFACE

This thesis describes the investigation on the CVD growth and the characterization of a widegap semiconductor silicon carbide(SiC) and its application to fundamental electronic devices. The author investigated these subjects as a graduate student at Matsunami Laboratory, Department of Electrical Engineering, Kyoto University. SiC, especially 3C-SiC, is the most hopeful candidate for the material of electronic devices which operate under harsh circumstances because of its wide bandgap and physical and chemical stability. SiC is, in truth, an old and well known material. However, dimensions of crystals obtained by a conventional growth method are too small and some other problems in crystal growth exist as a barrier to the investigation as a semiconductor material. Although many investigators tried to grow 3C-SiC on Si, a large lattice mismatch of 20% between them prevented successful single crystal growth. "A carbonized buffer layer" introduced to overcome the large lattice mismatch by the senior workers of the author opened the way to use 3C-SiC as a "new" semiconductor material. The author took over the work to bring up 3C-SiC.

This thesis consists of seven chapters. In Chapter I, features and properties of SiC and its history are introduced, and purposes of this investigation are explained. 3C-SiC grown on a Si substrate is treated in Chapter II to Chapter V. The crystal growth of 3C-SiC on Si is discussed in Chapter II. The structure of "a carbonized buffer layer" and influences exerted by the lattice mismatch were studied. Through the characterization of the grown layers, a growth technique was optimized to improve their crystallinity. In Chapter III, the antiphase disorder which is peculiar to heteroepitaxial growth and its elimination by the introduction of off-orientation into substrates are described. Electrical properties of undoped and doped crystals are mentioned in Chapter IV. Some problems due to the introduction of off-orientation and doping are also

discussed. Properties of ion implanted layers were investigated as a preparation of device fabrication and results are explained in Chapter V. Successful fabrication of MOSFET's as a compilation of studies is presented also in Chapter V. In Chapter VI, growth on 6H-SiC attempted to seek a new direction is mentioned. An innovation was achieved in homoepitaxial growth of 6H-SiC by the introduction of off-orientation into the substrate. Chapter VII summarizes conclusions of this investigation.

New materials must experience many seasons before ripe. SiC just spent a few seasons as a semiconductor material. The author hopes that this thesis serves as a seedbed for successors and the season of good harvest will come around.

Kentaro Shibahara
December 1987

ACKNOWLEDGMENTS

The author would like to express his deep gratitude and appreciation to Professor Hiroyuki Matsunami for his constant guidance, critical supervision and encouragement throughout the work. The author would also like to thank Professors Akio Sasaki and Shigeo Fujita for their critical reading of the manuscript and valuable comments.

Special thanks are due to Associate Professor Shigehiro Nishino, Kyoto Institute of Technology and Dr. Takashi Fuyuki for their guidance and invaluable discussion. Thanks are also due to Mr. Masahiro Yoshimoto who gave the author valuable advice and good stimulus.

Much appreciation is due to Messrs Naotaka Kuroda, Tatsuya Takeuchi, Kouji Matsumoto, Syunji Takase and Takeshi Yoshida for their valuable participation in the work. Thanks are due to Messrs Hajime Suhara and Yoshihisa Fujii for their kind advice. The author also thanks many other members of Matsunami Laboratory.

The author is grateful to Dr.Masahiro Akiyama, Oki Electric Industry Company for his valuable advise.

The author is indebted to Drs. Tadashi Ohachi and Hidetaka Moriyama, Doshisya University for their facilities for RHEED observation. The experiments are also partly supported by facilities due to staffs and students of Sasaki Laboratory and Kawabata Laboratory.

Si wafers, SiC crystals and C_2H_2 gas used in the crystal growth were supplied by the kindnesses of Shin-Etsu Semiconductor Co. Ltd., Sanyo Electric Co. Ltd. and Nichi-Go Acetylene Co. Ltd., respectively.

The author really thanks his friends who cheered up and encouraged him.

CONTENTS

I. INTRODUCTION

As our ancestors abandoned stones and adopted bronze, human beings are always seeking new materials to satisfy personal curiosities and ambitions and social desires. An invention of a triode vacuum tube in 1906 gave rise to electronics. However, soon peoples found the limitation of size, reliability and power of the vacuum tube. After triode action of Ge in 1948[1], semiconductors, especially Si, have held a leading part of evolution of industries and our lives. Nowadays, we are living surrounded by uncountable semiconductor-devices and computer-aided technology. Needless to say, Si dominates electronics and semiconductor fields. At the same time, other semiconductors hold important parts. Now microwave and optical communications are supported by III-V semiconductor devices. And beside us CD(compact disk) players which need semiconductor lasers can be easily found. Even in the field of a super computer which is one of the symbol of Si technology, a product which uses GaAs IC's(integrated circuit) for its CPU(central processing unit) is announced to ship in 1989[2].

However, still there are many fields where new materials are expected to satisfy needs. Wide-bandgap semiconductors are necessary for high-temperature operation of devices and blue light-emitting devices. IV-IV compound semiconductor SiC treated in this thesis is one of the most hopeful candidates for such uses.

SiC is well known as an example of polytypism. Structure of every polytype of SiC is described by stacking sequence in the [0001] direction*). Atoms occupy one site out of three in the close packed structure. Three sites of A, B and C have the relative arrangement shown in Fig.1. Stacking sequences and bandgaps of popular polytypes are listed in Table 1. Each polytype is described by a number of layers in the repeat distance of a primitive cell and three types of crystal structures. The crystal structures are expressed by H for

*): See notes at P.7.

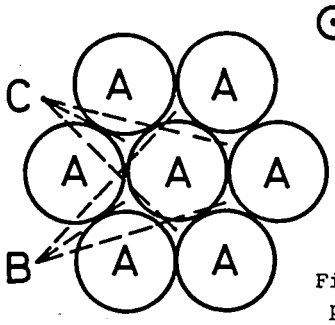

Fig.1 Atom position in close-packed layers.

polytype	stacking sequence	exciton bandgap(eV)
2H(wurtzite)	AB	3.330
3C(zinc blende)	ABC	2.390
4H	ABAC	3.265
6H	ABCACB	3.023
15R	ABCACBCABACABCB	2.986

Table 1 Stacking sequences and bandgaps of popular polytypes.

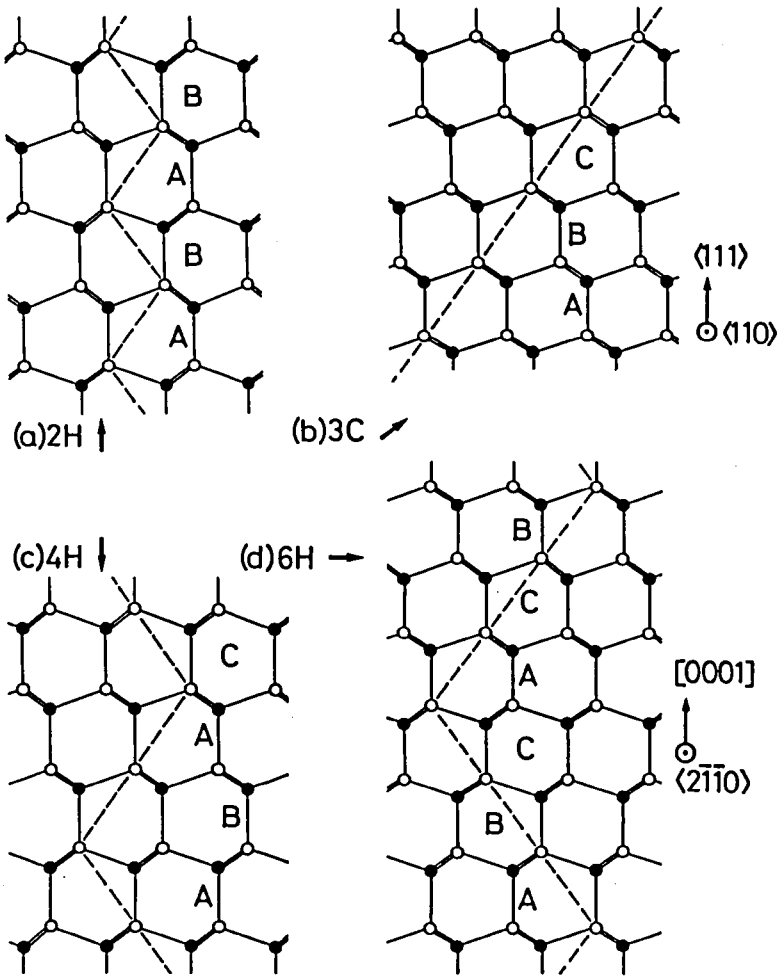

Fig.2 Crystal structures of (a)2H-, (b)3C-, (c)4H- and (d)6H-types.

	band structure	E_g (eV)	μ (cm^2/Vs)	v_s (cm/s)	E_b (V/cm)	λ (W/cm°C)	lattice constant(Å)	crystal structure
3C-SiC	I	2.4	1000	2.7×10^7	-	-	4.36	ZB
6H-SiC	I	3.1	600	2×10^7	5×10^6	5.0	a_0=3.09 c_0=15.1	6H
Si	I	1.12	1500	1×10^7	2×10^5	1.5	5.43	DI
GaAs	D	1.42	8500	2×10^7	3×10^5	0.5	5.65	ZB

I:indirect D:direct E_g:energy gap μ:electron mobility at 300K
v_s:saturated electron drift velocity E_b:break down field
λ:thermal conductivity at 300K ZB:zinc blende DI:diamond

Table 2 Physical properties of 3C-SiC, 6H-SiC, Si and GaAs.

hexagonal, R for rhombohedral and C for cubic. 3C-type is the only cubic structure. Generally its structure is known as a zinc-blende structure. 3C-SiC is often called β-SiC and others are called α-SiC. The structures of 2H-, 3C-, 4H- and 6H-SiC are shown in Figs.2(a)-(d). There are many polytypes except for those shown here. As far as the author knows, the longest repeat distance of a primitive cell corresponds to 594 layers[3]. Off course usually, easily obtainable several polytypes are used and investigated. In this thesis the most popular two polytypes of 3C- and 6H-types are mainly treated.

Physical properties of 3C-SiC, 6H-SiC, Si and GaAs are listed in Table 2[5-11]. As mentioned above both 3C- and 6H-SiC are expected as materials for electronic devices which operate under harsh (high temperature and high radiation) circumstances. 3C-SiC has high electron mobility of 1000cm^2/Vs[5] in spite of its wide bandgap of 2.4eV. Therefore, potentiality for active devices of 3C-SiC is superior to that of 6H-SiC. SiC has higher thermal conductivity[6], higher saturated electron drift velocity[7,8] and higher breakdown electric field[9] than Si and GaAs as listed in Table 2. These features are desirable for high-power microwave electronic devices such as IMPATT(impact ionization avalanche transit time) diodes. 6H-SiC is also a promising material for blue LED's(light-emitting diode) in spite of its indirect bandgap structure. Because both p and n-type conduction are easily obtained for SiC different from other wide-bandgap semiconductors.

After an invention of synthesizing method by Acheson in 1892, SiC has been utilized in industry. SiC is very hard and it is well known as polishing powder named carborundum. SiC is very stable even at high temperature, and it is also used as a heat-resistant material and a heater. Recently its ceramics is used as package for VLSI. Because its ceramics simultaneously can realize high thermal conductance, high resistivity and the same thermal expansion coefficient as Si[12]. FRM(fiber-reinforced metal) using SiC whisker is utilized for a cylinder of a motorcycle engine. Composite materials using fiber and whisker of SiC are

actively investigated for the aerospace industry.

By the Acheson method 6H-SiC is mainly obtained. Therefore, 6H-SiC was used in industry and sometimes it was investigated as a semiconductor material. In 1907[13] and 1923[14] electroluminescence was reported. SiC was used as a crystal detector at the time. And utilizations for a varistor and a surge absorber are known. However, investigation for other electronic devices was difficult. Because crystals obtained by the Acheson method were not adequate for electronics use. In the Acheson method, SiC is synthesized in an electric furnace using silica, carbon and some additional sources. Such crystals usually contain many impurities and they are small and irregular in shapes. Usually usable area for the investigation is smaller than $1cm^2$. In 1955, Lely invented a growth method of pure crystals utilizing sublimation[15]. By this method 6H-SiC was mainly obtained. This innovation motivated investigation for ingot growth of 6H-SiC and its electronic devices. Since in the Lely method nucleation for crystal growth takes place randomly, the problems of size and shapes were not solved. Based on the Lely method some modification was carried out. By the introduction of a seed crystal, growth of large crystals became possible[16,17]. Recently growth of 6H-SiC ingots which were 30mm in diameter and 13mm in height was reported[18]. However, the technology of ingot growth still stays at research level.

Epitaxial growth technique was utilized to fabricate electronic devices of 6H-SiC. By sublimation technique impurity control of thin layers is difficult. And diffusion technique is hard to apply for device fabrication because of very low diffusion coefficient of impurities in SiC[19]. Fabrication of blue LED's with 6H-SiC was investigated by CVD(chemical vapor deposition)[20,22] and LPE(liquid phase epitaxy)[21,22] methods. Recently investigation continues to achieve higher efficiency using the LPE method[23] in the aim of marketing. P-n junction diodes[7,9], FET's(field effect transistor)[19] and bipolar transistors[24] were fabricated to investigate properties of 6H-SiC as semiconductor materials and potentiality of high-

temperature use. However, recently investigation for such purpose is not active. Difficulty in preparation of substrates with good quality and high epitaxial-growth temperature are probably main reasons. Typical growth-temperatures are higher than 1650°C and 1800°C for LPE and CVD, respectively. Success of growth of 3C-SiC on Si is also a reason.

In the case of 3C-SiC, crystals are obtained by sublimation and solution growth methods. However, such crystals are too small for investigation as electronic materials. Typical area usable for investigation is smaller than several mm^2. Rising of trend for investigation began in 1980's by the success of heteroepitaxial growth of 3C-SiC on Si[25] by Nishino, Matsunami and co-wokers. They were members of the laboratory where now the author belongs. 3C-SiC is considered to be stable at lower temperatures(<1600°C) compared with other polytypes. Therefore, heteroepitaxial growth of 3C-SiC by CVD has been attempted by many investigators[26]. Si is the most popular substrate for heteroepitaxial growth of 3C-SiC. Since Si wafers are cheap and they have controlled high quality. However, lattice mismatch between Si and SiC reaches 20% and reproducible growth of thick single crystals was impossible. To overcome the large lattice mismatch, Matsunami et al.[27] proposed introduction of an intermediate thin layer between a substrate and a grown layer which was called as "a buffer layer". They tested several methods to form a buffer layer[27,28] and chose a carbonization method[25,29]. By carbonization of Si surface using C_3H_8 before CVD growth, single crystalline SiC was reproducibly obtained. However, the role of "a buffer layer" is not clear and investigation as a semiconductor material just started. Since 3C-SiC has higher potential for active devices than 6H-SiC and single crystal with large area is easily obtained by this method[30], many groups began to take part in the investigation.

In the former part, features, history and present situation of SiC were explained. Based on this knowledge the following subjects are listed as the purpose of this thesis.

To establish growth technique of 3C-SiC on Si,

(1)Characterization of carbonized layers and grown layers;
(2)Optimization of factors concerning crystal growth
are investigated. Based on the results, if necessary,
(3)Improvement of grown layers
is attempted. And to apply 3C-SiC for electronic devices,
(4)Impurity doping;
(5)Fabrication of devices
are attempted. And to seek future of SiC the next subject is added:
(6)Growth on 6H-SiC(0001) under 1500°C.
CVD growth under 1500°C was not well investigated. This subject includes two meanings. One is to know whether 6H-SiC(0001) is usable for a lattice-matched substrate of 3C-SiC or not. The other is to investigate whether control of polytypes is possible or not by changing the growth conditions.

*)Note: Usually for 3C-SiC, Miller indices (e.g. (hkl)) for a cubic lattice are used. However, in chapter VI to treat both 3C-SiC and 6H-SiC at the same time, hexagonal-lattice Miller-Bravais indices[4] are also used. This notation explicitly expresses symmetrical relationship between various faces. Popular faces such as (0001), $(2\bar{1}\bar{1}0)$ and $(10\bar{1}0)$ are idiomatically identified by this notation. However, to discuss diffraction phenomena of various polytypes, vector calculation is necessary and Miller indices for hexagonal lattice is convenient for all polytypes. In this thesis from chapter II to chapter V, faces of 3C-SiC and Si are identified by Miller indices for cubic lattices. In chapter VI and APPENDIX, diffraction phenomena are explained by Miller indices for hexagonal lattices, and Miller-Bravais indices are used to identify popular faces. Correspondence between these notations are shown in APPENDIX.

References

[1] J.Bardeen and W.H.Brattain, Phys. Rev. 74(1948) 230.
[2] Nikkei Electronics, no.428(1987)8-24 p.88, in Japanese.
[3] C.Kittel, *Introduction to Solid State Physics*, (John Wiley & Sons, New York, 1986) 6th edition, p.22.
[4] B.D.Cullity, *Elements of X-ray diffraction*, (Addison-Wesley, Massachusetts, 1956), Chapter 2.
[5] W.E.Nelson, F.A.Halden and A.Rosengreen, J. Appl. Phys. 37(1966) 333.
[6] G.A.Slack, J. Appl. Phys. 35(1964) 3460.
[7] W.von Muench and E.Pettenpaul, J. Appl. Phys. 48(1977) 4823.
[8] D.K.Ferry, Phys. Rev. 1B 12(1975) 2361.
[9] W.von Muench and I.Pfaffeneder, J. Appl. Phys. 48(1977) 4831.
[10] S.M.Sze, *Physics of Semiconductor Devices*, (John Wiley & Sons, New York, 1981) 2nd edition, p.850.
[11] Mitsushi Ikeda, Doctoral Thesis, Faculty of Engineering, Kyoto University, 1980.
[12] K.Nakamura, K.Maeda, Y.Takeda and M.Ura, Oyo Buturi 53(1984) 311, in Japanese.
[13] H.J.Round, Electrical World 19(1907) 309.
[14] O.V.Lossev, Wireless Telegraphy and Telephony 18(1923) 16.
[15] von J.A.Lely, Ber. Deut. Keram. Ges. 32(1955) 229, in German.
[16] Yu.M.Tairov and V.F.Tsvetkov, J. Crystal Growth 52(1981) 146.
[17] G.Ziegler, P.Lanig, D.Theis and C.Weyrich, IEEE Trans. Electron Devices ED-30(1983) 277.
[18] K.Koga, T.Tanaka and T.Niina, Extended Abstr. 17th Conf. Solid State Devices and Materials, Tokyo, 1985(Business Center for Academic Societies Japan, Tokyo, 1985), p.249.
[19] R.B.Campbell and H.-C.Chang, *Semiconductor and Semimetals* vol.7-B, (Academic Press, New York, 1971) edited by R.K.Willardson and A.C.Beer, p.625.
[20] for an example of CVD grown blue LED
S.Nishino, A.Ibaraki, H.Matsunami and T.Tanaka, Jpn. J. Appl.

Phys. 19(1980) L353.
[21] for examples of LPE growth
(a) R.W.Brander and R.P.Sutton, Brit. J. Appl. Phys. 2(1969) 309.
(b) M.Ikeda, T.Hayakawa, S.Yamagiwa, H.Matsunami and T.Tanaka, J. Appl. Phys. 50(1979) 8215.
[22] for an example of both CVD and LPE
W.von Muench, W.Kuerzinger and I.Pfaffeneder, Solid-State Electron. 19(1976) 871.
[23] Y.Matsushita, Y.Ueda, T.Nakata and T.Niina, Extended Abstr. 17th Conf. Solid State Devices and Materials, Tokyo, 1985(Business Center for Academic Societies Japan, Tokyo, 1985) p.253.
[24] W.von Muench and P.Hoeck, Solid-State Electron. 21(1978) 479.
[25] S.Nishino, H.Suhara and H.Matsunami, Extended Abstr. 15th Conf. Solid State Devices and Materials, Tokyo, 1983 (Business Center for Academic Societies Japan, Tokyo, 1983)p.317.
[26] for examples
(a) P.R-Choudhury and N.P.Formigoni, J. Electrochem. Soc. 116(1969) 1440.
(b) S.Nishino, H.Matsunami and T.Tanaka, J. Crystal Growth 45(1978) 138.
[27] H.Matsunami, S.Nishino and H.Ono, IEEE Transact. Electron. Devices 28(1981) 1235.
[28] S.Nishino, Y.Hazuki, H.Matsunami and T.Tanaka, J. Electrochem. Soc. 127(1980) 2674.
[29] S.Nishino, J.A.Powell and H.A.Will, Appl. Phys. Lett. 42(1983) 460.
[30] S.Nishino, K.Shibahara, S.Dohmae and H.Matsuanami, Late News Abstr. 16th Int. Conf. Solid State Devices and Materials, Kobe, 1984(Business Center for Academic Societies Japan, Tokyo, 1984) p.8.

II. CVD GROWTH OF 3C-SiC ON Si SUBSTRATES

1. Introduction

In this investigation, 3C-SiC was grown on Si substrates by the combination of the carbonization and the CVD growth. First in this chapter, the apparatus and the procedures for growth are introduced. Next, the characterization of carbonized layers and grown layers and the optimization of various conditions concerning growth are mentioned. The structure of the carbonized layers is discussed based on the characterization by various methods. Variations of crystallinity due to flow rates of source gases and film thickness are described. Through the RHEED observation of grown layers on various faces of Si substrates, a model of a carbonization mechanism is brought up. Finally attempts for lowering of growth temperature using C_2H_2 are also mentioned. These subjects were investigated with the aim of obtaining "good crystals" for the fabrication of electronic devices.

2. CVD apparatus and growth procedures

(CVD apparatus)

Figure 1 shows a schematic diagram of a CVD growth system. The appearances of a reaction tube and mass-flow-control units are shown in Figs.2 and 3. The epitaxial growth of 3C-SiC by CVD was carried out in a horizontally set quartz reaction-tube at ordinary atmospheric pressure. A cross section of the reaction tube was a circle of 5cm in diameter and it had a water cooling jacket. A carrier gas was refined hydorgen(H_2) by a purifier and its typical flow rate and linear velocity were 3 SLM and 5 cm/s, respectively. Source gases were, hereafter if not specially annotated, silane(SiH_4) and propane(C_3H_8). Methane(CH_4) and acetylene(C_2H_2) were also used for carbon sources. Diborane(B_2H_6)

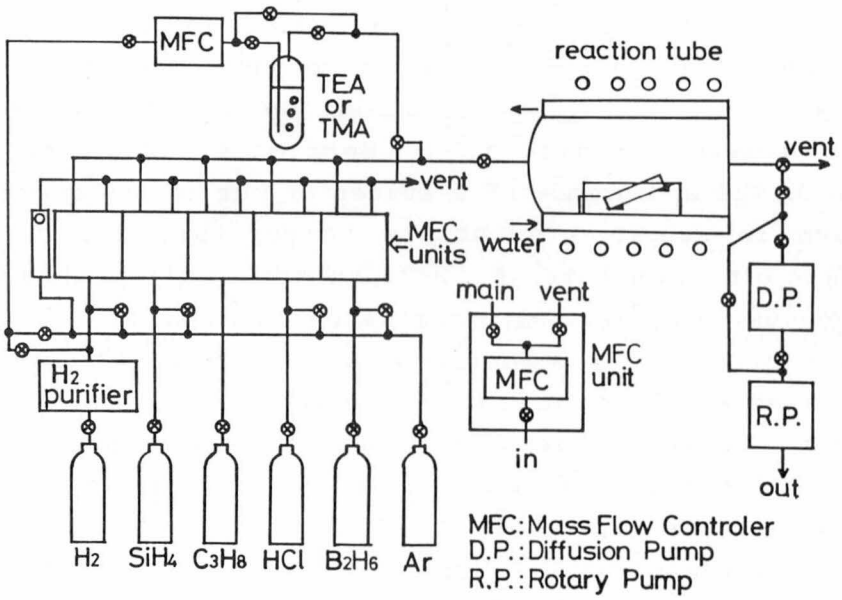

Fig.1 Schematic diagram of CVD growth system.

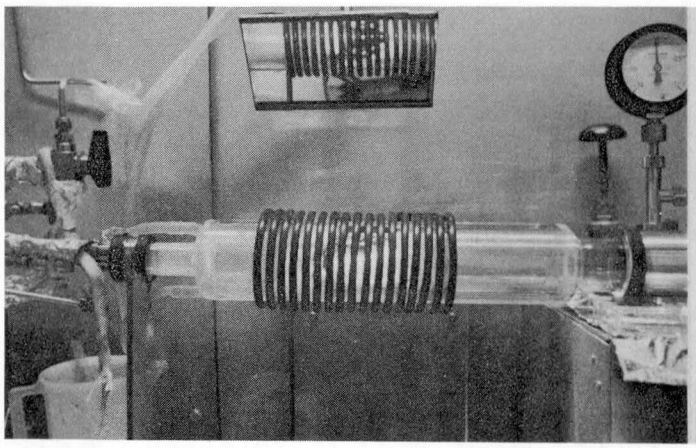

Fig.2 Reaction tube for CVD growth.

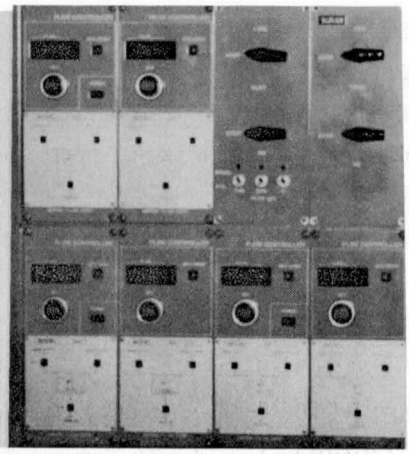

Fig.3 MFC(mass-flow controller) system.

and organic aluminum were used for doping. Source gases and B_2H_6 were diluted with H_2. The used organic aluminum is liquid at room temperature and they were introduced by a bubbling method. Hydrogen chloride(HCl) was used for etching of substrates.

A substrate was put on a graphite susceptor coated with SiC and they were heated by RF induction. The quality of the coating affects growth conditions. In Section 4-1 this problem is mentioned. The appearance of a susceptor set in its quartz holder is shown in Fig.4. A substrate temperature was decided by measuring a temperature of a hole formed at the backside of the susceptor using an optical pyrometer.

The susceptor was inclined at an angle of 10° towards the upper stream as shown in Fig.4 in order to improve the uniformity of film thickness. Figures 5(a) and (b) represent the variation of film thickness as a function of the distance from the front edge of a substrate for horizontally set and inclined susceptors, respectively. The linear velocity of a carrier gas was increased from 0.85cm/s to 5cm/s in the latter case by the increase of a flow rate of a H_2 carrier gas and a modification of the susceptor holder. When the susceptor was set horizontally and linear velocity was low, the film thickness at the front edge was 5 times greater than that at the back edge as shown in Fig.5(a). The uniformity of the film thickness was much improved as shown in Fig.5(b) by the inclination and the increase of the linear velocity. The combinations of an inclined susceptor and the low linear velocity or a horizontal susceptor and the high linear velocity did not give such improvement as shown in Fig.5(b).

These results are explained by "a stagnant layer model" brought up by Everstyen et al.[1]. Around an object in a moving fluid with low viscosity such as water or the air, there is a layer named the boundary layer where the velocity of the fluid gradually decreases and reaches to zero[2]. Everstyen et al. used a simplified model for the boundary layer, namely, the stagnant layer where the velocity of the fluid is zero and the temperature of the fluid is constant in order to estimate the growth rate of a crystal in CVD system. When this model can be

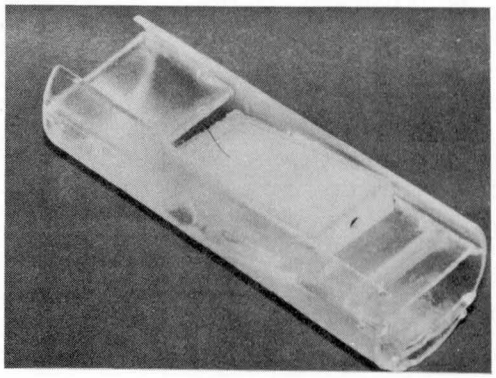

Fig.4 Susceptor and its quartz holder.

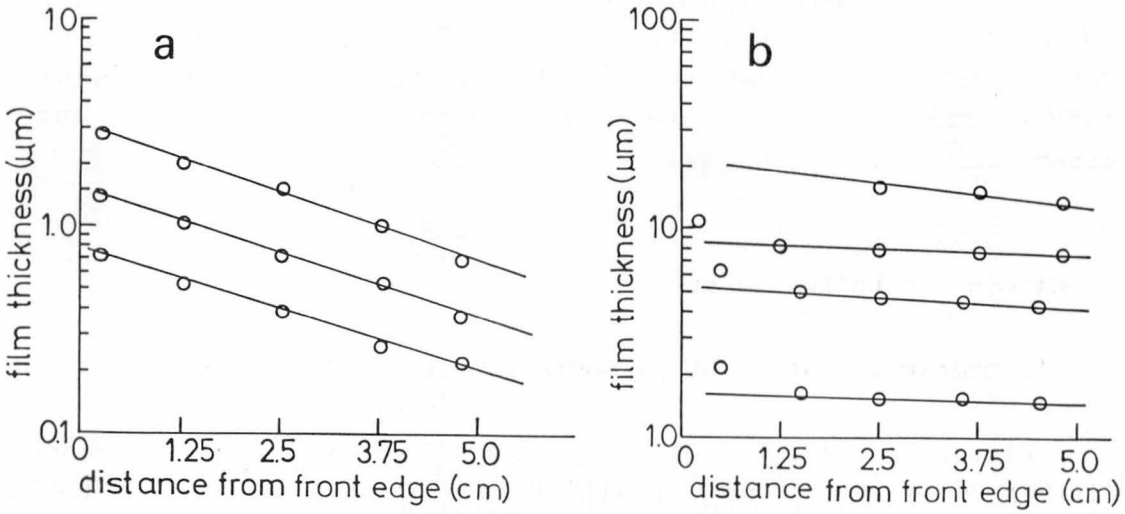

Fig.5 Relationship between film thickness and the distance from the front edge of a substrate. Susceptors were set (a)horizontally and (b)tilted at 10°.

applied, similar to Fig.5(a), film thickness changes proportional to the reciprocal of an exponential function of the distance from the front edge of a sample. Through calculation and experiments they found that the uniformity of the film thickness was improved by the inclination of substrates and the high linear velocity of a carrier gas.

In the case of this investigation, the further increase of the linear velocity to 10cm/sec showed no meaningful improvement of the uniformity. Therefore, by taking economy into consideration the linear velocity was fixed to 5cm/sec.

(Growth procedure)

The temperature program of CVD growth procedure is shown in Fig.6. The crystal growth procedure consists of three processes. The first process is etching of a Si substrate by HCl gas at 1180°C. The flow rates of HCl and H_2 for etching were 10sccm and 1SLM, respectively. The second step is carbonization of the Si substrate with C_3H_8 at 1360°C for 2min. The typical flow rate of C_3H_8 and H_2 during carbonization were 1.2sccm and 1SLM, respectively. The last is CVD growth with SiH_4 and C_3H_8 at 1350°C. The typical flow rate of SiH_4 and C_3H_8 was 0.3sccm and about 0.25sccm, respectively.

3. Carbonized buffer layers

3-1. Characterization of carbonized buffer layers

Figure 7 shows a RHEED pattern of a carbonized layer on Si(100). When conditions for the carbonization were optimized, a spot pattern of single crystalline 3C-SiC was obtained. There are three important parameters for the carbonization. They are time, temperature and flow rate of C_3H_8. If the conditions were far from the optimized situation, carbonized layers were polycrystalline as shown in Figs.8(a) and (b). The samples whose RHEED patterns are shown in Figs.8(a) and (b) were prepared

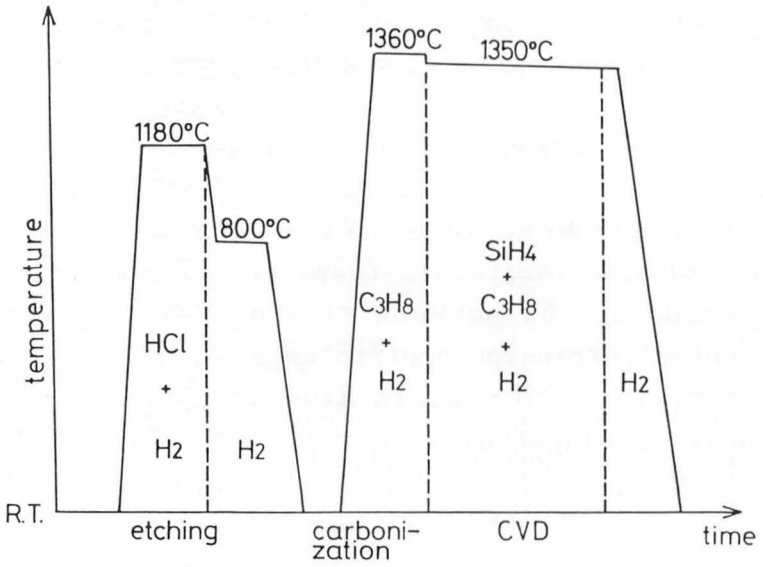

Fig.6 Temperature program of CVD growth procedures.

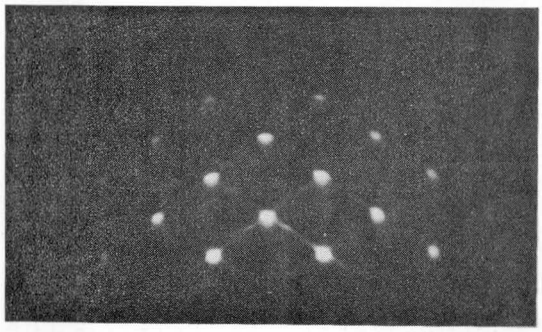

Fig.7 ‹011› azimuth RHEED pattern of a carbonized layer on Si(100) under the optimum condition.

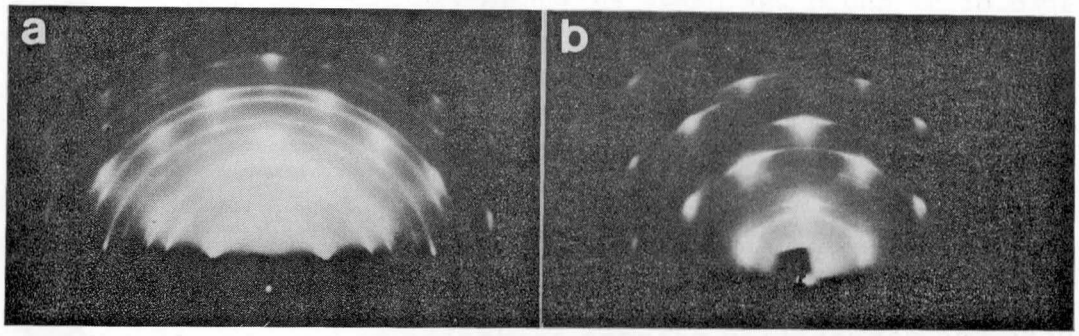

Fig.8 RHEED pattern of a carbonized layers on Si(100) under the off-optimum condition. (a)Too low flow rate of C_3H_8. (b) Too long carbonization time.

under the conditions of too low C_3H_8 flow rate and too long carbonization time[3], respectively. To obtain single-crystalline grown layers, single-crystalline carbonized buffer layers are preferable.

A careful observation of Fig. 7 reminds us of the existence of extra-spots and streaks spreading to $\langle 111 \rangle^*$. The extra-spots and streaks are considered to be originated from the existence of twinning and stacking faults[4], respectively. There is a large lattice mismatch of 20% between Si and 3C-SiC, and they have different thermal expansion coefficients. Therefore, thin grown layers are considered to contain high-density crystal defects induced by lattice mismatch and stress due to the difference in thermal expansion.

As mentioned above, the carbonized layers were confirmed to be single crystalline by RHEED observation. (In the strict sense, since twin-spots were slightly observed, they were not single crystalline. However, to avoid repeated troublesome explanations hereafter they are called to be simply "single crystalline".) However, the information obtained by RHEED observation was due to the area just close to the surface of samples. Because, the incidence angle of electron beams for RHEED observation is very low and the penetration depth of electron is not deep[5]. To discuss the mechanism of carbonization of Si, the information from the interface should be utilized.

An AES(Auger electron spectroscopy) depth profile of the carbonized layer on Si(100) is shown in Fig.9. The composition ratio of Si and C was close to 1.0 in the surface layer of 7nm in depth. Gradual change in the composition from SiC to Si was observed in the layer of 22nm in depth under the surface layer of SiC. Then the total thickness from the surface to the Si substrate was 29nm. These values were estimated using an etching rate of 3nm/min. Similar results were obtained for the carbonized layer on Si(111). Except for SiC, no crystalline compounds of $Si_xC_{1-x}(x<1)$ are known. Therefore, the existence of the layer where the composition changes gradually is hard to understand. Figure 10 shows a surface of a carbonized layer observed by a

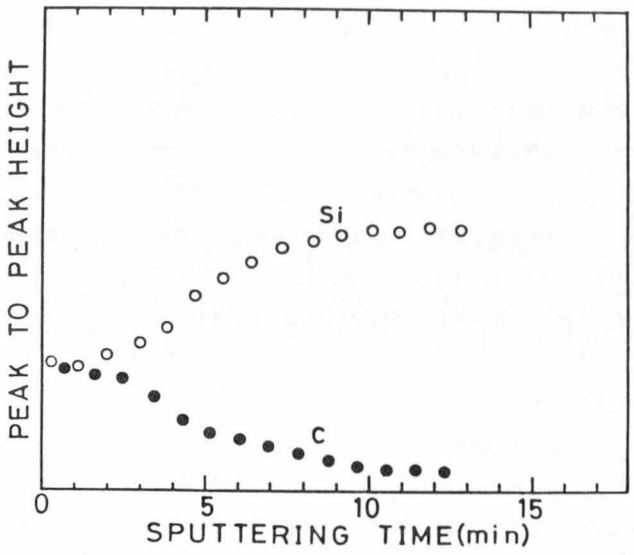

Fig.9 Auger electron spectroscopic depth profile of a carbonized buffer layer. An etching rate was about 3nm/min.

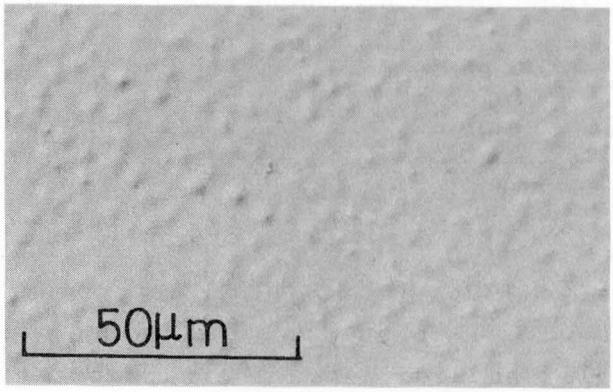

Fig.10 Nomarski microphotograph of the surface of a carbonized buffer layer on Si(100).

Nomarski microscope. Slight roughness was observed. If this roughness means that the thickness of SiC was not uniform because of island growth, there is a possibility that the difference in the thickness was observed as the gradual change of the composition around the interface in the depth profile of AES. Evaluation of the carbonized layer by ellipsometry gave a thickness of about 13-20nm and a refractive index of 2.7. This value of the refractive index is close to that of 3C-SiC of 2.64. A simple two-layer model was used to calculate the thickness and the refractive index of the film. If there are some intermediate layers, a multilayer model should be adopted[6].

TEM(transmission electron microscope) observation of the interface was carried out. A CVD grown layer on (100) with a thickness of 100nm was used. Figure 11(a) shows an XTEM(cross-sectional TEM) micrograph of the interface area observed from the ‹110› direction. Intervals of observed stripes correspond to the lattice spacing of (111) faces[7] and the stripes spread along one of the ‹111› directions forming an angle of 55° with the (100) face. Dark and light lines spread along another ‹111› direction and form 55° with the (100) face, which means the existence of plane defects. These plane defects are probably stacking faults or microtwins. The observed interface between SiC and Si was very sharp. Since the lattice spacings of the (111) faces differ in SiC and Si, all the stripes cannot be connected one by one. The enlarged picture of the interface area is shown in Fig.11(b). In this picture, one out of 4 or 5 lines of the stripes is disconnected at the interface. This interval of disconnections well agrees with the lattice mismatch of 20% between Si and 3C-SiC. Therefore, these disconnections indicate that periodically induced defects are important for lattice-mismatched epitaxial growth of 3C-SiC on Si(100).

3-2. Epitaxial relationship

Epitaxial relationship of substrates and heteroepitaxially

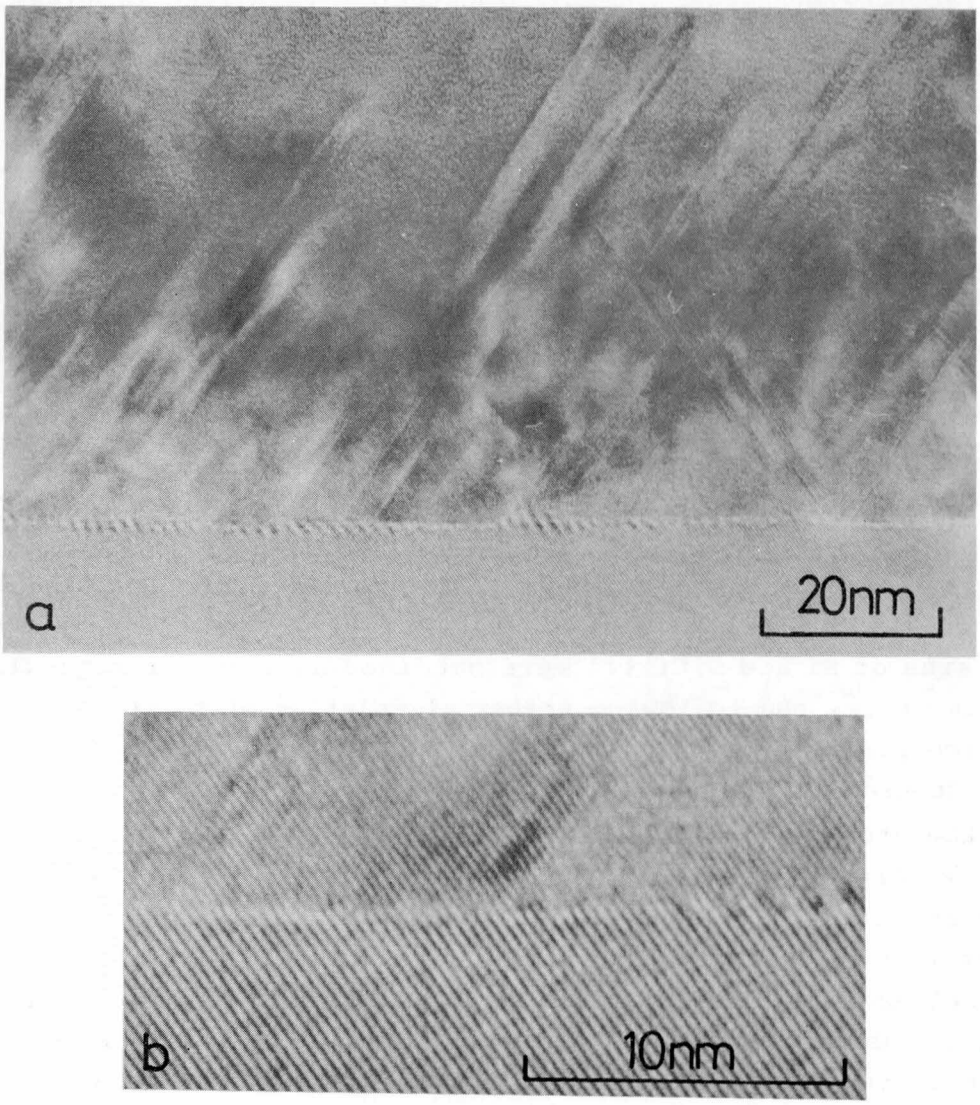

Fig.11 (a)XTEM photograph of a grown layer. (b) Magnified picture of (a).

grown layers can be identified utilizing etch pits, cleaving or a diffraction technique. In this subsection, a direct observation technique of the epitaxial relationship using electron diffraction is demonstrated. Electron beam was exposed to the edge of a sample as shown in Fig.12. The superposition of a transmission pattern from a substrate and a reflection pattern from a grown layer or a carbonized layer was obtained. Figs.13(a) and (b) show obtained patterns of grown layers on Si(100) and (111) substrates, respectively. Though CVD grown layers were used to take these patterns, the obtained epitaxial relationship was the same as that for carbonized layers. A schematic explanation of Fig.13 is shown in Fig.14. For a (100) substrate in Fig.14(a) superposition of <100> azimuth patterns of both Si and SiC(100) was obtained. In the previous sentence the index of a plane was given only to SiC, because transmission and reflection diffraction took place for a Si substrate and a SiC grown layer, respectively. In the case of a (111) substrate <211> azimuth patterns of Si and SiC(111) were obtained as shown in Fig14.(b). Conclusively, the following epitaxial relationships are obtained. For the growth on Si(100):

3C-SiC(100)//Si(100), 3C-SiC[011]//Si[011], and

for the growth on Si(111):

3C-SiC(111)//Si(111), 3C-SiC[$0\bar{1}1$]//Si[$0\bar{1}1$]

However, this conclusion does not describe the strict epitaxial relationship. Because, in spite that for 3C-SiC (111) and ($\bar{1}\bar{1}\bar{1}$) are not equal and for both Si and 3C-SiC [$0\bar{1}1$] and [$01\bar{1}$] are not equal, they are not distinguished here. To obtain the strict relationship utilization of other techniques may be necessary.

4. Crystallinity of grown layers

4-1. Dependence on Si/C ratio

Surface morphology and crystallinity of the grown layers are severely affected by the Si/C ratio(atomic ratio of Si and C in

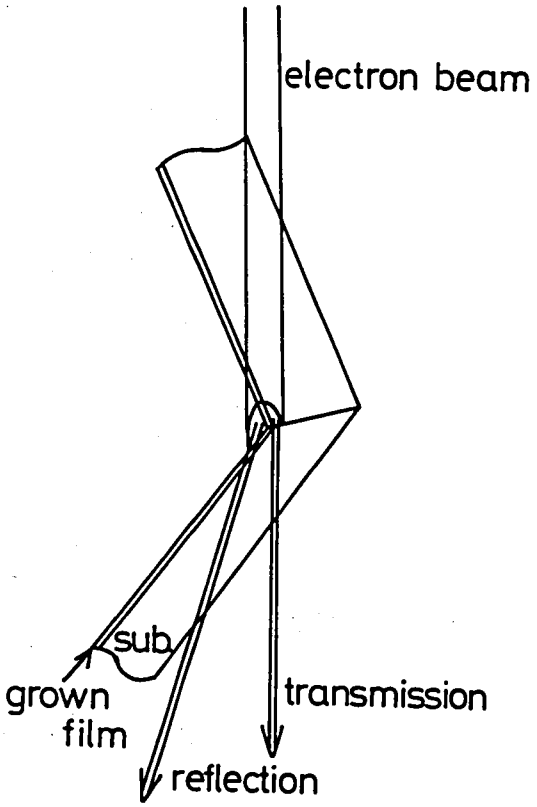

Fig.12 Electron beam which hits on the edge of a sample gives rise to both reflection and transmission diffraction.

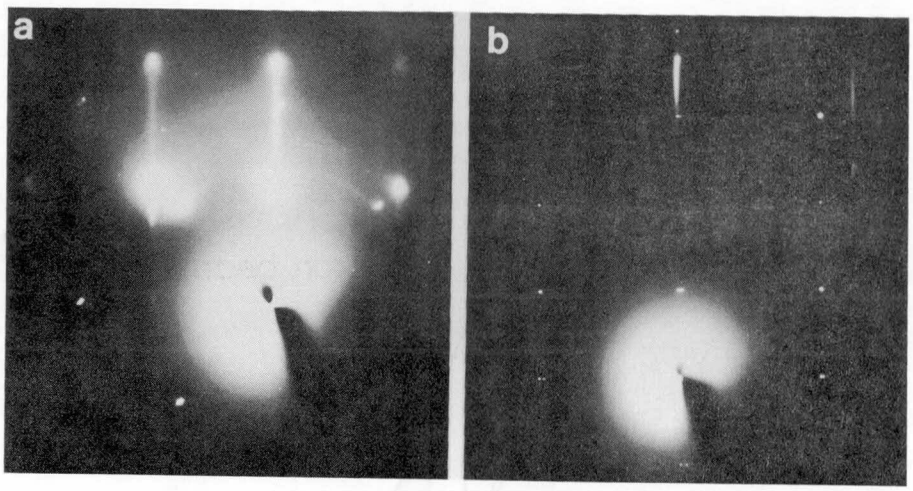

Fig.13 RHEED pattern of a SiC grown layer and the simultaneously obtained TED pattern of a Si substrate. (a) SiC(100) on Si(100). <010> azimuth. (b)SiC(111) on Si(111). <2$\bar{1}\bar{1}$> azimuth.

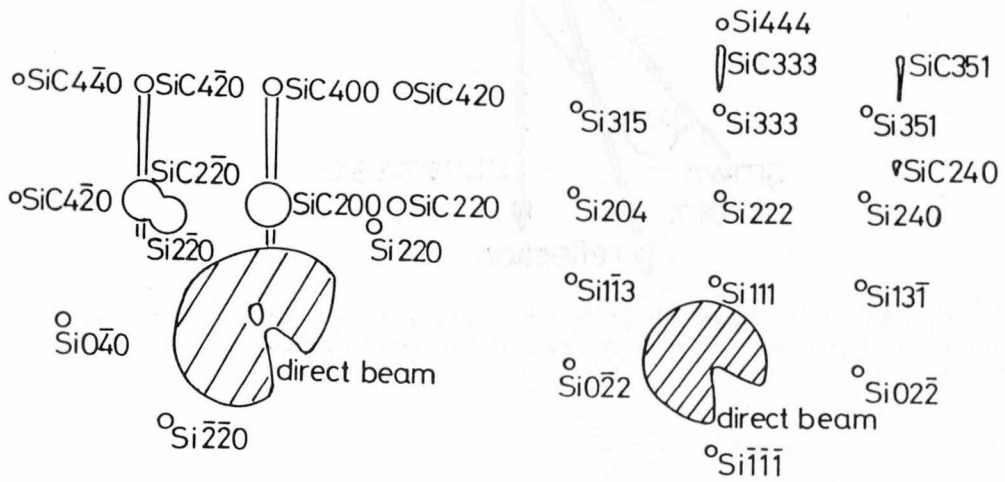

Fig.14 Schematic explanation of Fig.13. (a)SiC(100) on Si(100) and (b)SiC(111) on Si(111).

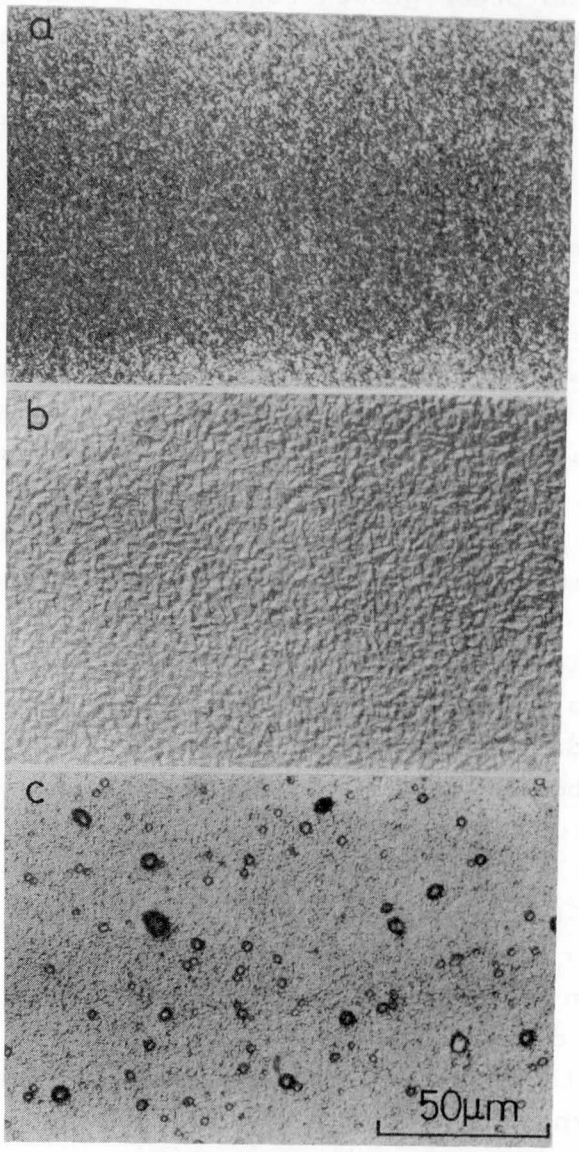

Fig.15 Si/C ratio dependence of surface morphology on Si(100). (a)Si-rich condition, Si/C=0.97, (b)moderate Si/C ratio, Si/C=0.34 and (c) C-rich condition, Si/C=0.27.

supplied source gases). Optimum Si/C ratio varies according to the change of a carbon source, growth temperature, orientations of substrates and other growth conditions. However, the feature of variation in surface morphology and crystallinity mentioned below were common to all cases. Here, examples of the grown layers on Si substrates oriented 4° off (100) towards (010) are shown. C_3H_8 was used for the carbon source and growth temperature was 1350°C.

The feature of the surface morphology was classified by the Si/C ratio into three types of Si-rich, moderate Si/C ratio and C-rich. Examples of the surface morphology are shown in Figs.15(a)-(c). Under the moderate Si/C ratio($Si/C \simeq 0.4$) condition, the surface of the grown layer became flattest. The surface was very rough and a random shape morphology was observed for the Si-rich condition ($Si/C >> 0.4$). For the C-rich condition ($Si/C << 0.4$), many needlelike crystals were observed. When CH_4 was used as the carbon source, a typical moderate Si/C ratio was about 0.15.

The crystals grown under the moderate Si/C ratio and the C-rich conditions gave streak and spot RHEED patterns of single crystalline 3C-SiC, respectively. Under the Si-rich condition, as the Si/C ratio became larger, the RHEED pattern gradually changed to a ring pattern of polycrystals. An example of the RHEED pattern of such a grown layer and its schematic explanation are shown in Figs.16(a) and (b), respectively. The polycrystals grown under the Si-rich condition contain both 3C-SiC and Si. Crystallization of excessively supplied Si was considered to obstruct single crystal growth of 3C-SiC.

The moderate Si/C ratio was severely affected by susceptor coating. Two types of susceptors were used. One was a graphite susceptor which was coated in the reaction tube using SiH_4 and C_3H_8 before growth. Hereafter susceptors of this kind are called in situ-coated susceptors. The other was a SiC-coated graphite susceptor which was produced for epitaxial growth of Si in factories. The coating of the latter susceptors looks denser by observation with the naked eyes. When the in situ-coated

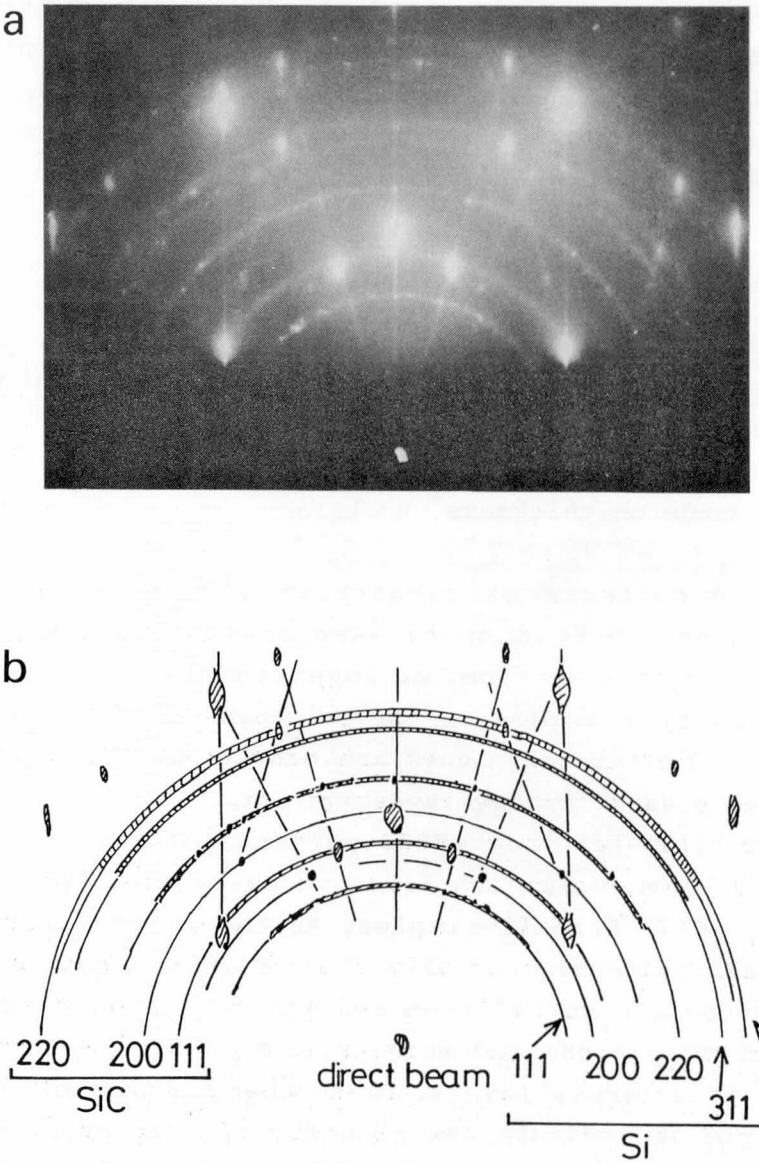

Fig.16 (a)RHHED pattern of a layer grown under the Si-rich condition. (b)Schematic explanation of (a). Solid arcs represent theoretically obtained Debye rings for Si and 3C-SiC. Observed patterns are drawn as shaded bands and spots.

susceptors were used, the flow rate of C_3H_8 must be decreased. Such a result indicates that graphite susceptors with a poor coating work as a carbon source. Surface morphology of the edge area was also affected by coating. Irrespective of the quality of coating, the surface in the edge part was rougher than that in the middle part. When in situ-coated susceptors were used, the area of such a part was wider. Carbon or some impurities which were contained in graphite were considered to affect the surface morphology. Even for epitaxial growth of Si whose typical growth temperature is lower than 1200°C, the prevention of contamination from susceptors are very important[8]. Since the growth temperature for SiC is very high, more solid and durable coating is demanded.

4-2. Dependence on thickness

In RHEED patterns of carbonized layers streaks due to stacking faults and twin spots were observed as described in Section 3-1. In this section, an investigation of the change in the crystallinity according to the thickness of the grown layers using RHEED and other techniques are mentioned. The grown layers on Si(100) were used for the investigation.

Figures 17(a)-(c) show RHEED patterns of the grown layers which were 0.15μm, 0.9μm and 5.4μm in thickness. The incidence azimuth was <011> for all samples. As the grown layers became thicker, RHEED patterns gradually changed from a spot pattern to a streak pattern. Kikuchi lines and Kikuchi bands were clearly observed and twin spots and streaks along <111>* disappeared in the case of thick grown layers. These changes in RHEED patterns are considered to indicate the reduction in the crystal defects which were observed in the carbonized layer. In other words, the crystallinity of the grown layer was improved as the film grew. To confirm the improvement of the crystallinity, channeling and X-ray diffraction techniques were utilized. The channeling spectra of Si atoms in the grown layers were obtained with 1MeV He^+. As shown in Fig.18, yields of backscattered ions decreased

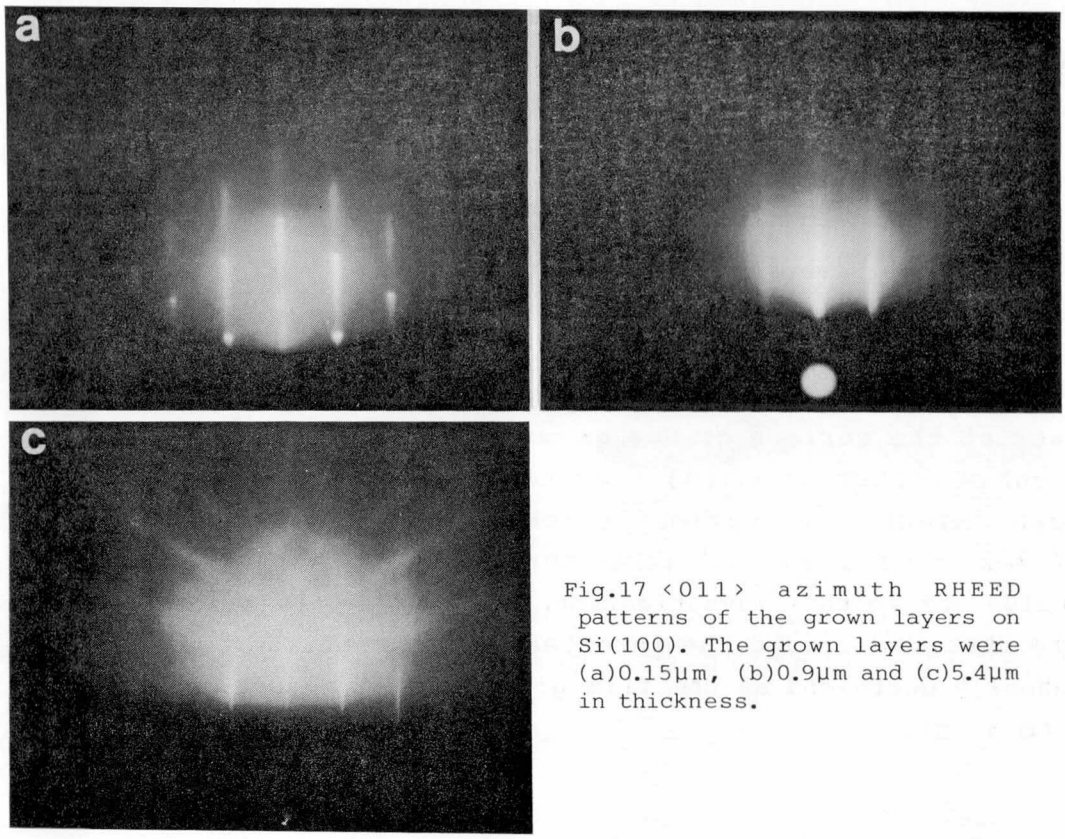

Fig.17 <011> azimuth RHEED patterns of the grown layers on Si(100). The grown layers were (a)0.15μm, (b)0.9μm and (c)5.4μm in thickness.

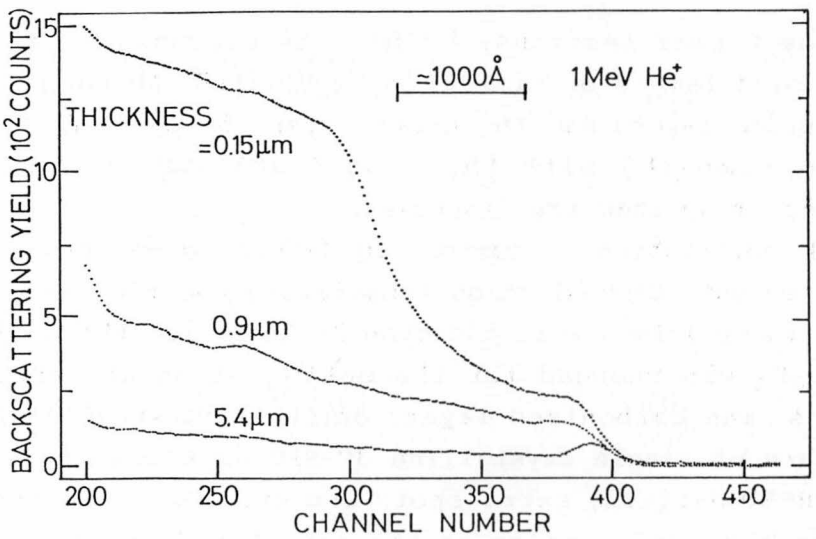

Fig.18 Channeling spectra of grown layers on Si(100).

as the film became thicker, which means improvement of crystallinity. In the case of X-ray diffraction, FWHM(full width at half maximum) of X-ray rocking curves decreased monotonously as the film became thicker as shown in Fig.19. These results obtained by both channeling and X-ray diffraction methods supported the improvement of the crystallinity of the grown layer by the increase of the film thickness.

In Section 3-1 an XTEM photograph of a CVD grown layer with a thickness of 100nm was shown. Many plane defects were observed as shown in Fig.11(a). The density of the plane defects was lower at the surface of the grown layer than at the interface. Recently Carter et al.[9] reported XTEM observation of 3C-SiC grown layers with various thicknesses. 3C-SiC was grown on Si(100) by a similar method to ours. They also obtained similar conclusions to this investigation. Stacking faults and microtwins were observed around the interface. They reported that defects gradually decreased as the film grew and such reduction continued up to 3-4μm.

5. Growth on Si(111), (110) and (211)

In the former sections, mainly the carbonized layers and the CVD grown layers on Si(100) were treated. In this section, the carbonized layers and the grown layers on Si(111), (110) and (211) are compared with those on (100) and the origin of differences among them are discussed.

RHEED observation of carbonized layers on various Si faces were carried out. Carbonization temperature and time were 1360°C and 2min. These values were the same as those for (100). The flow rate of C_3H_8 was changed for the optimization of carbonizing conditions. The carbonized layers on (111) substrates showed a spot pattern of single crystalline 3C-SiC as shown in Fig.20(a). In this RHEED pattern, extra-spots and streaks spreading along $\langle 111 \rangle^*$ are observed similar to the carbonized layers on (100). The carbonized layers on Si(111) were also considered to contain

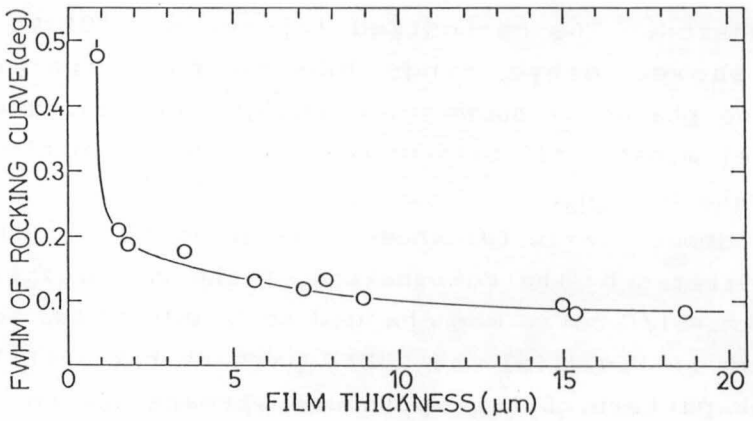

Fig.19 Film thickness dependence of FWHM of X-ray rocking curves of grown layers.

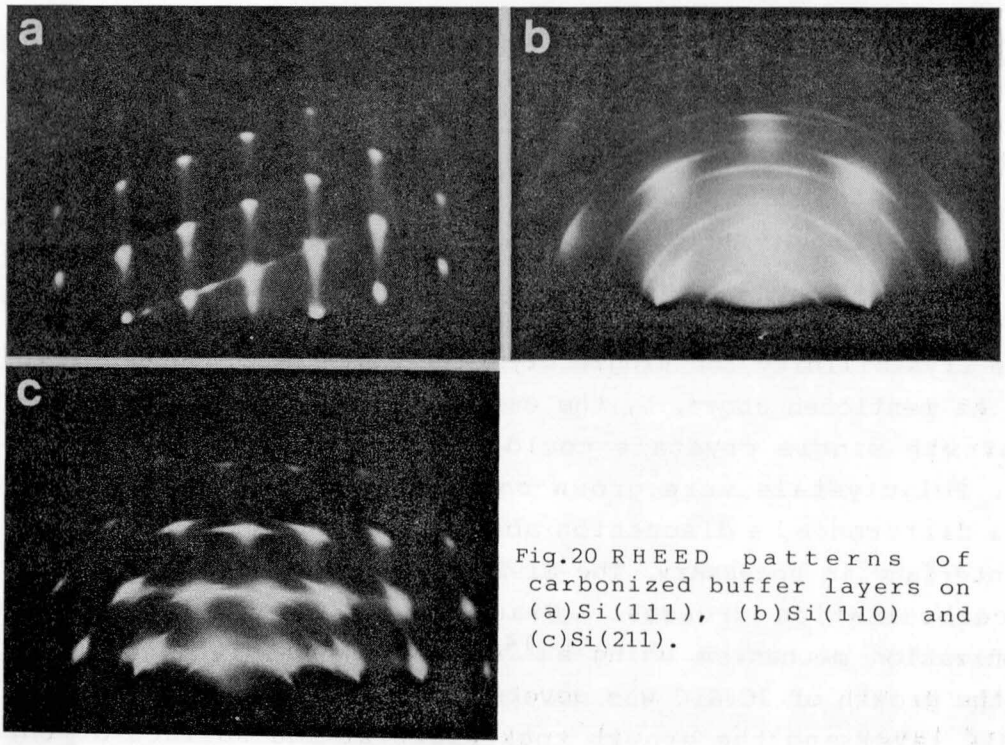

Fig.20 RHEED patterns of carbonized buffer layers on (a)Si(111), (b)Si(110) and (c)Si(211).

crystal defects due to the lattice mismatch or the difference in thermal expansion. The carbonized layers on (110) and (211) substrates showed Debye rings due to the existence of polycrystalline phases as shown in Figs.20(b) and (c). The rings could not be eliminated in spite of attempts for the optimization of the flow rate of C_3H_8.

3C-SiC of about 2μm in thickness was grown on Si(111), (110) and (211) substrates by the combination of the carbonization and the CVD growth. Si/C ratio was changed to be optimized for each face. As shown in Fig.21(a) the RHEED pattern for a (111) face was a streak pattern. Extra-spots and streaks due to crystal defects disappeared. Similar to the case of (100) mentioned in Section 4-2, the crystallinity of the grown layers on (111) was improved as the film became thicker. In contrast with (100) and (111), the grown layers on (110) and (211) showed no significant improvement in the crystallinity due to the increase of the thickness. As shown in Figs.21(b) and (c), grown layers on the (110) and (211) substrates gave extra-spots and Debye-rings in RHEED patterns. The surfaces of the grown layers on (110) and (211) substrates were very rough as shown in Figs.22(a) and (b). The optimization of the Si/C ratio was of no use for improvement of crystallinity and surface flatness. The crystallinity of the carbonized layers on (110) and (211) was considered to be too bad in the crystallinity for single crystal growth by subsequent CVD.

As mentioned above, by the carbonization and the subsequent CVD growth single crystals could be grown only on (100) and (111). Polycrystals were grown on (110) and (211). To explain such a difference, a discussion about the formation of the Si-SiC interface is necessary. The Si-SiC interface is formed during the carbonization process. Graul et al. investigated the carbonization mechanism using a ^{14}C tracer method and concluded that the growth of 3C-SiC was governed by diffusion of Si through the SiC layer and the growth took place at the surface of the sample[10]. Based on their conclusion, the initial stage of the carbonization was assumed to be composed of two steps as follows. [step 1] Growth of the first layer: Decomposed C_3H_8 molecules

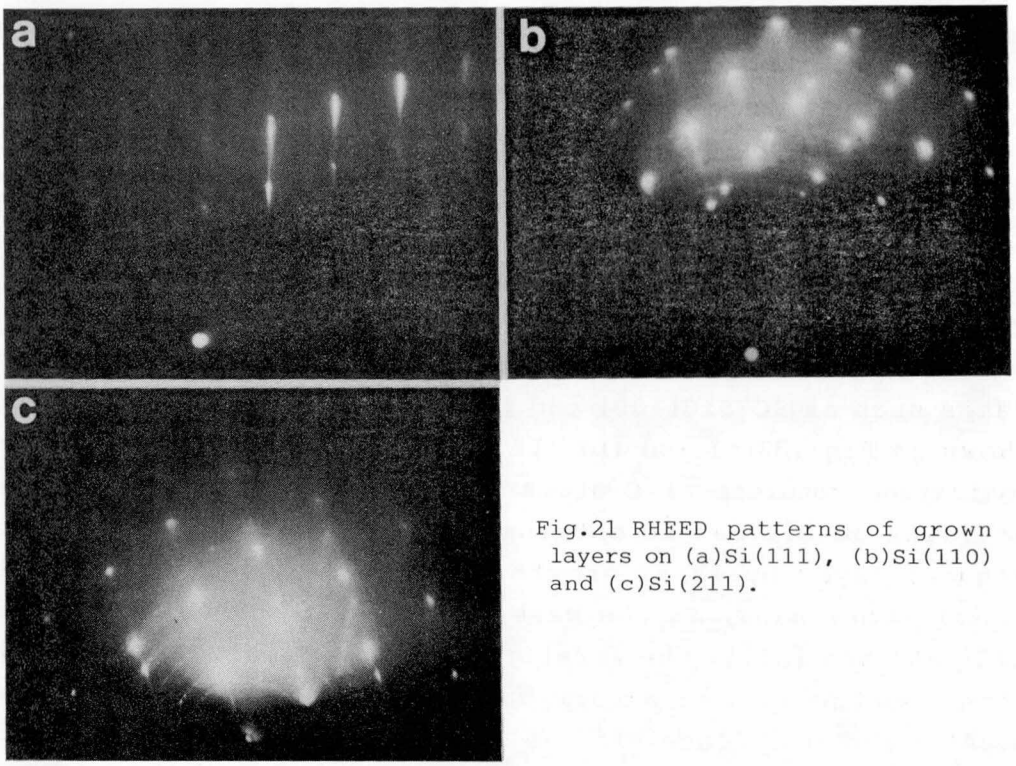

Fig.21 RHEED patterns of grown layers on (a)Si(111), (b)Si(110) and (c)Si(211).

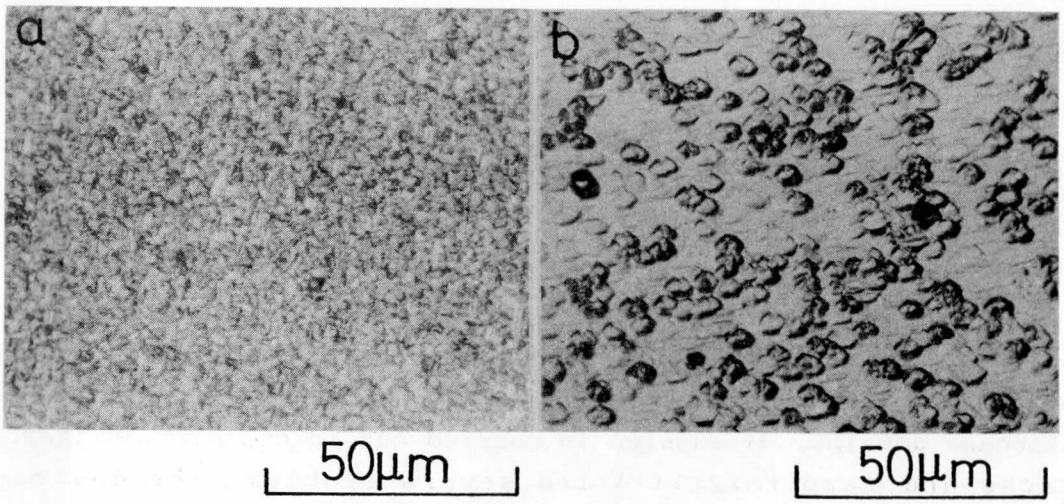

Fig.22 Nomarski microphotographs of surface morphology of the grown layers on (a)Si(110) and (b)Si(211).

adhere to the Si surface, and C atoms of a monoatomic layer cover the Si surface. [step 2] Subsequent growth: 3C-SiC grows at the surface of the carbonized Si substarate consuming out-diffused Si atoms and gaseous C_3H_8.

The step 1 of this assumption means that the first grown layer consists of C atoms only. Figures 23, 24(a) and 24(c) show the arrangements of the atoms around the ideal Si-SiC interface for various orientations. To make the discussion simple, the large lattice mismatch of about 20% between Si and 3C-SiC is neglected in Figs.23 and 24. The ideal first grown layer of polar surfaces such as 3C-SiC(100) and (111) should have only C atoms as shown in Figs.23(a) and (b). If the first grown layer by the carbonization consists of C atoms only as assumed above, single crystalline 3C-SiC can be obtained on (100) and (111) faces by subsequent layer-by-layer growth in the order of Si, C, Si and C. On the other hand, in the case of nonpolar surfaces such as 3C-SiC(110) and (211), the first grown layer should be composed of both C and Si atoms to form the 3C-SiC lattice as shown in Figs.24(a) and (c). Hence, if the first layer is a carbon layer as assumed, single crystalline 3C-SiC cannot be obtained by the subsequent growth on (110) and (211) faces. By assuming that the first grown layer by the carbonization consists of carbon atoms only, the difference in the crystallinity of the carbonized layers due to the crystal faces was explained. This assumption is important for the discussion of the origin of antiphase domains in Chapter III.

Thus, by the combination of carbonization and subsequent CVD growth single crystalline 3C-SiC was obtained on Si(100) and (111) substrates. However, problems remain in the grown layers on these substrates. For (100) antiphase domains and for (111) warp and cracks are major problems. Concerning the elimination of antiphase domains, discussion is carried out in the next chapter. Cracks and warp for (111) are severe problems for device application. An example of cracks is shown in Fig.25. The cracks were not observed during the grown layers were thinner than 10μm. While the grown layers were thin, the warp or wavy surfaces were

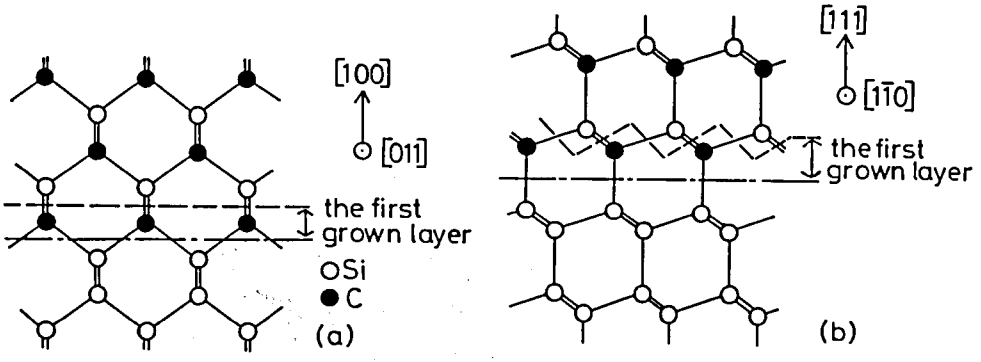

Fig.23 Ideal atomic arrangements of interfaces between Si and SiC. (a)SiC/Si(100) and (b)SiC/Si(111).

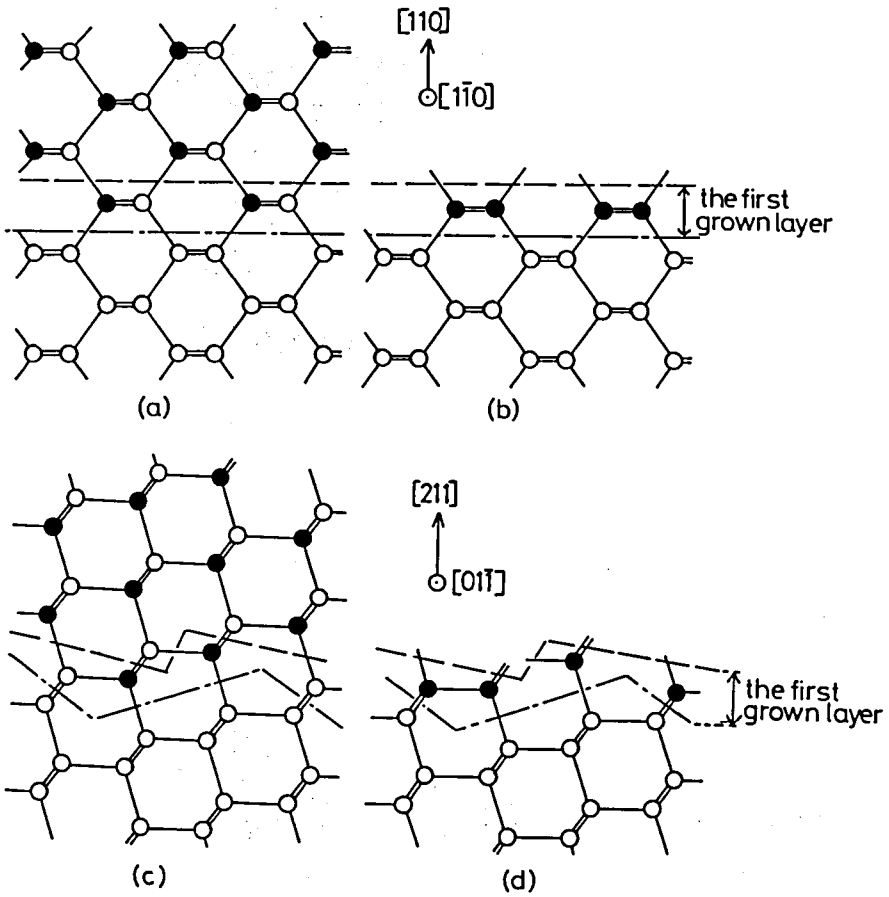

Fig.24 Atomic arrangements of interfaces between Si and SiC. Ideal cases: (a)SiC/Si(110) and (c)SiC/Si(211). The first grown carbon layer formed by carbonization on (b)Si(110) and (d)Si(211).

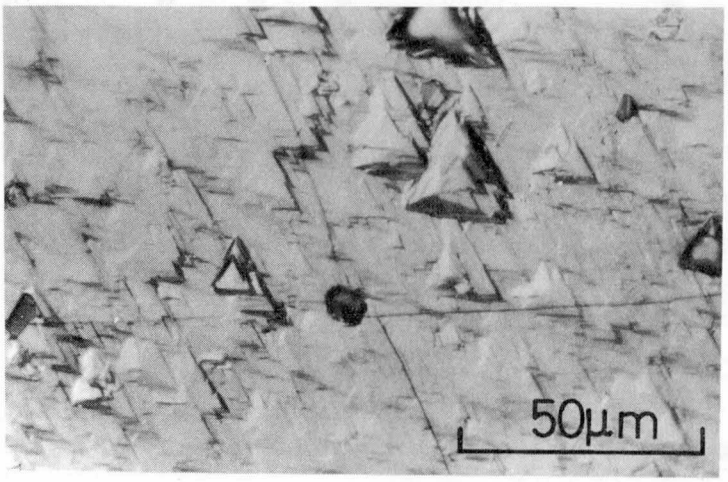

Fig.25 Cracks observed on a grown layer on Si(111).

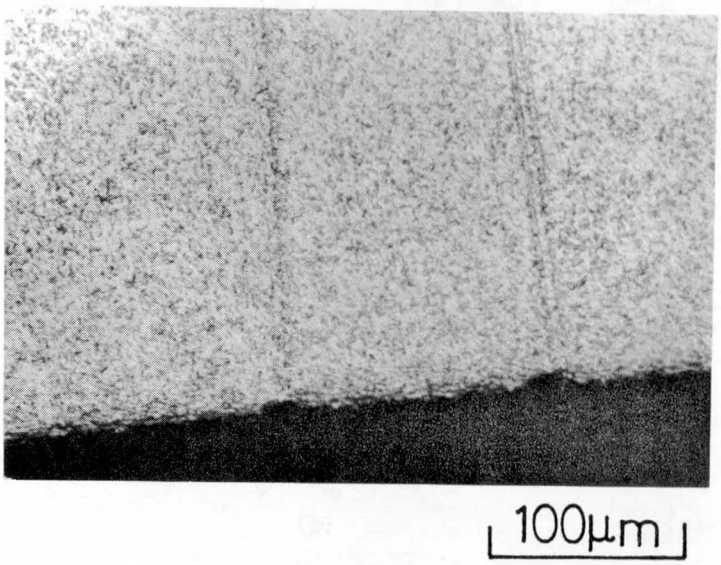

Fig.26 Slip lines observed on a grown layer on Si(100).

observed. There are two considerable origins of the warp such as the lattice mismatch and the difference in the thermal expansion coefficient. Suzuki[11] reported that the warp can be observed during growth. Hence, the main factor which gives rise to the warp and cracks are considered to be stress due to the difference in lattice constants. While the film is thin enough, the stress results in the warp. And when the thickness exceeds a certain limit, the stress gives rise to cracks.

6. Attempt for low temperature growth

In this section a trial to reduce growth temperature is mentioned. The ordinary growth temperature of 3C-SiC on Si substrates is 1350°C. This temperature is rather higher than process temperatures which are necessary for the fabrication of practical Si devices. High growth temperatures sometimes give rise to problems as follows. Contamination from the inside of a growth system easily takes place. As an example of such contamination the supply of carbon by the susceptor with poor coating was mentioned in Section 4-1. Since the growth temperature is close to 1420°C of the melting point of Si, deterioration of Si substrates in crystallinity is anticipated. In truth, slip lines are always observed after the HCl etching and the growth. An example of slip lines are shown in Fig.26. Flexibility in the fabrication process of devices is damaged by the high growth temperature.

In addition to the problems mentioned above, the diffusion of impurities due to high process temperature is an important problem in the case of growth of Si. Therefore, many attempts have been carried out to reduce growth temperature of Si. The selection of source gas is important to reduce the growth temperature of Si. A typical growth temperature of Si using a $SiCl_4$-H_2 system is 1150-1250°C. By using SiH_4, the growth temperature was reduced to 950-1050°C[12]. Recently growth at 700°C using Si_2H_6 was reported[13].

In this work, growth of 3C-SiC using C_2H_2 as a carbon source was carried out with the aim of the reduction in growth temperature. C_2H_2 was diluted with H_2. Si(100) well-oriented substrates were used. The crystal growth procedure was the same as those mentioned in Section 2. The carbonization temperature was fixed at 1360°C. The optimization of carbonizing conditions was carried out by varying the flow rate of C_2H_2. The growth temperatures were changed in the range of 1150-1350°C.

First, the growth rate was fixed at about 1.8μm/hr and the growth temperature was reduced. This growth rate was a typical one for CVD growth using C_3H_8 at 1350°C. Figure 27 shows the surface morphology and the RHEED patterns of 3C-SiC grown at various temperatures. The growth time was 1hr. The Si/C ratio was optimized at each growth temperature. Single crystalline 3C-SiC was obtained at 1350°C and 1300°C. The surface morphology was almost similar to that obtained using C_3H_8.* In the case of 1250°C twin spots were slightly observed in the RHEED pattern. When the growth temperature was reduced again, ringlike spots(1200°C) and complete ring(1100°C) patterns were observed. In other words, under 1250°C the grown layers contained twinning or polycrystals. The surface morphology also changed from a single-crystal-like orderly pattern to a polycrystal-like random pattern as the growth temperature reduced.

(*A typical surface morphology of 3C-SiC grown with C_3H_8 on similar substrates is shown in Section III-2-1.)

As growth temperatures are reduced, surface migration becomes inactive. In order to make up for the insufficiency of migration, the growth rate was reduced. The growth time was prolonged to keep comparable thickness. RHEED patterns of the grown layers are shown in Fig.28. At 1250°C and 1200°C single crystals were obtained at growth rates of 0.72μm/hr and 0.54μm/hr, respectively. Surface morphology changed from one with a random feature to the similar one obtained at 1350°C by the reduction in the growth rate. At 1150°C the growth rate was reduced to 0.45μm/hr. The RHEED pattern of this grown layer in Fig.28(c) showed an improvement in the crystallinity compared

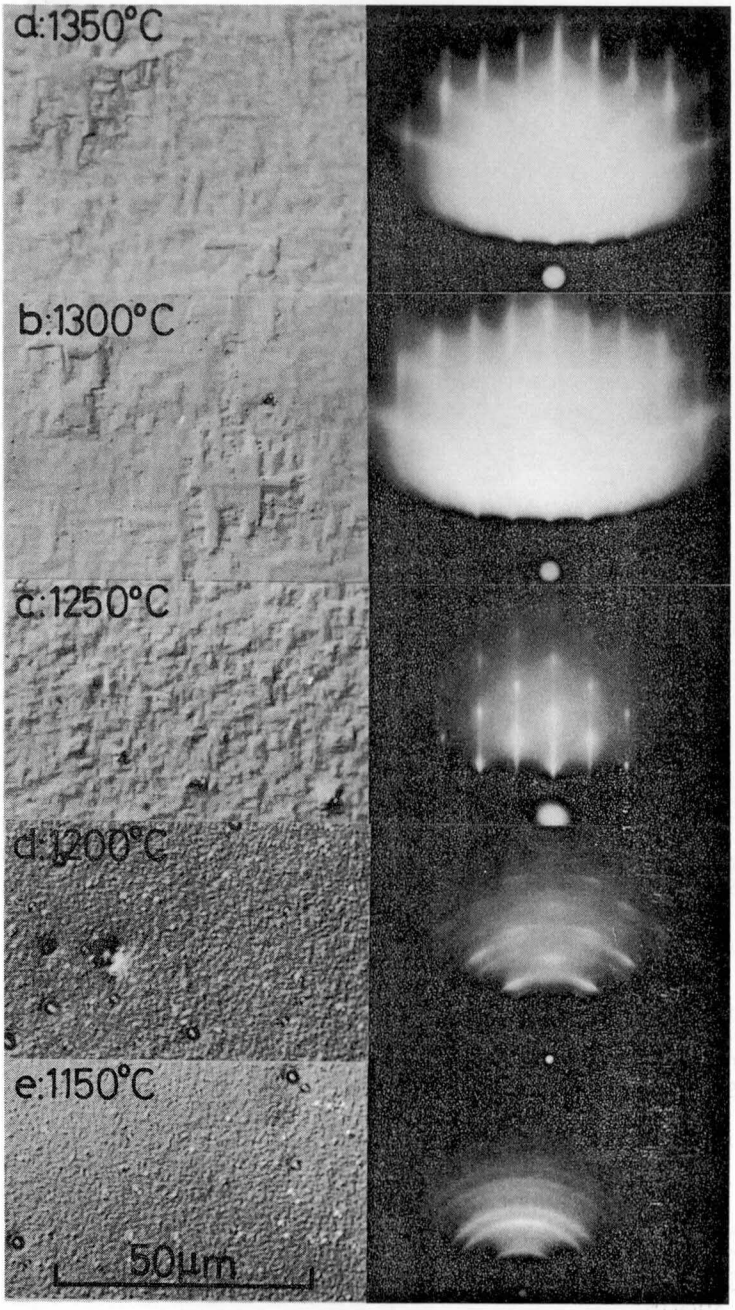

Fig.27 Nomarski microphotographs of surface morphology and [011] azimuth RHEED patterns of 3C-SiC grown using C_2H_2. Growth temperatures were (a)1350°C, (b)1300°C, (c)1250°C, (d)1200°C and (e)1150°C. Growth rate was about 1.8μm/hr.

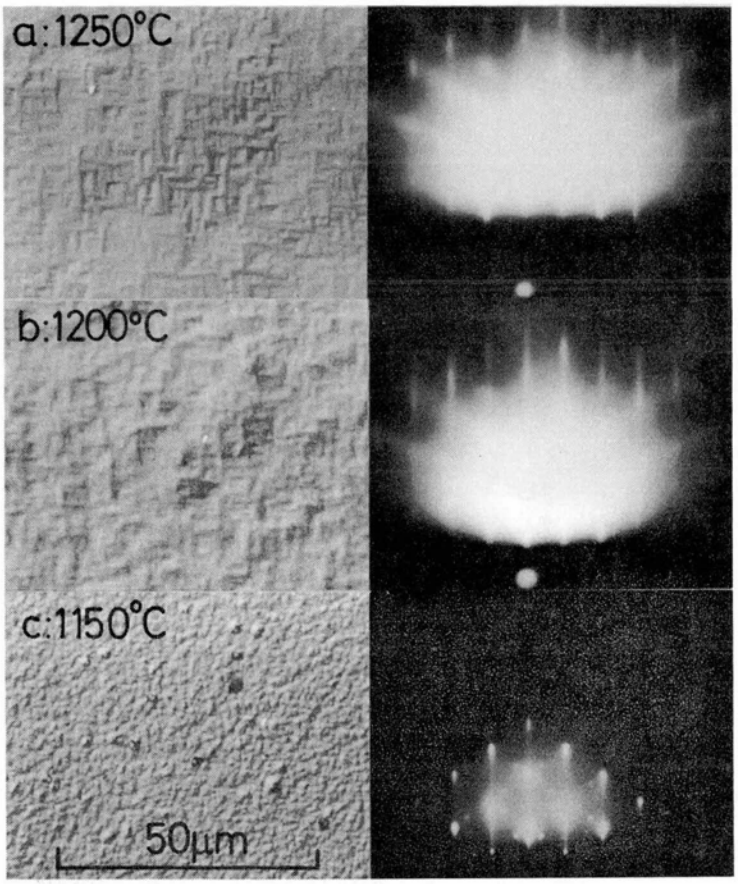

Fig.28 Nomarski microphotographs of the surface morphology and RHEED patterns of 3C-SiC grown using C_2H_2. By the reduction in growth rates, crystallinity was improved compared with Fig.27. Growth temperatures and growth rates were (a)1250°C and 0.72μm/hr, (b)1200°C and 0.54μm/hr and (c)1150°C and 0.54μm/hr, respectively.

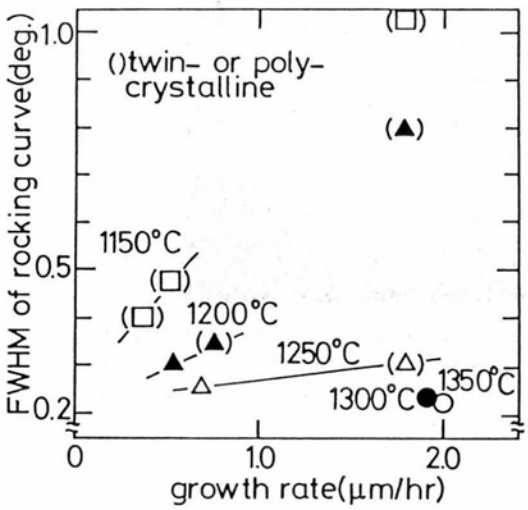

Fig.29 Growth rate dependence of FWHM of x-ray rocking curves of grown layers.

with Fig.27(e). Debye-rings disappeared and extra-spots were reduced. However, twin-spots remains slightly. Though optimization of the Si/C ratio was carried out, twin-spots did not disappear. Surface morphology in Fig.28(c) still remains a random feature. Thus, by the reduction in the growth rate single crystals were obtained at low temperatures of 1250°C and 1200°C.

A further evaluation of the grown layers prepared with C_2H_2 was carried out. The FWHM of X-ray rocking curves of these grown layers are shown in Fig.29. When the growth rate was fixed at about 1.8μm/hr, as the growth temperature was reduced, the FWHM of rocking curves became wider. And by the reduction in the growth rate, the FWHM became narrower. These results agree with the change in the crystallinity observed by RHEED technique. However, in spite that the samples grown at 1250°C and 1200°C showed single crystalline streak patterns by RHEED observation, their FWHM of X-ray rocking curves were wider than those of the samples grown at over 1300°C. This fact indicates that the lack of migration effect due to low growth temperature was not sufficiently made up for by the reduction in the growth rate.

The characteristics of Au-SiC Schottky barriers were evaluated using the samples which showed single crystalline features in RHEED observation. Figure 30 shows an example of the current-voltage characteristics of the Schottky diodes. The layers grown at low temperatures showed worse rectification than those grown at high temperatures. Figure 31 shows a variation of barrier height(ϕ_{bn}) and ideal factor *n*. As the growth temperature was reduced, the barrier height became lower and ideal factor *n* became larger. Such variations are considered to support the change in the crystallinity due to growth temperature observed as the change of FWHM of X-ray rocking curves. However, electron mobility and electron concentration obtained by the van der Pauw measurement showed no meaningful difference. Electron mobility is often governed not only by crystallinity but also by ionized impurity scattering and some other scattering mechanisms. Hence, the temperature dependence of electron mobility should be investigated to discuss the effects of crystallinity upon the

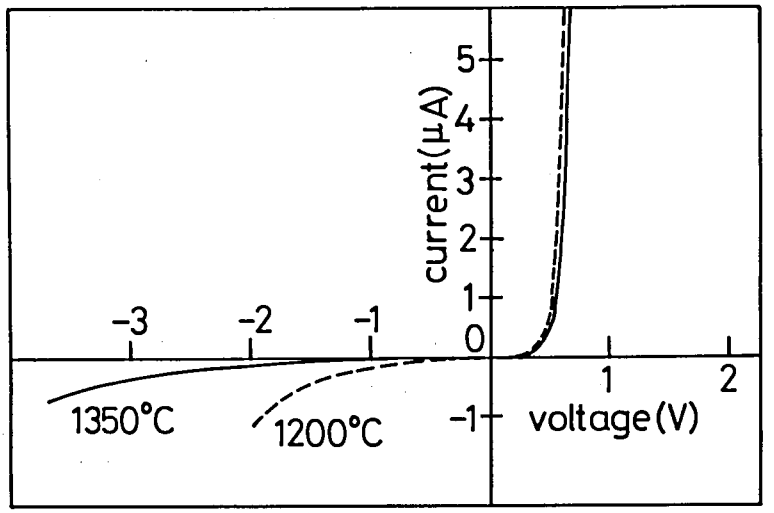

Fig.30 Example of rectification of Au-3C-SiC Schottky barrier. 3C-SiC grown at low temperatures(<1250°C) showed poor rectification.

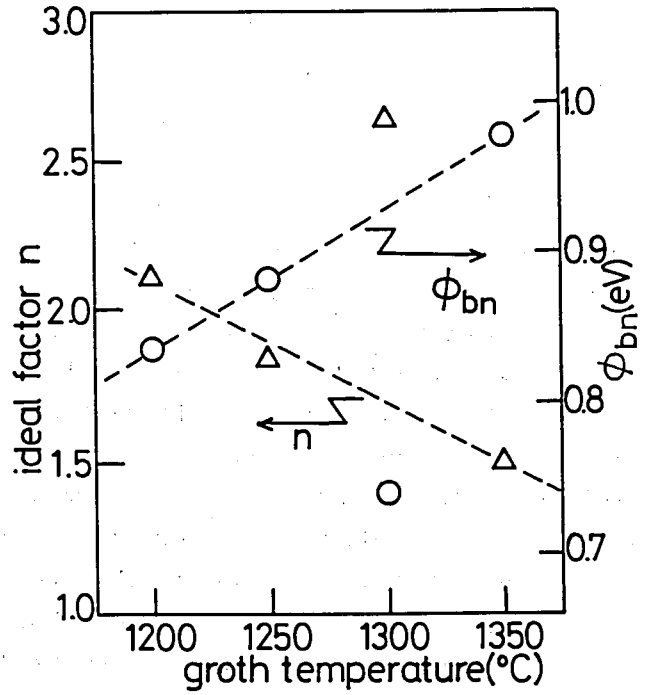

Fig.31 Growth temperature dependence of *n* value and barrier height(ϕ_{bn}) of Au-3C-SiC Schottky barrier.

electron mobility.

*Note: Recently the conversion of C_2H_2 into C_2H_4 under a H_2 ambience in cylinders was found[14]. The same phenomenon was considered to take place in the used cylinders for this investigation. Because, the moderate Si/C ratio always varied after the replacement of the cylinders of C_2H_2. In other words, the used carbon source was a mixture of C_2H_2 and C_2H_4. Therefore, the Si/C ratio was not discussed in detail in this section.

7. Summary

Characterization of carbonized layers was carried out. By RHEED observation the carbonized layers grown under optimized conditions were found to be single crystalline 3C-SiC. However, they contained crystal defects such as stacking faults and twinning. The density of these defects in CVD grown layers was reduced as the film grew, which was supported by RHEED, X-ray diffraction, channeling measurement and XTEM.

Single crystal growth of the 3C-SiC polar faces such as (100) and (111) was successful. However, the growth of nonpolar faces such as (110) and (211) was unsuccessful, which was explained by assuming the first grown layer by the carbonization to be a carbon layer. The grown layer on (111) has a severe problem of cracks and warp.

Temperature for single-crystal growth could be reduced to 1200°C by the reduction in growth rate. The reduction in the growth rate was effective to make up for the insufficiency of migration effect. However, crystals grown at low temperatures were inferior to those grown at high temperatures in crystallinity. If further reduction in the growth temperature will be attempted, some innovations which enhance migration may be necessary.

By considering all results mentioned in this section the

following factors which are necessary to obtain "good crystals" are selected. The current best substrate is Si(100). To improve crystallinity the grown layers had better be thicker than several microns. The carbonizing condition and the Si/C ratio must be optimized and the growth should be carried out at 1350°C. The growth of 3C-SiC on Si for the investigation of the following chapters was carried out in accordance with this guideline.

References

[1] F.C.Everstyen, P.J.W.Severn, C.H.J.v.d.Brekel and H.L.Peek, J. Electrochem. Soc. 117(1970) 925.

[2] I.Tani, *Nagaregaku(Hydrodynamics)*, (Iwanami, Tokyo, 1967), p.131, in Japanese.

[3] H.Suhara, Master Thesis, Faculty of Engineering, Kyoto University, 1983.

[4] P.B.Hirsch, A.Howie, R.B.Nicholson, D.W.Pashley and M.J.Whelan, Electron Microscopy of Thin Crystals, (Butterworths, London, 1965), Chapter 6.

[5] M.Plutton, *Surface Physics*, (Oxford Univ. Press, Oxford, 1975), Chapter 3.

[6] C.J.Dell'Oca, J. Electrochem. Soc. 120(1973) 1225.

[7] T.Ito, T.Inuzuka, *Kessyou No Hyouka(Characterization of Crystals)*, (Corona, Tokyo, 1982), p.107, in Japanese.

[8] T.Ohmi, S.Kuroiwa, S.Yoshitake, H.Iwabuchi, G.Sato and J.Murota, Extended Abstr. 19th Conf. Solid State Devices and Materials, Tokyo, 1987(Business Center for Academic Societies Japan, Tokyo, 1987) p.239.

[9] C.H.Carter, Jr., R.F.Davis and S.R.Nutt, J. Mater. Res., 1(1986) 811.

[10] J.Graul and E.Wagner, Appl. Phys. Lett. 21(1972) 67.

[11] A.Suzuki, private communication.

[12] C.W.Pearce, *VLSI Technology*, (McGraw-Hill, Auckland, 1983) edited by S.M.Sze, Chapter 2.

[13] F.Mieno, Y.Furumura and M.Maeda, Extended Abstr. 18th Int.

Conf. Solid State Devices and Materials, Tokyo, 1986(Business Center for Academic Societies Japan, Tokyo, 1986) p.49.
[14] H.Shiomi, private communication.

III. GROWTH ON OFF ORIENTED SUBSTRATES

1. Introduction

In this chapter, some attempts to improve grown layers on Si(100) and (111) by the introduction of off orientation are mentioned.

The main interest in the grown layers on (100) is concerned with antiphase domains(APD's). APD's are crystal defects which are observed in compound crystals. Especially, they are often observed in a heteroepitaxially grown crystal with a zinc-blende structure on a (100) face of a crystal with a diamond structure[1-5]. In the case of a zinc blende crystal like 3C-SiC, APD's are defined as follows. Zinc-blende structures consist of two sublattices of a face centered cubic structure. Usually each sublattice consists of atoms of a kind. When these atoms belong to the opposite sublattice in the both sides of some boundaries, the boundaries are called antiphase boundaries(APB's). Domain structures made by APB's are called APD's. A model of APD's(APB's) in a zinc blende structure is shown in Fig.1. In a zinc-blende structure each atom has four bondings with the nearest atoms of the opposite kind. However, APB's consist of bondings with atoms of the same kind as shown in Fig.1. When a crystal containing APD's is observed from [100], [011] direction in one domain is 90° different from that in a adjoining domain separated by APB's. In other words, when grown layers on Si(100) are observed from the upper side, it looks that there are two phases which are rotated by 90° each other.

APB's in semiconductor materials should be eliminated. In the case of epitaxial layers of GaAs on Si, APB's work as origins of lowering of electron mobility[6], roughness of surfaces[6] and recombination centers[7]. In this chapter, the origin and how to eliminate APD's in 3C-SiC are discussed based on various observations. Electrical properties are mentioned in the next chapter.

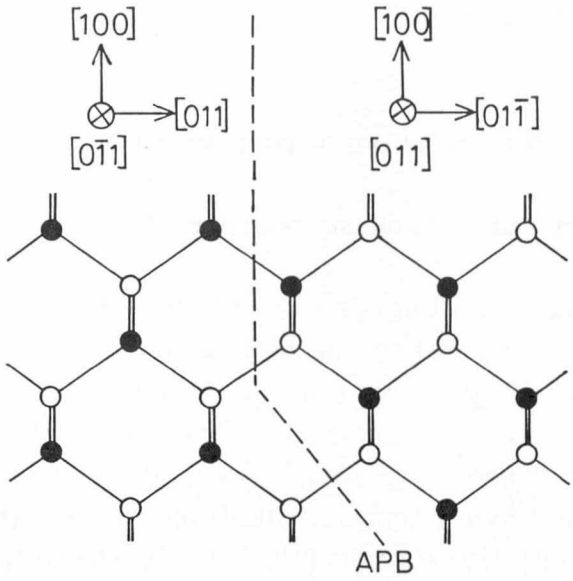

Fig.1 Antiphase boundary in a zinc blende crystal.

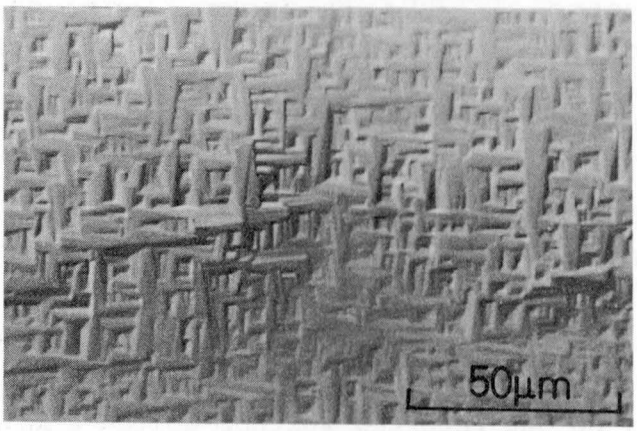

Fig.2 Nomarski microphotograph of typical surface morphology of the grown layer on a (100) well oriented substrate.

In Section 4, a fundamental experiment to investigate effects of the introduction of off orientation into (111) substrates is mentioned.

2. Antiphase disorder in grown layers on Si(100)

2-1. Observation of antiphase boundaries

APD's were always observed in 3C-SiC grown layers on (100) well oriented Si substrates. Figure 2 shows a typical surface morphology of grown layers on (100) well oriented substrates. The observed texture-like morphology consists of wedge shapes perpendicularly intersecting each other. Here, the existence of two phases which have perpendicular relationships should be noted. As explained above, two phases separated by APB's show a perpendicular relationship. Therefore, the surface morphology in Fig.2 is considered to indicate the existence of APD's. Such morphology was reported in the case of GaP grown layers on Si(100) which contained APD's.[1].

The existence of APD's in grown layers on (100) well oriented substrates was inferred by the surface morphology. By utilizing other techniques the existence of APD's was confirmed clearly. In this section etching and B-doping methods are mentioned. APB's were visualized using these methods. The utilization of a RHEED technique for the identification of the existence of APD's is mentioned in Section 2-3.

First, an etching method for the observation of APB's is introduced. Molten-alkali etching is known to be a good defect-observation tool for (0001)Si faces of various polytypes of SiC[8]. However, no one reported whether molten-alkali etching is useful for the 3C-SiC(100) face or not as far as the author knows. In this investigation it was confirmed that defects were observed by molten KOH etching as hollows on the SiC(100) surface. Figure 3 shows an etched surface by molten KOH at about 600°C. Three types of hollows were observed : A:type-1

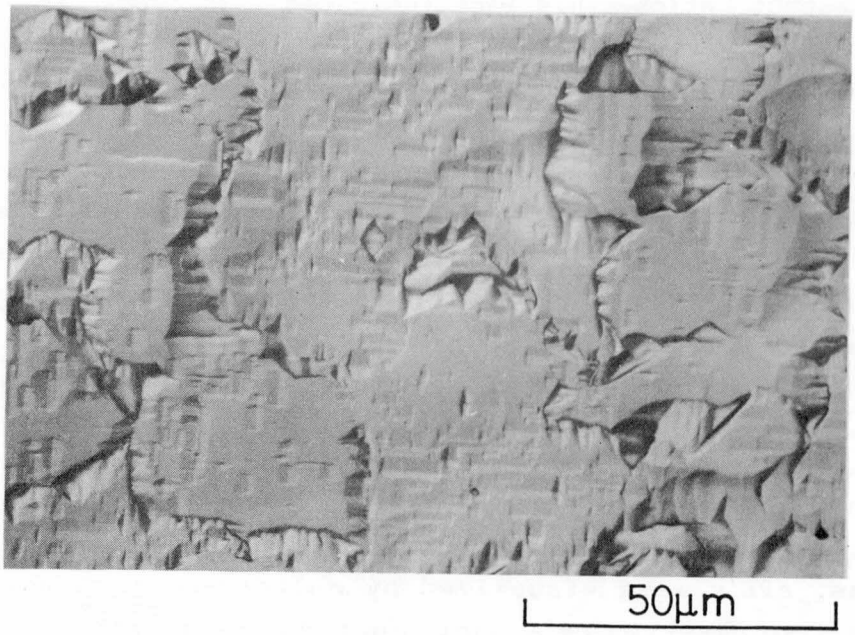

Fig.3 Nomarski microphotograph of the surface of a grown layer etched by molten KOH on (100) well-oriented substrate. APB's were observed as random grooves.

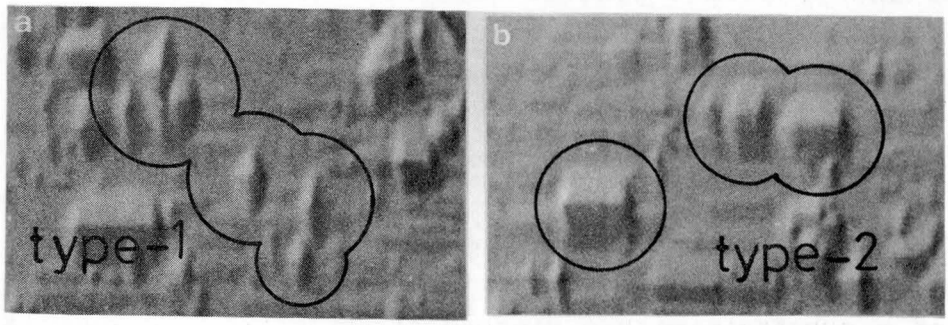

Fig.4 Etch pits formed by molten KOH etching. (a)type-1 pits and (b)type-2 pits.

pits(Fig.4(a)), B:type-2 pits(Fig.4(b)) and C:random grooves. Every type-1 pit has a similar figure and type-2 pits have various aspect ratios. This fact indicates that type-1 and 2 pits originate from line defects(dislocation) and plane defects(stacking faults), respectively. Random grooves are visualized APB's, because the pits are placed perpendicularly each other in adjoining regions separated by the grooves.

Figures 5(a)-(c) show Nomarski microphotographs of etched surfaces of grown layers with various thicknesses. APD's became broader and the concentration of APB's was reduced as a film grew thicker. Figures 6(a)-(c) indicate a reduction mechanism of APB's. As the film becomes thicker, APB's spread upward with lateral movements(Figs.6(a) and (b)). And once two APB's collide, they connect each other and stop spreading(Fig.6(c)). Thus, APB's reduce and the area of a single domain becomes broader, as the film grows.

Thus, APB's were visualized by molten KOH etching. APB's could be also observed by B-doping during CVD growth. A B-doped layer was grown after etching by HCl at 1330°C on an undoped grown layer of 10μm thick. The thickness of the B-doped layer was about 1μm. APB's were clearly observed as grooves as shown in Fig.7. However, the area where grooves were formed was very narrow and sometimes grooves were not formed. Therefore, the molten KOH etching method was mainly used for the identification of the elimination of APD's.

2-2. Elimination of antiphase boundaries

Kroemer et al. indicated two necessary conditions to obtain an APD-free grown layer with a zinc-blende structure on the (100) face of a substrate with a diamond structure[2]. The conditions are the followings.

(A): There is a chemical preference for A-S bonding over B-S bonding. Where A and B are elements which constitute the zinc blende grown layer and S is an element of the substrate.

(B): The substrate should not have steps with a mono(or odd

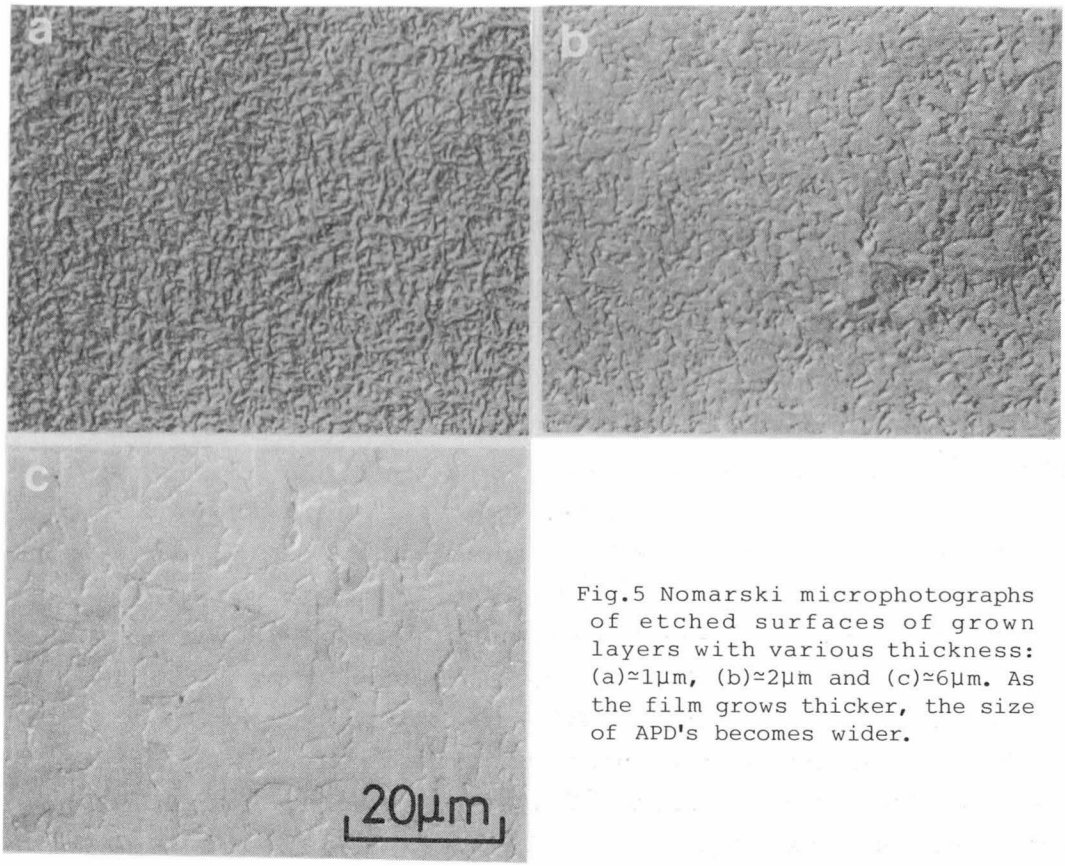

Fig.5 Nomarski microphotographs of etched surfaces of grown layers with various thickness: (a)≃1μm, (b)≃2μm and (c)≃6μm. As the film grows thicker, the size of APD's becomes wider.

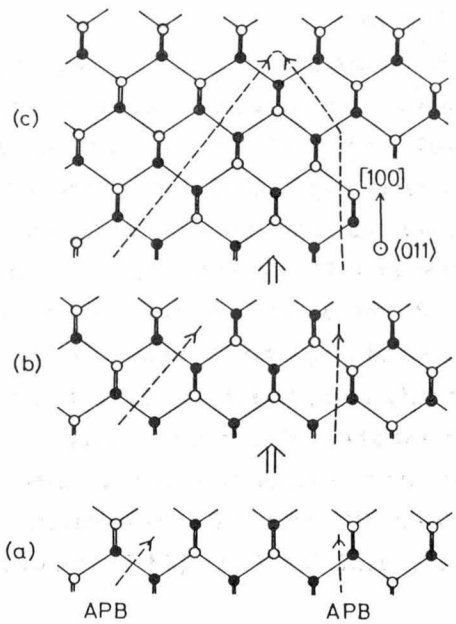

Fig.6 Model of the reduction mechanism of APB's. The crystal is viewed in the ⟨011⟩ direction.

number)-atomic layer height.

The condition (A) means that the first grown layer must consist of atoms of one kind. As discussed in Chapter II, the first grown layer formed by the carbonization of Si was considered to consist of C atoms only. So that, the condition (A) is satisfied. Hence, if the surface where only steps with a bi(or even numbers)- atomic layer height is obtained, an APD-free growth is expected as shown in Fig.8(a). However, APD's actually existed in the grown layer. Steps with a mono-atomic layer height which existed on the surfaces of etched Si substrates by HCl were considered to be origins of APB's as shown in Fig.8(b). Some methods to obtain a Si surface with bi-atomic layer steps are necessary for an APD-free growth. Modification of the step height on Si(100) under an ultra high vacuum was observed by LEED and RHEED[9-11]. The introduction of off orientation into Si(100) or surface treatment at high temperatures were effective to obtain bi-atomic layer steps. In this investigation, the elimination of APD's by the introduction of off orientation was attempted.

The off orientation consists of two important factors of the direction and the magnitude of an off angle. In order to treat these two factors at the same time, 3C-SiC was grown on a spherically polished Si(100) substrate. The radius of the curvature of the spherically polished substrate was 14cm. Figure 9(a) shows a photograph of the surface of the grown layer on the spherically polished substrate. Two black crossing lines were observed. These lines crossed at the (100) pole, and spread towards the directions which are equivalent to the [011] direction. The surface on the two black lines was mirrorlike, and that on the other area was rough. Figures 10(a)-(d) show Nomarski microphotographs of the surfaces at various points which are indicated in Fig.9(b). Point A corresponds to the (100) pole. In other words, the grown layer on point A corresponds to that on the (100) well-oriented surface. A texture-like morphology which indicates the existence of APD's was observed as shown in Fig.10(a). The grown layers on points B1 and B2 correspond to those on the surfaces oriented 1° and 3° off (100) towards

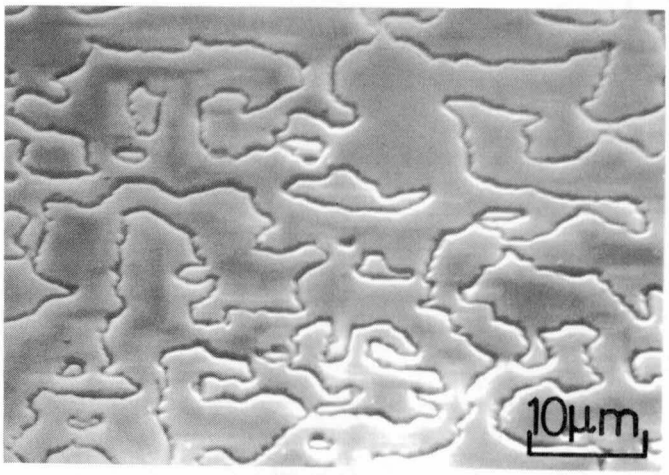

Fig.7 SEM microphotograph of the visualized APB's by the growth of a B-doped layer.

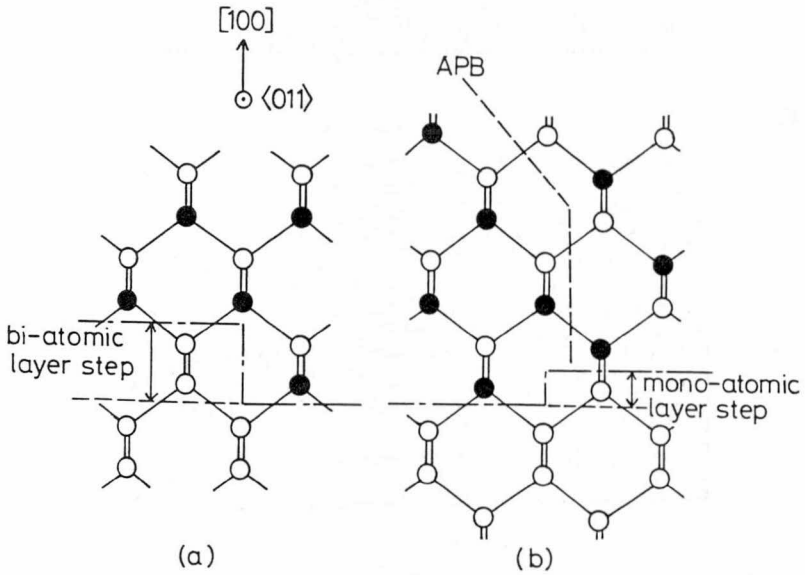

Fig.8 Model of origin of APD. On the assumption that the first grown layer consists of C atoms only, (a)steps with bi-atomic layer height result in APD-free growth. (b) Steps with mono-atomic layer height result in formation of APB's.

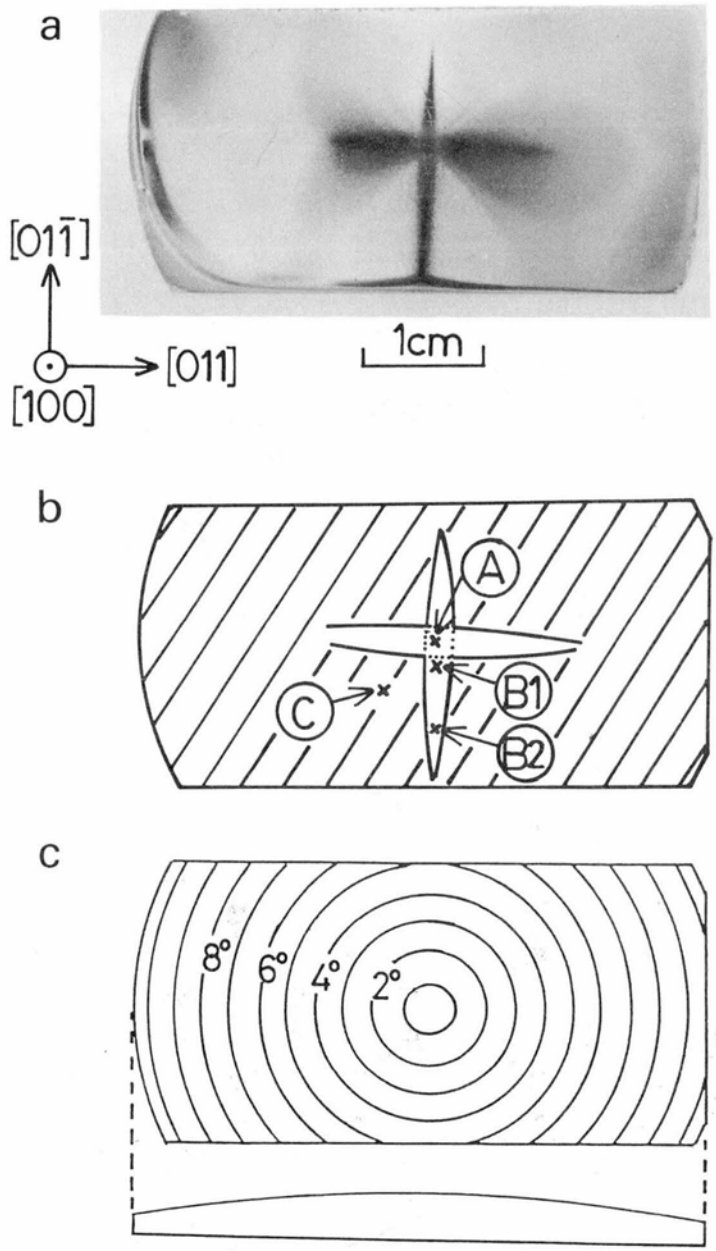

Fig.9 (a)Photograph of a grown layer on a spherically polished (100) substrate. The rough surface area looked white or grey because of random reflection of lighting. The surface of two black lines was mirrorlike. (b)Positions of points *A*, *B1*, *B2* and *C* on the spherically polished substrate. The surface morphology of the grown layers on these points is shown in Fig.10. The surface of the unshaded area was mirrorlike and that on the shaded area was rough. (c)Schematic explanation of relationship between position and off angle.

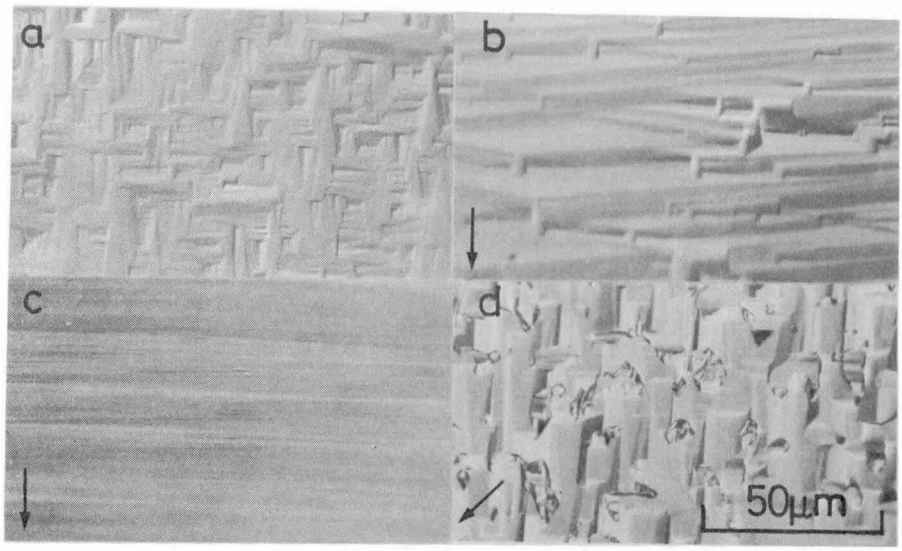

Fig.10 Nomarski microphotographs of the surfaces at various points of the grown layer on the spherically polished (100) substrates. Points *A*, *B1*, *B2* and *C* are located at (a)(100) pole, (b)the point inclined at 1° towards (011), (c)the point inclined at 3° towards (011) and (d) the point inclined at 4° towards (010).

(011), respectively. From point A to point B2 the surface morphology changed gradually. As the magnitude of the off angle became larger, the wedge-like crystal habit which pointed the perpendicular direction to the off direction became dominant like in Fig.10(b). Even when the magnitude of the off angle reached to 1°, antiphase domains were still observed like small islands(Fig.10(b)). Beyond 2° of the magnitude of the off angle, antiphase domains were not observed as shown in Fig.10(C). Up to 5° the single-domain area was observed. Beyond 5° the existence of antiphase domains was not clear because of surface roughness which was brought about by the disturbance of gas flow due to the thick and curved substrate. Off orientations except for towards [011] resulted in very rough surfaces with APD's like on point C(Fig.10(d)).

These results were applied to the growth on Si(100) wafers. The substrates used were oriented 2° off (100) towards (011). The surface morphology was similar to Fig.10(c). In order to confirm the elimination of APD's, the grown layer was etched with molten KOH at about 600°C. As shown in Fig.11, the etched surface of the grown layer on the substrate oriented 2° off (100) towards (011) showed no grooves, and all etch pits have the same direction different from the grown layers containing APD's. This result means that APD's were eliminated by the introduction of the off orientation towards (011). Substrates oriented 4° and 6° off (100) towards (011) were also used. The surface morphology for these substrates was quite similar to that for 2° off.

Figure 12 explains the relationship between the off orientation and surface morphology or etch pits. This relationship was constant. By using this, a strict epitaxial relationship between off substrates and grown layers is discussed as follows. The top view of type-2 pits is rhombic. In 6H-SiC, the $(000\bar{1})$C face is chemically more active than the (0001)Si face, and the former has a higher etch rate for molten alkali. The $(000\bar{1})$ and (0001) faces correspond to the $(11\bar{1})$ and (111) faces of 3C-SiC, respectively. If the sidewalls of the etch pits consist of only the $(11\bar{1})$ and (111) faces, the longer

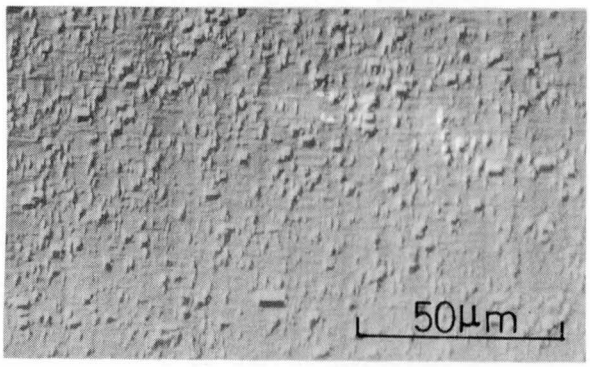

Fig.11 The surface of the grown layer etched with molten KOH on a Si substrate oriented 2° off (100) towards (011). No APB's are observed.

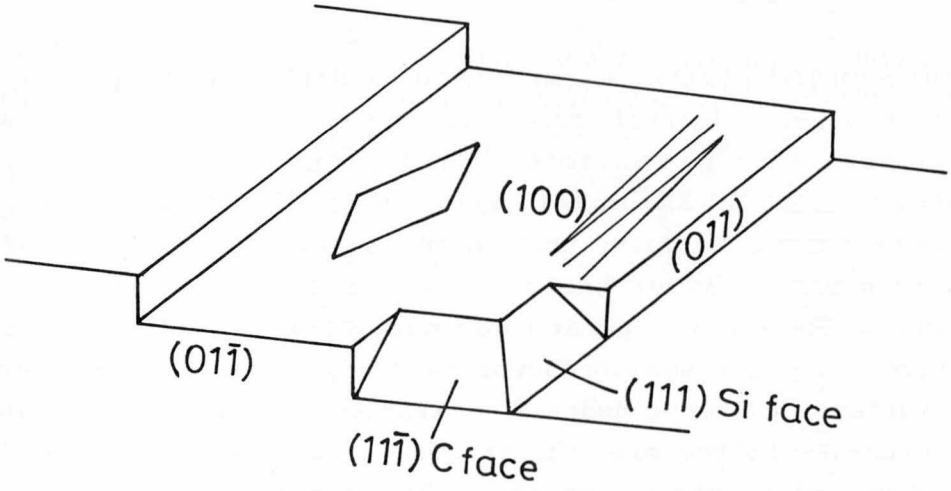

Fig.12 Schematic explanation of the relationship between off direction and etch pits or wedge-shaped surface morphology.

diagonal line of the rhombic shape should point the direction of the higher etch rate as shown in Fig.13. Therefore, the relationship between the off orientation and the $(11\bar{1})$ or (111) faces are obtained as shown in Fig.12.

An example of the surface morphology of the grown layers on Si oriented 4° off (100) towards (010) is shown in Fig.14. The surface was rough and the existence of APD's was confirmed by molten KOH etching. Thus, the grown layers on spherically polished (100) substrates and various (100) wafers well agreed concerning the existence of APD's and surface morphology.

In this investigation, the off orientation was introduced to eliminate APD's. Recently this method is often used for the growth of III-V semiconductors on Si[3,12,13]. Growth on Si(211) is also known as a method to obtain APD-free grown layers for GaP and GaAs[14,15]. However, this method cannot be adopted for 3C-SiC, because single crystals could not be grown on Si(211) as mentioned in Section II-5.

2-3. Surface observation by RHEED

In Section 2-1 the observation of APB's was described. In this section, the identification of the existence of APD's using a RHEED technique is mentioned. This method utilizes a surface 5x1 structure of 3C-SiC grown layers. This surface structure was very persistent. In spite that samples were exposed to the air for a long period after growth, the surface structure did not disappear. The longest period was over several months. Surface structures of other semiconductor materials are usually observed after surface treatment under an ultrahigh vacuum and they vanish after exposure to the air[16]. The 5x1 structure was observed as the fifth order extra streaks in RHEED patterns. In addition that, curved streaks due to reciprocal planes were observed. The relationship between the 5x1 surface structure and the curved streaks is also discussed.

Two types of Si substrates were used. One was a (100) well oriented Si substrate and the other was a Si substrate oriented

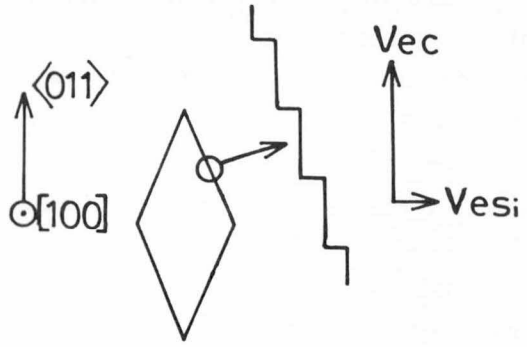

Fig.13 If the sidewall of etch pits consists of only $(11\bar{1})$C and (111)Si faces, a longer diagonal line of rhombic shape points $[11\bar{1}]$ direction because of the difference in etch rates.

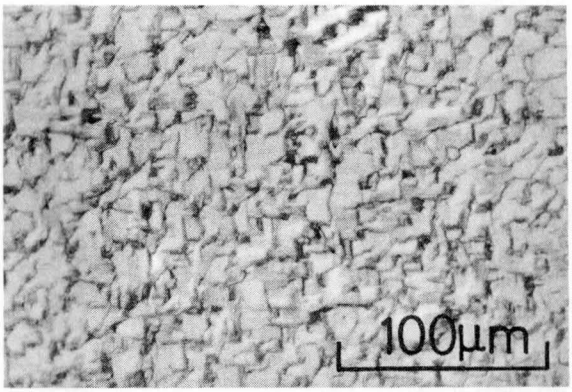

Fig.14 Nomarski microphotograph of surface morphology of a grown layer on Si substrates oriented 4° off (100) towards (010).

2° off (100) towards (011). The former and the latter substrates are hereafter called as (100) substrates and off substrates in this section, respectively. The grown layers on (100) substrates contained APD's as described in Section 2-1.

RHEED observations were carried out using a JEOL JEM-120B electron microscope with an attachment for high resolution RHEED. The acceleration voltage of incident electrons was 80kV. Samples were left in the air after growth. No surface treatment was carried out in the microscope. Sometimes samples were cleaned with organic solvents, deionized water or HF acid. However, cleaning seemed to give no difference in RHEED patterns. Surface structures were reproducibly observed when the grown layers were thicker than 0.5μm. RHEED patterns used hereafter were taken with the grown layers of 0.5μm in thickness.

Figures 15(a)-(d) show RHEED patterns for the ‹011› azimuth. In the case of the grown layers on (100) substrates(Figs.15(a) and (b)), both [0$\bar{1}$1] and [011] azimuth patterns showed the fifth order extra streaks. The pattern was schematically represented in Fig.16. In the [001] azimuth no extra streaks were observed as shown in Fig.17(a). Hence, these RHEED patterns originated from a mixture of the 5x1 and 1x5 surface structures; i.e. two phases existed on the surface of the grown layer on the (100) substrates. The grown layers on the (100) substrates contained APD's. If these two phases originated from APD's, APD-free grown layers on off substrates should contain a 5x1 structure. The RHEED pattern for the [011] azimuth of the grown layer on the off substrate actually showed no extra streaks as shown in Fig.15(d) and the [0$\bar{1}$1] azimuth pattern in Fig.15(c) showed the fifth order streaks similar to Figs.15(a) and (b). Thus, CVD grown layers of 3C-SiC on the off substrates showed the 5x1 surface structure. A 6x1 surface structure was rarely observed.

Two kinds of unusual streaks were observed in addition to the fifth order streaks. One is a curved streak and the other is an unusually long streak. The curved streaks were observed in the [010] azimuth patterns of Figs.17(a) and (b). In the case of ‹011› azimuth patterns on the off substrates, streaks for

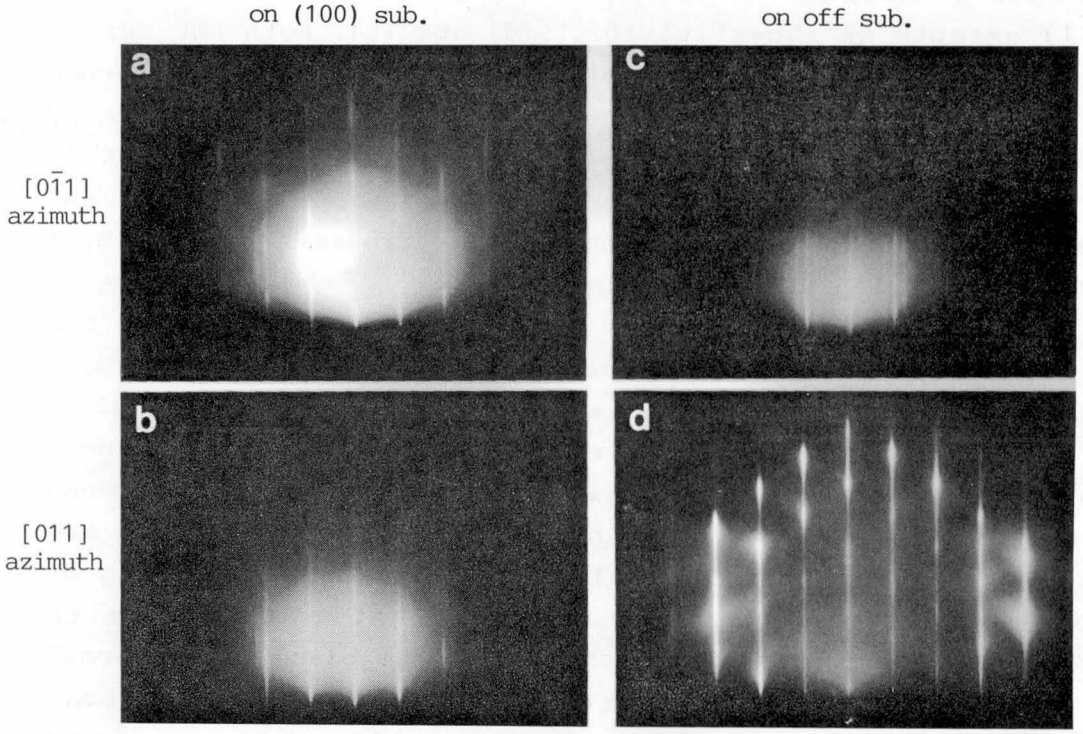

Fig.15 [0$\bar{1}$1] and [011] azimuth RHEED patterns of the grown layers on a (100) substrate and a 2° off substrate.

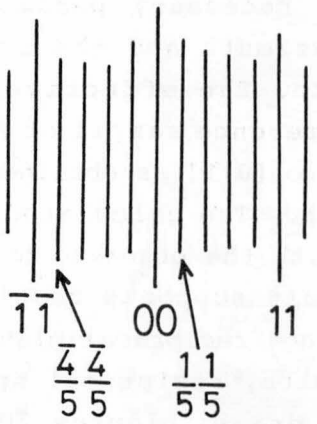

Fig.16 Schematic explanation of Fig.15 (a), (b) and (c).

the [011] azimuth were much longer than those for the [0$\bar{1}$1] azimuth as shown in Figs.15(d) and (c). Both the curved streaks and unusually long streaks are explained by the existence of reciprocal planes[17-19]. When a structure composed by parallel linear rows exists, the reciprocal lattice of this structure is formed by reciprocal planes normal to the rows. And when the each row consists of components periodically spaced by a distance of d in the real space, the reciprocal planes have an interval of $1/d$ as shown in Fig.18. The projection of the intersectional lines made by the Ewald sphere and the reciprocal planes are observed as the curved streaks on a screen or a film. If the incidence azimuth is parallel to the reciprocal planes, projected intersectional lines are observed as straight streaks as shown in Fig.19(a). If it is not parallel, curved streaks are observed as shown in Fig.19(b). The [011] azimuth pattern of Fig.15(d) showed unusually long straight streaks due to reciprocal planes. Therefore, the reciprocal planes are normal to [0$\bar{1}$1] direction. The interval of the observed reciprocal planes corresponds to the distance between 00 and 1$\bar{1}$ streaks as shown in Fig.15(d), which means that the period of the components composing the each row corresponds to the lattice spacing of (011) faces.

The projected curves can be easily obtained by calculation[18,19]. The necessary parameters are the angle between the incidence azimuth and the reciprocal planes and effective camera length. The effective camera length was determined by using a reference sample of Au. If the reciprocal planes are perpendicular to [0$\bar{1}$1] as obtained above, the angle is 45° for the [010] azimuth. The calculated curves assuming the angle to be 45° agreed with the observed curves in Fig.17 of the [010] azimuth. This result supports that the observed curved streaks originated from the reciprocal planes normal to [0$\bar{1}$1].

Based on these results, reciprocal space diagrams of the surface structures were drawn. Figures 20(a) and (b) show the diagrams on the (100) substrates and the off substrates, respectively. Figure 20(a) corresponds to the superposition of

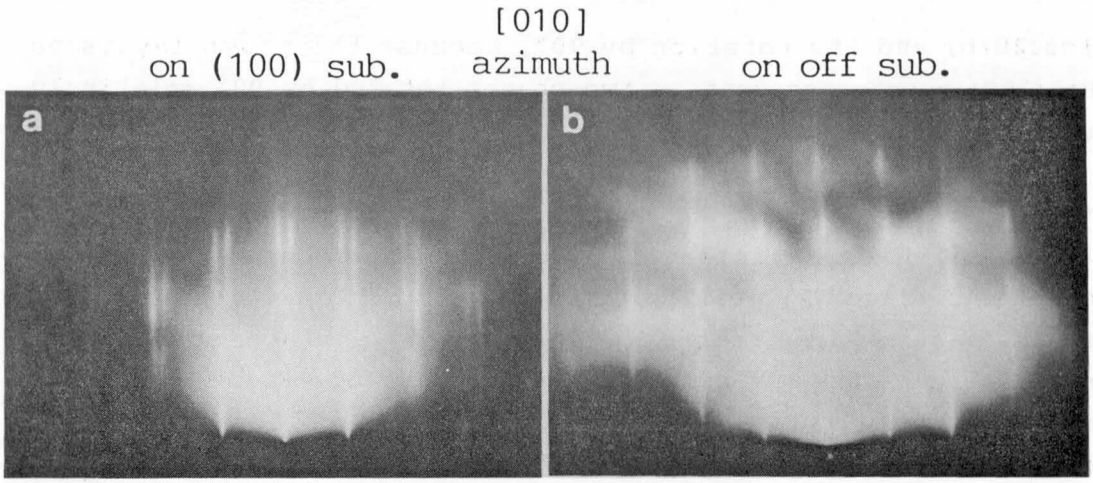

Fig.17 [010] azimuth RHEED patterns of the grown layers (a)on a (100) substrate and (b)on a off substrate.

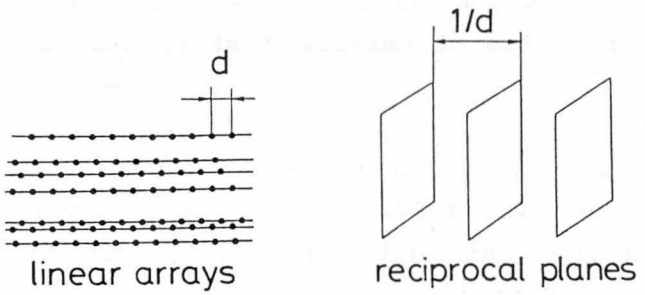

Fig.18 Reciprocal planes are formed in the reciprocal space by linear arrays in the real space. (After Delescluse, Ref.[18]).

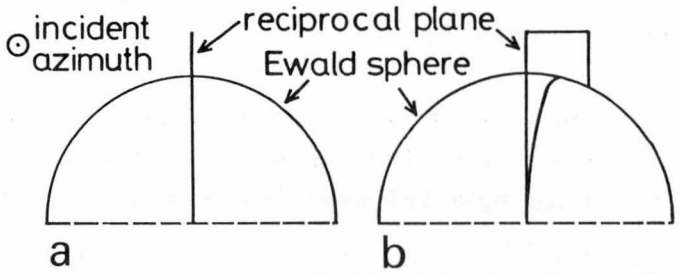

Fig.19 When incident azimuth is (a) parallel and (b) not parallel to a reciprocal plane, intersectional lines made by the Ewald sphere and the reciprocal plane are projected as (a) a straight line and (b) a curved line.

Figs.20(b) and its rotation by 90°, because the grown layers on the (100) substrates contain two phases rotated by 90° relatively due to APD's.

The 5x1 surface structure and the reciprocal planes simultaneously existed as mentioned above. As an example of the structure which satisfies the observed results, a partially occupied surface 5x1 mesh structure shown in Fig.21 is discussed. If the mesh points are fully occupied by surface structures, curved streaks are not observed. In the case of Fig.21, parallel rows are constructed by the missing of surface structures. The rows point the $[0\bar{1}1]$ direction, and each of them is composed by surface structures which lie at intervals of the lattice spacing of (011). A preliminary simulation of diffraction of waves by the 5x1 surface mesh was carried out to discuss the origin of the reciprocal planes. Dynamical theory was not utilized for the simulation. The position of surface mesh points is described as follows:

$$\boldsymbol{R}_m = m_1\boldsymbol{a} + m_2\boldsymbol{b} \ , \qquad (1)$$

where m_1 and m_2 are integer and $\boldsymbol{a}$ and $\boldsymbol{b}$ fundamental translation vectors of the mesh. The difference in the phase angle between scattered waves from the mesh point at $\boldsymbol{R}_m$ and the origin $\boldsymbol{O}$ is written as follows[20]:

$$2\pi(\boldsymbol{s}-\boldsymbol{s}_0)\boldsymbol{R}_m/\lambda = 2\pi\boldsymbol{S}(m_1\boldsymbol{a}+m_2\boldsymbol{b}) \ , \qquad (2)$$

where

$$\boldsymbol{S} = (\boldsymbol{s}-\boldsymbol{s}_0)/\lambda \ , \qquad (3)$$

and $\boldsymbol{s}$ and $\boldsymbol{s}_0$ are wave vectors of incoming and outgoing waves. For the whole mesh points, scattering amplitude F is written as

$$F = \sum_{m_1,m_2} \exp((2\pi i\boldsymbol{S})\cdot(m_1\boldsymbol{a}+m_2\boldsymbol{b})) \ . \qquad (4)$$

Here, since the discussion about the absolute amplitude is not necessary, the scattering factor at mesh points is neglected. To treat the diffraction by a 5x1 mesh, parameters are defined as follows.

$$\boldsymbol{a} = \begin{pmatrix}5\\0\\0\end{pmatrix} \ , \quad \boldsymbol{b} = \begin{pmatrix}0\\1\\0\end{pmatrix} \ , \quad \boldsymbol{s}_0 = \begin{pmatrix}0\\0\\1\end{pmatrix} \ , \quad \boldsymbol{s} = \begin{pmatrix}p\\q\\r\end{pmatrix}, \quad \lambda = 10^{-2} \ . \qquad (5)$$

Then F is described as

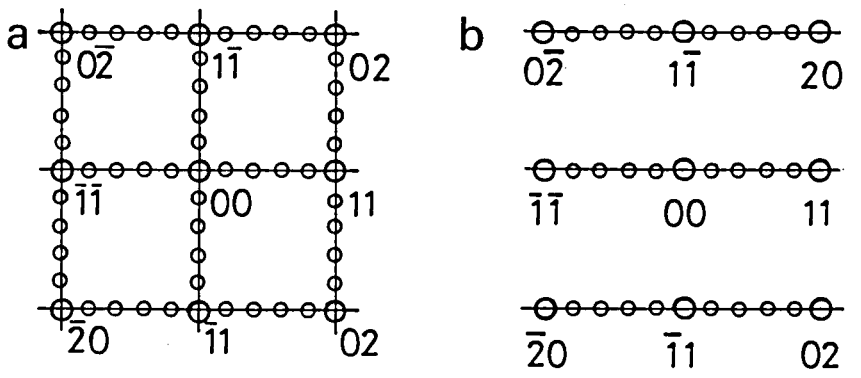

Fig.20 Reciprocal-space diagrams of the surface structure (a)on (100) substrates and (b)on off substrates.

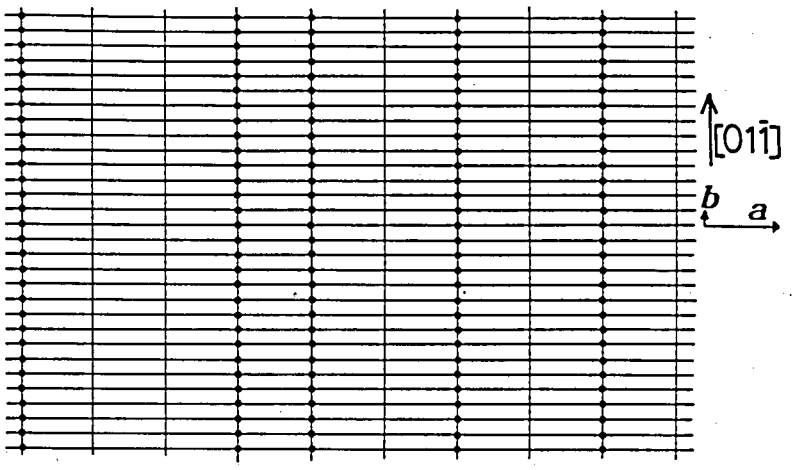

Fig.21 Partially occupied 5x1 surface mesh structure. Solid circles mean that the net points are occupied by surface structures. Length of unit mesh for [01̄1] is equal to lattice spacing of (100).

$$F = \sum_{m_1} \exp(2\pi i \cdot 500 m_1 p) \sum_{m_2} \exp(2\pi i \cdot 100 m_2 q) \quad . \qquad (6)$$

In this investigation an electron energy for RHEED observation was 80KeV ,and the wavelength of electron beam was 0.042Å and $|\boldsymbol{b}|$(lattice spacing of SiC(011)) was 3.2Å, therefore, the value of λ was decided to be 10^{-2}. Using eq.(6), the scattering intensity is obtained as $F \cdot F^*$. When $r >> p,q$, the scattering intensity for a small scattering angle is obtained. Figure 22 shows the intensity distribution of the diffracted waves on a screen for the waves perpendicularly incident upon the mesh. In this case, the intensity distribution represents the reciprocal space diagram of the mesh structures. Figure 22(a) shows the diffraction by a fully occupied 5x1 mesh. Peaks correspond to the fifth order streaks observed in the RHEED pattern. The introduction of the parallel rows pointing $\boldsymbol{b}$ shown in Fig.21 results in the increase of the intensity on the lines which are normal to $\boldsymbol{b}$ and connect the peaks as shown in Fig.22(b). Figure 22(b) agreed with the obtained reciprocal space diagram of the surface of 3C-SiC indicated in Fig.20(b). When parallel rows are formed normal to $\boldsymbol{b}$, reciprocal planes are formed normal to $\boldsymbol{a}$ as shown in Fig.22(c). The random missing of mesh points results in the increase of the background intensity as shown in Fig.22(d).

3. Growth on spherically polished Si(111)

In this section, an investigation concerning the introduction of off orientation into (111) substrates is described. Growth was carried out on a spherically polished (111) substrate similar to Si(100). Figure 23(a) shows the surface of a grown layer on the spherically polished substrate. Three narrow black lines spread from the (111) pole to the directions equivalent to $\langle 2\bar{1}\bar{1} \rangle$. Figures 24(a)-(c) show Nomarski microphotographs of the surfaces of the three points on the sample. The positions of the points are schematically indicated in Fig.23(b). The surfaces on the lines are clearly flatter than

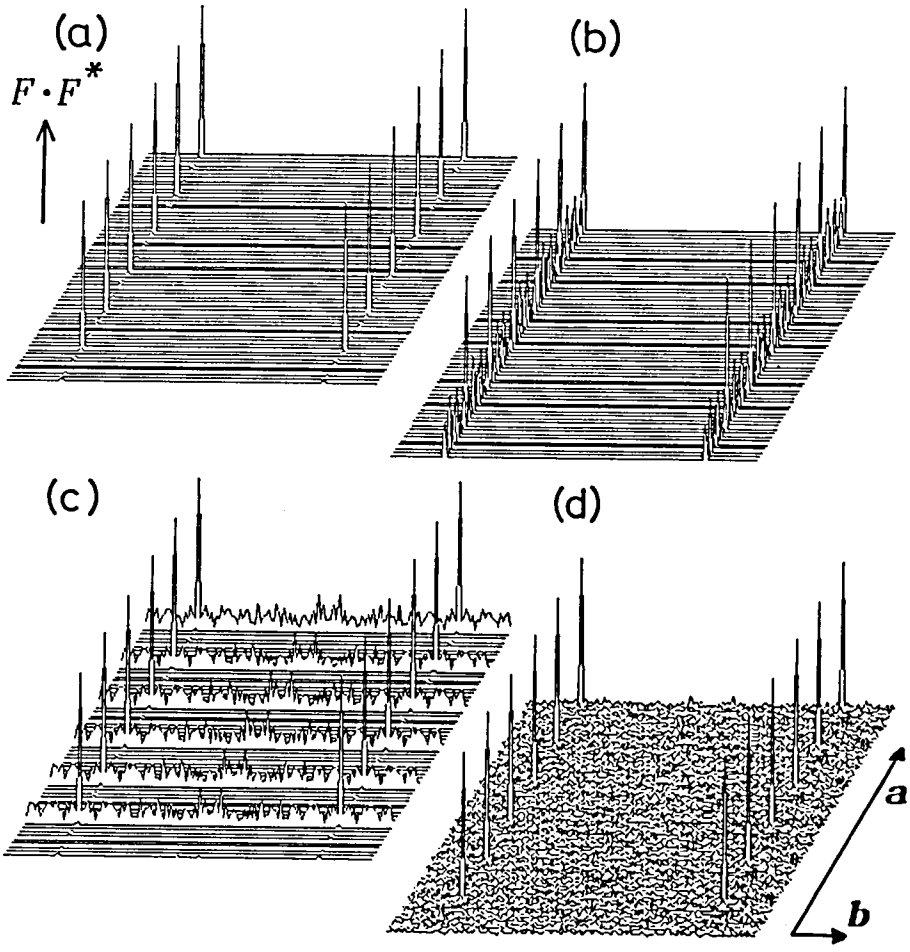

Fig.22 Intensity distribution of diffracted waves on a screen for the incidence azimuth of waves normal to the mesh. (a)Diffraction by fully occupied 5x1 mesh. (b)Diffraction by partially occupied 5x1 mesh which consists of linear arrays pointing to [0$\bar{1}$1]. (c)Diffraction by partially occupied 5x1 mesh which consists of linear arrays pointing to [0$\bar{1}\bar{1}$]. (d)Diffraction by randomly occupied 5x1 mesh.

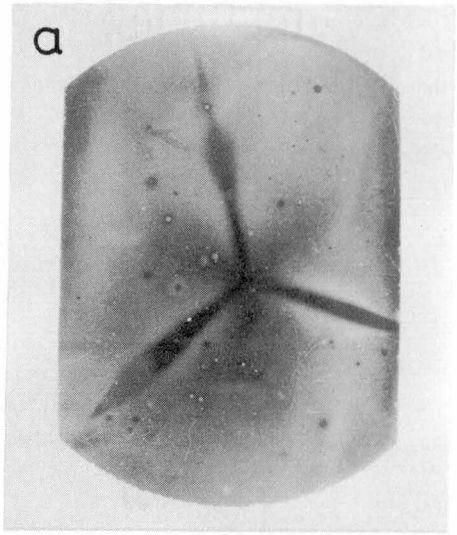

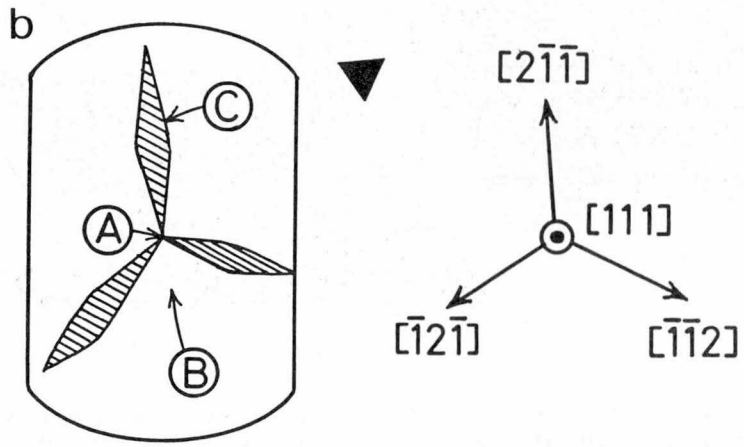

Fig.23 (a)Photograph of the grown layer on a spherically polished (111) substrate. (b)Schematic representation of (a). A solid triangle indicates orientations of etch pits on the Si substrate.

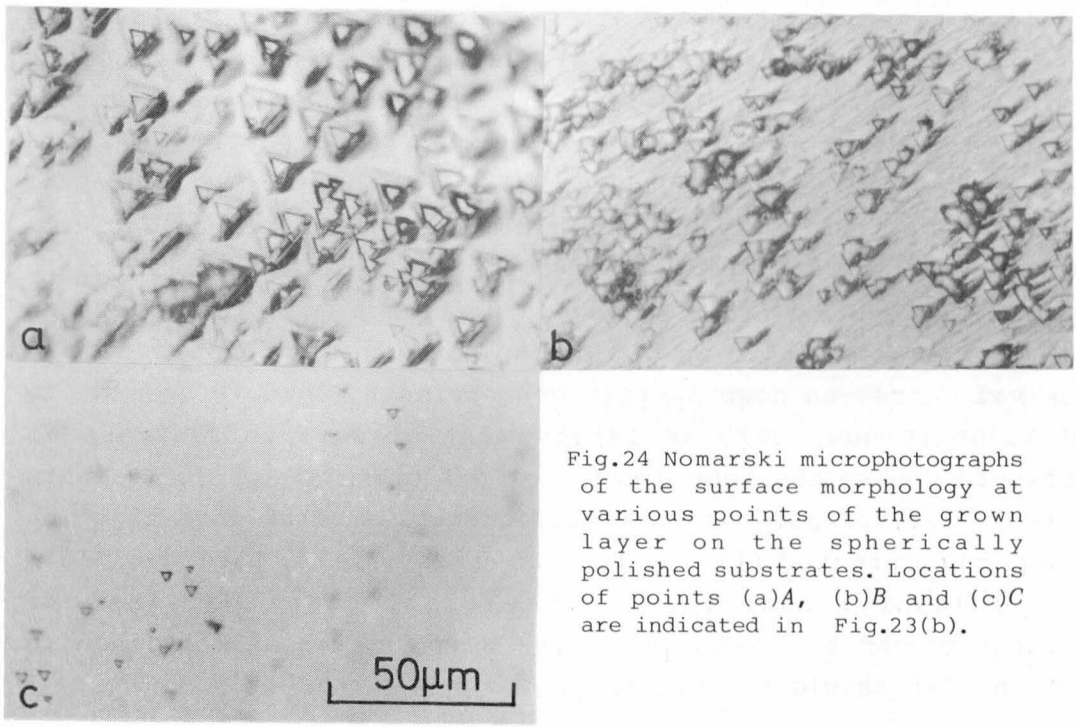

Fig.24 Nomarski microphotographs of the surface morphology at various points of the grown layer on the spherically polished substrates. Locations of points (a)*A*, (b)*B* and (c)*C* are indicated in Fig.23(b).

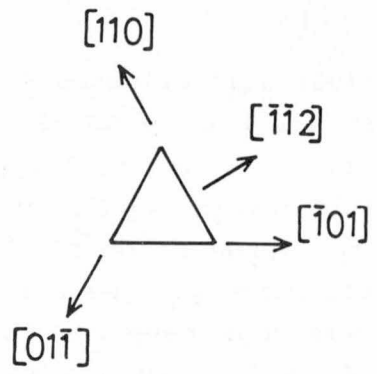

Fig.25 The relationship between orientation and geometry of etch pits on Si(111). (After Runyan, Ref.[21]).

the other part. In the strict sense, $[2\bar{1}\bar{1}]$ is not equivalent to $[\bar{2}11]$ for Si. To distinguish these directions an observation of etch pits was utilized. Pits were formed by boiling spherically polished Si in aqueous KOH at 80°C for 30sec. Triangular pits were formed. The orientation of such pits is known as shown in Fig.25[21]. The directions perpendicular to the three sides of the triangles are $\langle 2\bar{1}\bar{1}\rangle$. The relationship of the orientation between the pits and the three lines are schematically indicated in Fig.23(b). Conclusively, the directions of the off orientation which are effective to improve surface flatness were obtained to be $[\bar{1}\bar{1}2]$, $[\bar{1}2\bar{1}]$ and $[2\bar{1}\bar{1}]$. However, different from the growth on Si(100) the dependence on off orientation was not reproducibly observed. Some unknown factors concerning the growth seemed to exist. Up to now, only an improvement of surface flatness is confirmed due to the introduction of off orientation. To evaluate whether crystallinity was affected or not, further investigation using off oriented (111) wafers towards $[\bar{1}\bar{1}2]$, $[\bar{1}2\bar{1}]$ or $[2\bar{1}\bar{1}]$ are necessary. Especially, the relationship between off orientation and the problems of the warp and cracks mentioned in Section II-5 should be investigated.

4. Summary

Grown layers on (100) well oriented Si substrates contained APD's. As the grown layers became thicker, the area of APD's became broader. However, even for the thick(≃20μm) grown layers they were far from single domain. By the growth on a spherically polished substrate, the introduction of the off orientation to (011) was found to be effective for the elimination of APD's. The elimination of APD's was confirmed for the grown layers on Si wafers oriented 2°, 4° and 6° off (100) towards (011). The domination of steps with bi-atomic layer heights brought about by the introduction of off orientation was considered to be the origin of the elimination of APD's. Molten KOH etching at about 600°C was utilized for the observation of APB's and etch pits.

The identification of the existence of APD's was also possible by the RHEED observation. When the grown layers contained APD's, a mixture of 5x1 and 1x5 surface structures was observed. The surface structure showed extraordinary persistence. The curved and long straight streaks due to reciprocal planes were also observed. Growth on spherically polished Si(111) was also attempted. An improvement in surface flatness by the introduction of the off orientation to $[2\bar{1}\bar{1}]$ was observed.

References

[1] K.Morizane, J. Cryst. Growth 38(1977) 249.

[2] H.Kroemer, K.J.Polasko and S.C.Wright, Appl. Phys. Lett. 36(1980) 763.

[3] B-Y.Tsaur, J.C.C.Fan, G.W.Turner, F.M.Davis and R.P.Gale, Proceeding 16th IEEE Photovoltaic Specialists Conf., San Diego, 1982(IEEE, New York, 1982), p.1143.

[4] M.Akiyama, Y.Kawarada and K.Kaminishi, J. Cryst. Growth 68 (1984) 21.

[5] M.Akiyama, Y.Kawarada and K.Kaminishi, Jpn. J. Appl. Phys. 23(1984) L843.

[6] M.Akiyama, Y.Kawarada and K.Kaminishi, Extended Abstr. 15th Conf. of Solid State Devices and Materials, Tokyo, 1983 (Business Center for Academic Societies Japan, Tokyo, 1983) p.293.

[7] M.Sugo, A.Yamamoto and M.Yamaguchi, Extended Abstr. 33th Spring Meeting of the Japan Society of Applied Physics and of the Related Societies, Tokyo, April, 1986, 4p-W-3.

[8] J.W.Faust,Jr., *Silicon Carbide A High Temperature Semiconductor* (Pergamon Press, Oxford, 1960) edited by J.R.O'Connor and J.Smiltens, p.403.

[9] M.Henzler and J.Clabes, Proceeding 2nd Int. Conf. on Solid State Sufaces, 1974 Jpn. J. Appl. Phys. Suppl. 2, Pt. 2, 1974.

[10] T.Sakamoto and G.Hashiguchi, Jpn. J. Appl. Phys. 25(1986) L78.

[11] R.Kaplan, Surf. Sci. 93, 145(1980).
[12] R.Fischer, H.Morkoc, D.A.Neumann, H.Zabel, C.Choi, N.Otsuka, M.Longerbone and L.P.Erickson, J. Appl. Phys. 60(1986) 1640.
[13] T.Ueda, S.Nishi, Y.Kawarada, M.Akiyama and K.Kaminishi, Jpn. J. Appl. Phys., 25, (1986) L789.
[14] S.L.Wright, H.Kromer and M.Inada, J. Appl. Phys. 55(1984) 2916.
[15] P.N.Uppal and H.Kroemer, J. Appl. Phys. 58(1985) 2195.
[16] M.Tabe, K.Arai and H.Nakamura, Surf. Sci. 99(1980) L403.
[17] H.Lipson and K.E.Singer, J. Phys. C: Solid State Phys. 7(1974) 12.
[18] P.Delescluse and A.Masson, Surf. Sci. 100(1980) 423.
[19] P.J.Dobson, J.H.Neave and B.A.Joyce, Surf. Sci. 119(1982) L339.
[20] C.Kittel, *Introduction to Solid State Physics*, (Wiley, New York, 1986) 6th ed., Chapter 2.
[21] W.R.Runyan, *Semiconductor Measurements and Instrumentation*, (McGraw-Hill, New York, 1975), p.12.

IV. ELECTRICAL PROPERTIES OF GROWN LAYERS AND IMPURITY DOPING

1. Introduction

In this chapter, electrical properties of undoped 3C-SiC grown on Si are first mentioned. Characterization by Hall measurements, observation of EBIC(electron beam induced current) images and formation of Schottky barriers were carried out. Before the success of growth on Si by the combination of the carbonization and CVD growth, such evaluation of electrical properties was very difficult because of a small size of a crystal.

Acceptor doping of B and Al is also mentioned in this chapter. Since undoped crystals of SiC were usually n-type, acceptor doping was necessary for the fabrication of p-n junctions and active devices. III_b elements such as B, Al and Ga work as acceptors in SiC. Their activation energies in 3C-SiC were obtained by photoluminescence observation as 735[1], 254[2] and 343meV[3] for B, Al and Ga, respectively. The values of these activation energies are rather high. The ionization energies of P and As donors and a B acceptor in Si are 44, 49 and 45meV[4]. A deep activation energy will give rise to rapid increase of carrier concentration by raising temperature. Though Al has the most shallow level as an acceptor in 3C-SiC, doping of Al during CVD growth involves some technical difficulties. Because it does not have any gaseous compounds at room temperature. B has gaseous compounds for examples B_2H_6, BF_3 and BCl_3. In this work B_2H_6 and organic Al was used for p-type doping. Used organic Al's were TMA(trimethyl-aluminum) and TEA(triethyl-aluminum) which are liquid at room temperature. By a bubbling method using H_2 organic Al was introduced. The influence of doping on grown layers and electrical properties of doped layers is mentioned.

Note: In this and the following chapters (100) well oriented Si substrates and Si substrates oriented $n°$ off (100) towards (011)

are called as (100) substrates and $n°$ off substrates, respectively. Where n is 2, 4 or 6.

2. Electrical properties of undoped layers

2-1. Hall measurement

In this section electrical properties of undoped layers on both (100) and off substrates are mentioned. All undoped layers showed n-type conduction in Hall measurements as far as measurements were carried out.

(Grown layers on (100) substrates)

Figure 1 shows the relationship between electron mobilities and electron concentrations of undoped grown layers on (100) substrates. The grown layers contained APD's. Hall measurements were carried out by van der Pauw method. Si substrates were removed by a mixed solution of HNO_3 and HF before the measurement to avoid the errors due to current conduction through the substrates. The maximum electron mobility on (100) substrates was $488cm^2/Vs$ at a carrier concentration of $3.18x10^{16}cm^{-3}$. The thickness of this sample was about 5μm. Though all the samples in Fig.1 were undoped, the carrier concentration changed in the range of 10^{16}-$10^{19}cm^{-3}$. The undoped carrier concentration was usually lower than $2x10^{17}cm^{-3}$. The most probable origin of high carrier concentrations was impurities in H_2 carrier gas. Because, most of the samples which showed very high carrier concentrations were grown without a H_2 purifier. However, sudden increase up to about $1x10^{18}cm^{-3}$ was rarely observed. The origin of this phenomenon is not clear. The lowest resistivity unintentionally obtained was 0.0015Ωcm. This fact means that by an appropriate doping low resistive layers which are necessary for good ohmic contacts are easily obtainable. When a H_2 purifier was used, a typical carrier concentration was in the range of $3x10^{16}$-$2x10^{17}cm^{-3}$.

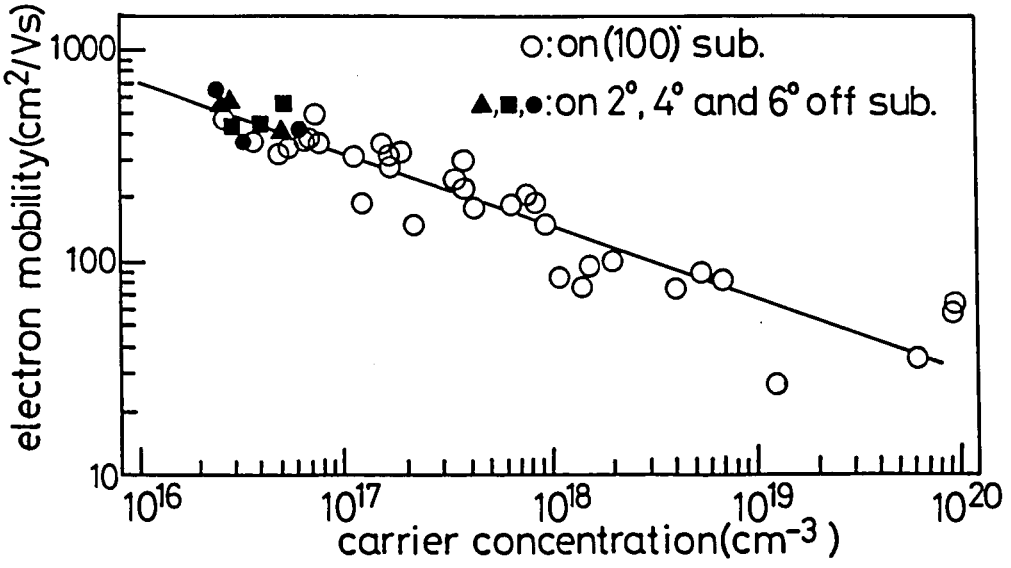

Fig.1 Relationship between electron mobilities and carrier concentrations of undoped grown layers. White circles and solid symbols represent grown layers on (100) and off substrates, respectively.

Recently Suzuki et al.[5] reported that nitrogen was detected by ESR(electron spin resonance) and SIMS(secondary ion mass spectroscopy) measurements for undoped grown layers. The amounts of nitrogen estimated from the ESR measurement were proportional to carrier concentrations. This is a noteworthy report though they added a comment that without a further investigation the residual impurity cannot be asserted to be nitrogen.

(Grown layers on off substrates)

The grown layers on off substrates showed electrical anisotropy, as explained below. In van der Pauw measurement using such a specimens as Fig.2, a value of R is defined by the following formulas.

$$r_{34}=V_{34}/I_{21},\ r_{41}=V_{41}/I_{32}\ , \qquad (1)$$

$$R\equiv r_{34}/r_{41} \text{ or } r_{41}/r_{34} \quad (R>=1)\ , \qquad (2)$$

where V_{mn} and I_{mn} are voltage and current between electrodes m and n(m,n: integer, $1\leqq m,n\leqq 4$). If the sample is exactly square and isotropic and electrodes are located symmetrically, R should be 1.0. When the grown layers on (100) substrates were measured, R was close to 1.0 as long as the samples were nearly square. However, when the grown layers on off substrates were used, the value of R was rather larger than 1.0. Such a result was considered to originate from electrical anisotropy. Based on results of van der Pauw measurement, the relationship between anisotropy and off orientation or wedge-like surface morphology was obtained as shown in Fig.3. When currents flow in parallel to the wedges, the grown layers showed lower resistivity. This direction is defined as the parallel direction. For the perpendicular direction higher resistivity was obtained. van der Pauw method is not suitable for samples with anisotropy. And so the standard Hall measurement was carried out. Bridge type specimens which have a complex shape as shown in Fig.4(a) are usually utilized for the standard Hall measurement. However, thin SiC films whose substrates were removed are too fragile to be cut into such a shape. Therefore, Hall measurements were carried out

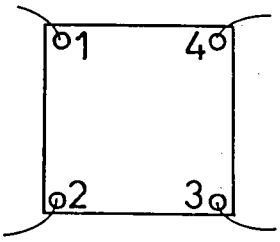

Fig.2 Specimen for van der Pauw measurement.

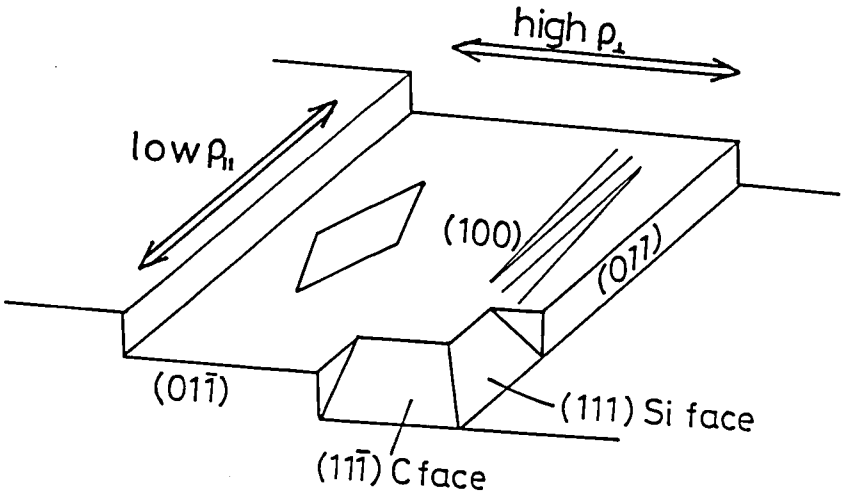

Fig.3 Directional relationship between the electric anisotropy and off orientation of substrates.

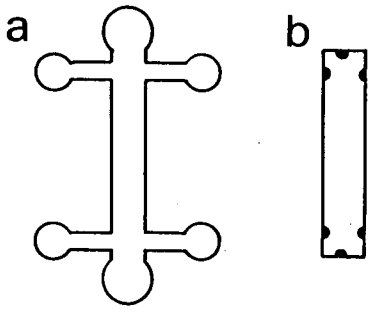

Fig.4 Shapes of specimens for Hall measurement. (a)Standard "bridge-type" and (b)used one for this investigation.

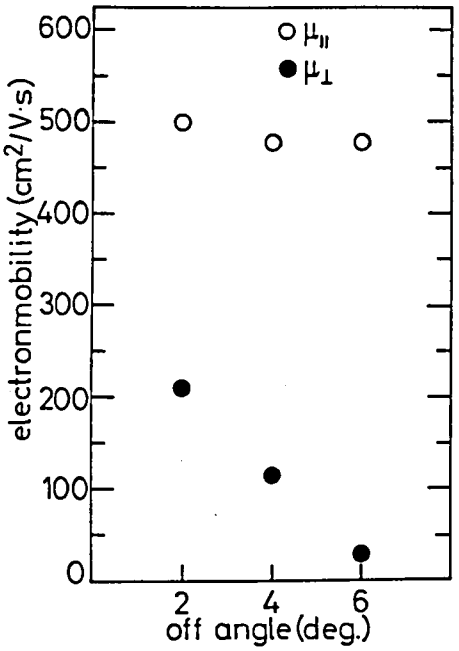

Fig.5 Electron mobility as a function of off angle.

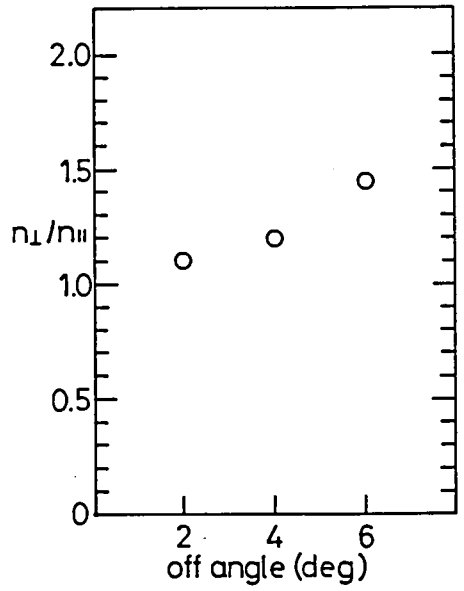

Fig.6 Ratio of $n_{\perp}$ and $n_{\parallel}$ as a function of off angle.

using the specimens which has a shape like Fig.4(b). The grown layers on the 2°, 4° and 6° off substrates were used. The thicknesses of the samples were 8-24μm. Figure 5 shows electron mobilities of the parallel and perpendicular directions. The horizontal axis of Fig.5 represents off angles of substrates. An average value of three samples were used as the electron mobility for each off angle. The electron mobility of the parallel direction($\mu_{\parallel}$) was independent of the off angle and its values were constantly about 500cm^2/Vs. However, the electron mobility of the perpendicular direction($\mu_{\perp}$) reduced as the off angle of the substrates became larger. Even at an off angle of 2°, $\mu_{\perp}$ was about half of $\mu_{\parallel}$. The electron concentrations of these samples were about 3-5x10^{16}cm^{-3}. The obtained maximum electron mobility was 650cm^2/Vs with a carrier concentration of 2.4x10^{16}cm^{-3}. The correlation between $\mu_{\parallel}$ and $n_{\parallel}$ on the off substrates are plotted in Fig.1 by solid symbols. Their correlation was similar to that for (100) substrates. Therefore, the improvement of electron mobility by the elimination of APD's was not observed. $\mu_{\perp}$ and $n_{\perp}$ showed no meaningful correlation. Figure 6 shows the ratio made by $n_{\perp}$ and $n_{\parallel}$. When the off angle was 2°, the ratio was close to 1.0. However, as the off angle increased, the ratio increased. It is not clear whether the observed anisotropy in the carrier concentration was due to some problems in measurements or not. Further characterization using a bridge type specimen shown in Fig.4(a) is expected.

2-2. EBIC observation

EBIC observation was carried out using Au-SiC Schottky barriers. Characteristics of the Schottky barriers are mentioned in the next section. Figures 7(a) and (b) show SEM(scanning electron microscope) and EBIC images of the grown layers on (100) substrates, respectively. The surface of the sample was ethced in molten KOH to visualize APB's as grooves. In the EBIC image of Fig.7(b) a random black and white pattern was observed, which indicates the existence of high-density recombination

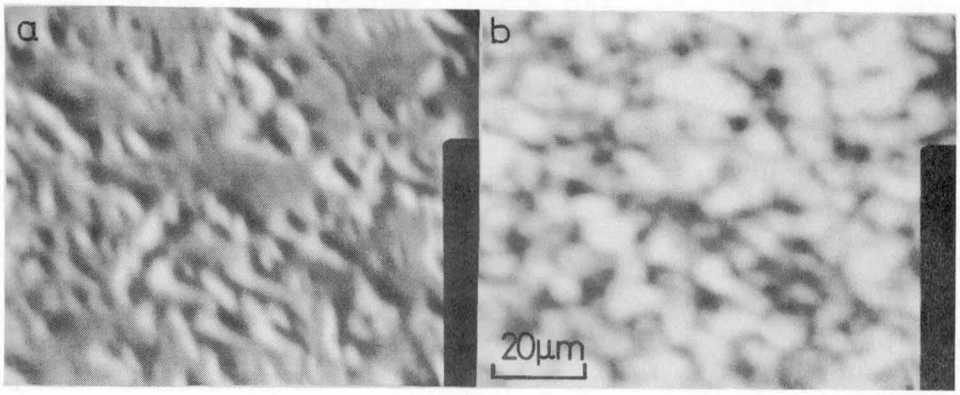

Fig.7 (a)SEM and (b)EBIC images of a grown layer on a (100) substrate. Surface of the sample was etched with molten KOH and APB's are observed as grooves.

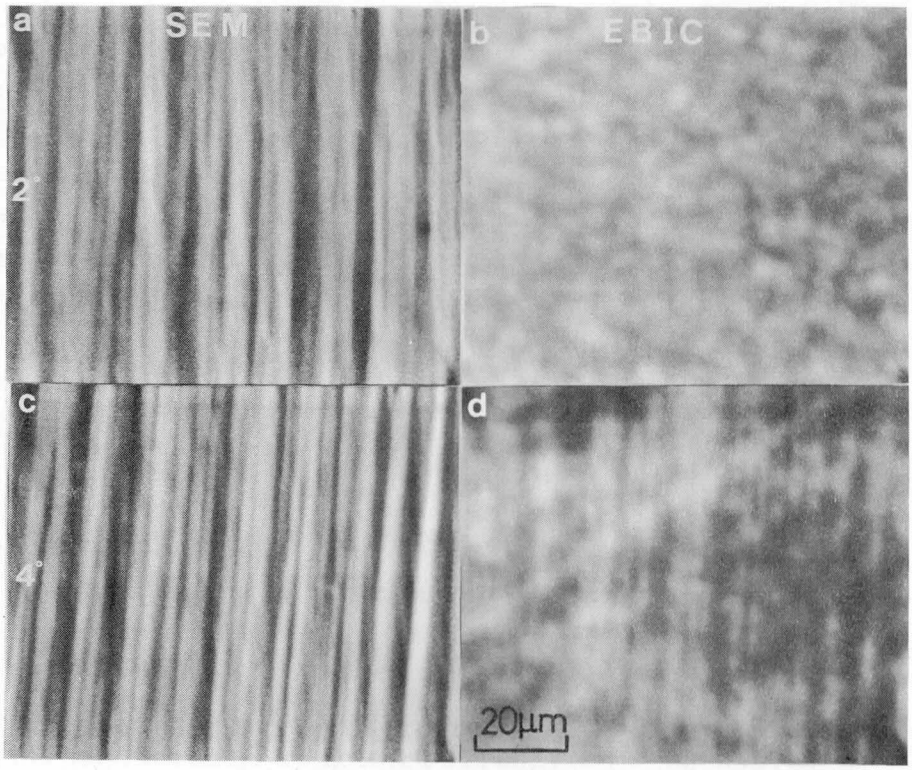

Fig.8 SEM and EBIC images of grown layers on off substrates.

centers. By comparing this EBIC image with its SEM image, the following two features were noticed. (1)The distribution pattern of grooves in the SEM image is similar to that of black lines in the EBIC image. (2)In the EBIC image there are many black parts which have no correspondent grooves in the SEM image. To sum up these two features, there are two types of recombination centers related and unrelated to APB's.

Figures 8(a)-(d) show SEM and EBIC images of the grown layers on the 2° and 4° off substrates. Grown layers on both the 2° and 4° off substrates showed similar surface morphology which consists of wedge patterns. The EBIC images showed different features due to the off angle. The EBIC image for the 2° off substrate in Fig.8(b) showed a random black and white pattern. However, the EBIC image for the 4° off substrate showed black lines in addition to a random pattern. These black lines point the same direction as a wedge-like morphology. The random black and white pattern observed for the 2° off substrates means that there exist recombination centers unrelated to APB. The black lines observed for the 4° off substrates indicate that the introduction of the off orientation with a large off angle gave rise to novel recombination centers. The black lines point the parallel direction defined in the previous section. The recombination centers observed as the black lines are considered to have some relation with the anisotropy mentioned in the previous section. The relationship between the recombination centers observed as the black lines and crystal defects is not clear. To discuss from a crystallographical standpoint characterization to observe crystal defects e.g. TEM (transmission electron microscope) should be utilized.

2-3. Schottky barrier

Au is the most popular metal to form Schottky barriers with n-type SiC. For 6H-SiC the barrier height of Au-SiC was obtained to be 1.40±0.05V by Wu and Campbell[6]. In this section characteristics of Schottky barriers of undoped n-type 3C-SiC

fabricated with Au are mentioned.

Before vacuum evaporation of Au, samples were cleaned in organic solvent, acids, deionized water and a 20% hot solution of K_2CO_3. Cleaning in this hot solution was introduced by Suhara, and it was confirmed to be effective for the improvement of current voltage(I-V) characteristics of Schottky barriers[7].

Figure 9 shows an example of I-V characteristics of a Schottky diode fabricated with a grown layer on a (100) substrate. Figure 10 shows its log$I$-V plotting. Grown layers on 2° off substrates showed no meaningful differences in characteristics of Schottky barriers. The breakdown voltage of the fabricated diodes was at most about -5V and they showed "soft" breakdown. About the breakdown discussion is given afterwards.

In log$I$-V plotting an ideal factor n and a saturation current density J_0 are obtained. Using them I-V characteristics of a Schottky barrier is given as follows[8].

$$J=J_0(\exp(qV/nkT)-1) , \qquad (3)$$

where J is current density, q elemental charge, V applied voltage, k Boltzmann constant and T absolute temperature. Though n should be 1.0 ideally, n is greater than 1.0 for real Schottky barriers. Using the value of J_0 the barrier height can be estimated[8]. However, J_0 showed wide variation in this investigation. Fundamentally the barrier height should be peculiar to the combination of a metal and a semiconductor and J_0 should not change. The values of n also showed wide variation. The smallest value of n was 1.27 and it was usually greater than 1.4. When the n value was close to the ideal value of 1.0, J_0 was relatively small. Therefore, some excess currents were considered to make J_0 larger. Since the introduction of guard rings showed no meaningful reduction of the current, surface leakage current was not a main factor of the excess currents. The barrier height estimated by capacitance-voltage characteristics also changed randomly. Photoelectric measurement[8] was attempted to estimate the barrier height. The obtained value for Au-SiC Schottky barriers by this method was 1.02eV. Yoshida et al.[9] reported a

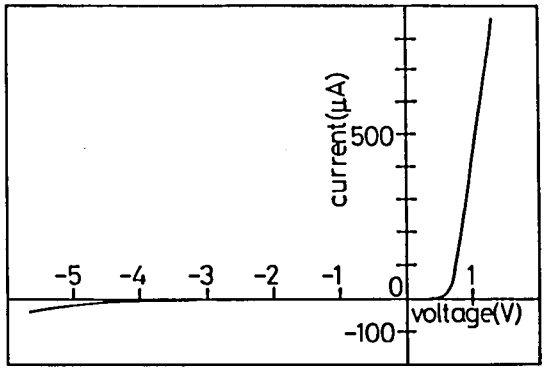

Fig.9 Current-voltage characteristics of a Au-3C-SiC Schottky diode.

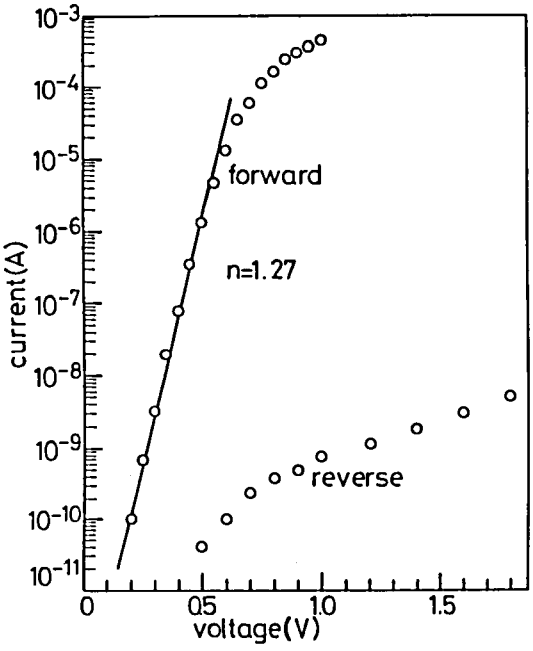

Fig.10 Log*I-V* plotting of current-voltage characteristics of a Au-3C-SiC Schottky diode.

value of 1.11eV by the same method. Schottky barriers were also fabricated using refractory metals such as Pt, Pd, Mo and W. The Schottky barriers with Pd showed comparable rectification to those fabricated with Au. Others were inferior in reproducibility. The barrier height of Pd-SiC measured by a photoelectric method was also 1.02eV.

No one reported about breakdown electric field in 3C-SiC up to now. Breakdown in Schottky diodes can be treated similar to a p^+n junction diode. Sze and Gibbsons[10] empirically achieved the following relationship between bandgap energy E_g and breakdown voltage V_b in one-sided p^+n and n^+p abrupt junctions.

$$V_B=60(E_g/1.1)^{3/2}(N_b/10^{16})^{-3/4} \quad (V) , \qquad (4)$$

where N_b is back ground impurity concentration. The maximum field E_m in a depletion layer is given as follows.

$$E_m= \left(\frac{2qN_b(V_B+V_d)}{\varepsilon_s}\right)^{1/2} \simeq \left(\frac{2qN_bV_B}{\varepsilon_s}\right)^{1/2} , \qquad (5)$$

where V_d is built-in potential and ε_s permittivity of a semiconductor. Since V_d is smaller than about 1V, it can be neglected for preliminary estimation. V_B and E_m were calculated as a function of N_b for 6H-SiC, 3C-SiC, GaAs, Si and Ge as shown in Figs.11(a) and (b). V_B and E_m obtained by Glover[11] using 6H-SiC Schottky diodes fabricated with Au were in accord with the Sze and Gibbsons's prediction. von Muench and Pfaffeneder[12] obtained higher E_m in one-sided p-n^+ junction diodes of 6H-SiC. In the case of 3C-SiC, V_B was calculated to be 30V for N_b of $1x10^{17}cm^{-3}$ and 60V for $4x10^{16}cm^{-3}$. A typical breakdown voltage of 4-5V was very small compared with these calculated values. There are many considerable origins of lowering the breakdown voltage such as tunneling[13], surface leakage, partial field enhancement, inappropriate surface treatment and crystal defects. Concerning these origins discussions are carried out one by one below. When the carrier concentration is very high and a depletion layer is very thin, tunneling takes place very easily. However, in the case of this investigation the carrier concentrations of most samples were lower than $1x10^{17}cm^{-3}$, and this value is not so high as tunneling conduction occurs. Since

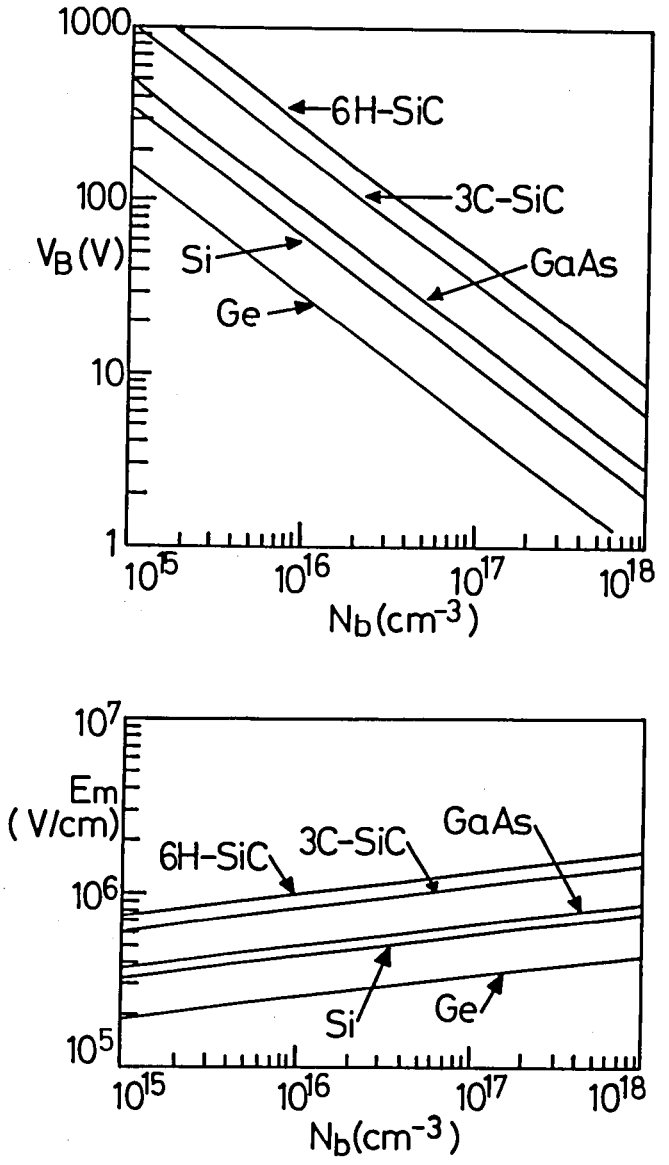

Fig.11 Predicted (a)breakdown voltage V_B and (b)maximum field E_m for onesided abrupt p-n junctions as a function of a background impurity concentration N_b. Used formulas were given by Sze and Gibbsons[10].

the reduction of the current due to the introduction of a guard electrode was very slight, surface leakage current was negligible. Surface roughness shown in the previous chapters can be an origin of partial field enhancement in Schottky barriers. However, there is no idea concerning how the breakdown voltage is really affected by the surface roughness. 3C-SiC is cleaned in a hot solution of K_2CO_3 before vacuum evaporation of Au in the current fabrication process. Suhara[7] reported that by the introduction of this cleaning an improvement of I-V characteristics in the forward biased region was observed as a reduction of the n value and saturated current density of J_0. And Suzuki[14] reported that samples without this cleaning sometimes showed very poor rectification. Thus, surface treatment seems very important for fabrication of Schottky barriers and some other cleaning or etching methods had better be attempted to improve their characteristics. As mentioned in Chapter II, 3C-SiC layers grown on Si substrates contains crystal defects, and the reduction of defect density due to the increase of the film thickness was observed. Schottky barrier diodes fabricated with grown layers with a thickness thinner than 1μm often showed very worse rectification. This result is considered to mean that characteristics of Schottky barriers are severely affected by defect density.

To sum up these discussion, there is no conclusive evidence for the low breakdown voltage, however, some following matters are probably effective to increase the breakdown voltage such as the improvement of surface flatness, a new surface treatment method and decrease of crystal defects.

3. B and Al doping

3-1 B-doping

Figures 12(a)-(c) show a variation of surface morphology due to the increase of a flow rate of B_2H_6 on (100) substrates. As

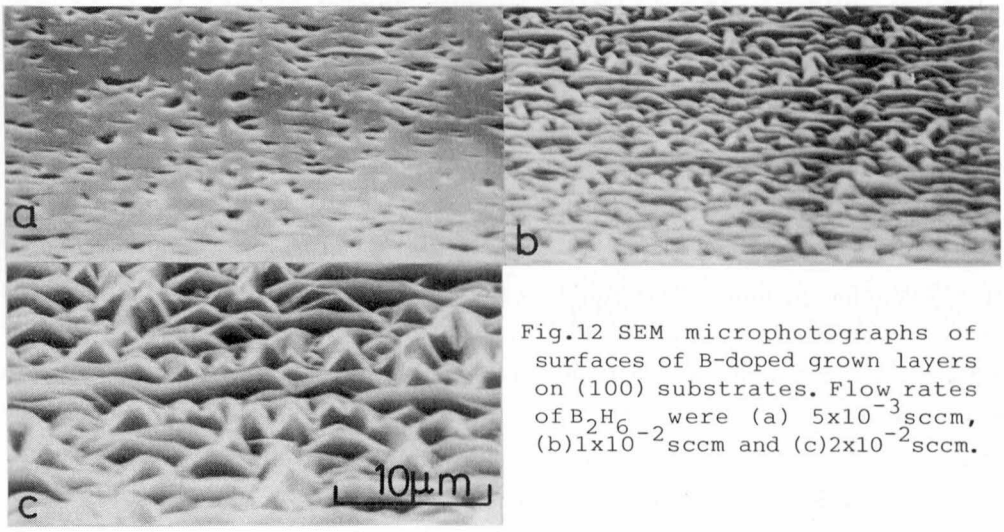

Fig.12 SEM microphotographs of surfaces of B-doped grown layers on (100) substrates. Flow rates of B_2H_6 were (a) $5x10^{-3}$sccm, (b)$1x10^{-2}$sccm and (c)$2x10^{-2}$sccm.

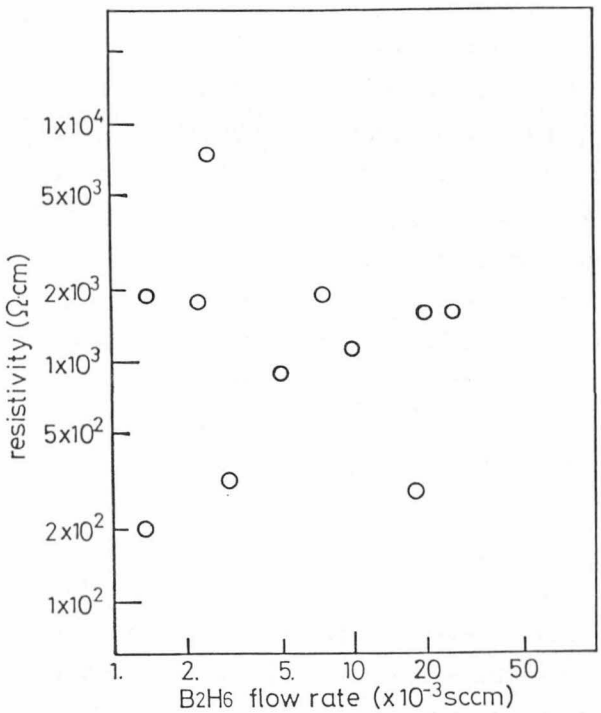

Fig.13 Resistivity of B-doped grown layers as a function of a flow rate of B_2H_6.

the flow rate increased surface roughness increased. When the flow rate of B_2H_6 was smaller than about $4x10^{-3}$sccm, flatness of the surface was comparable to that of the undoped layers. Figure 13 shows resistivities of the grown layers as a function of a B_2H_6 flow rate. When the flow rate of B_2H_6 was greater than about $1x10^{-3}$sccm, most of the grown layers showed resistivity higher than 200Ωcm. The highest resistivity was $8x10^{3}$Ωcm. By van der Pauw measurement of the grown layer for a flow rate of B_2H_6 of $4x10^{-3}$sccm, the resistivity, carrier concentration and hole mobility were obtained to be 320Ωcm, $1.1x10^{15}cm^{-3}$ and $18cm^2/Vs$, respectively. P-type conduction was confirmed at the same time. However, Al-Si electrodes which are usually used for p-type SiC mostly did not show good ohmic characteristics and Hall measurements by van der Pauw method was impossible and the values of the carrier concentration and hole mobility were not clear.

Thus by B-doping high resistive p-layers were obtained. If the high resistivity of the B-doped layer is maintained even at high temperatures, it is useful for device applications. However, rapid reduction of the resistivity was observed by heating as shown in Fig.14. The rapid reduction of the resistivity was due to a rapid increase of the carrier concentration. The carrier concentration was $8.6x10^{14}cm^{-3}$ at 25°C and it increased to $5.8x10^{16}cm^{-3}$ at 130°C as shown in Fig.15. Such a rapid change of electrical characteristics is due to a large activation energy of a B acceptor. Using the measured temperature dependence of the carrier concentration in Fig.15, the activation energy was estimated to be 413meV. This value is smaller than that of 735meV obtained by photoluminescence measurements[15]. Though further investigation is necessary to obtain an exact activation energy, there is no doubt that its value is extraordinary large.

3-2. Al-doping

For Al doping TEA and TMA were used. Figure 16 shows the relationship between their vapor pressure and temperatures. Since TEA has low vapor pressure at room temperature a vessel of TEA

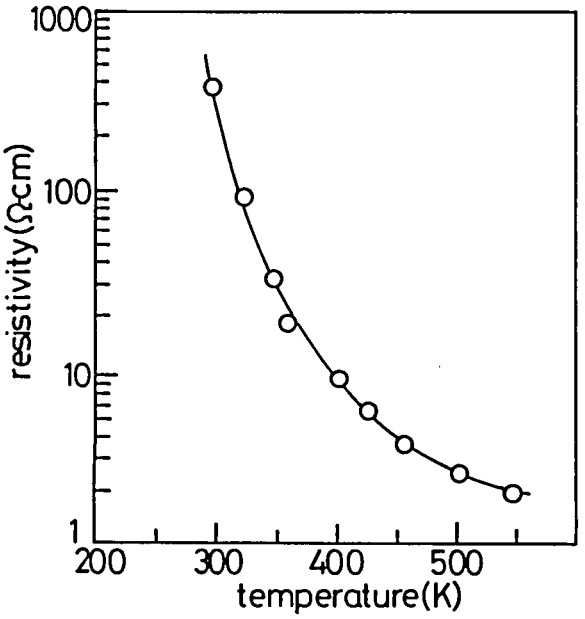

Fig.14 Temperature dependence of resistivity of a B-doped grown layer.

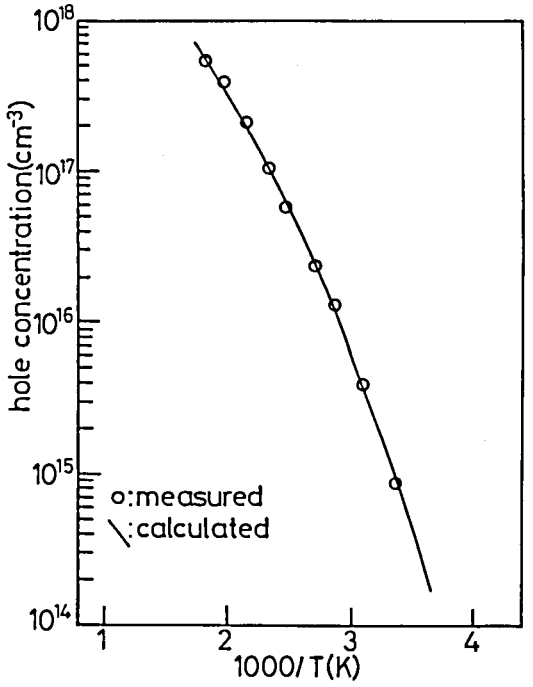

Fig.15 Temperature dependence of hole concentration of a B-doped grown layer.

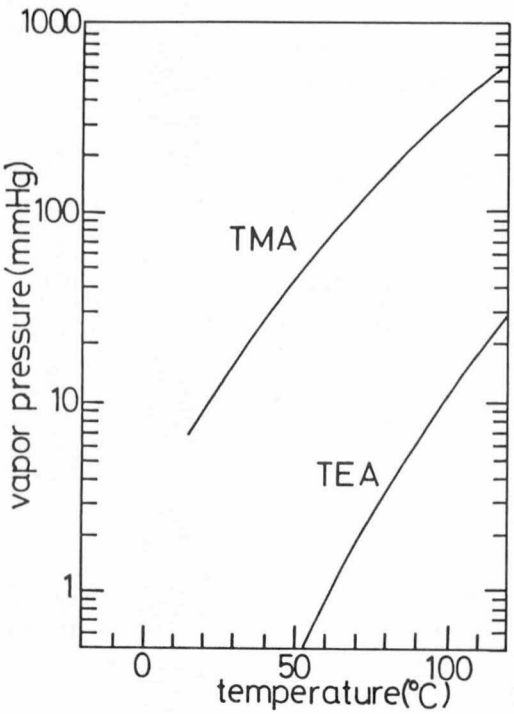

Fig.16 Vapor pressures of TMA and TEA as a function of temperature.

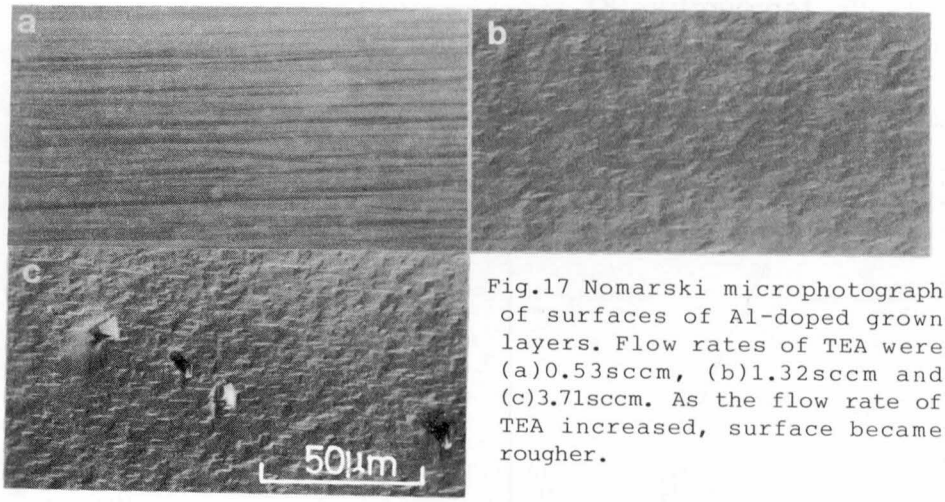

Fig.17 Nomarski microphotograph of surfaces of Al-doped grown layers. Flow rates of TEA were (a)0.53sccm, (b)1.32sccm and (c)3.71sccm. As the flow rate of TEA increased, surface became rougher.

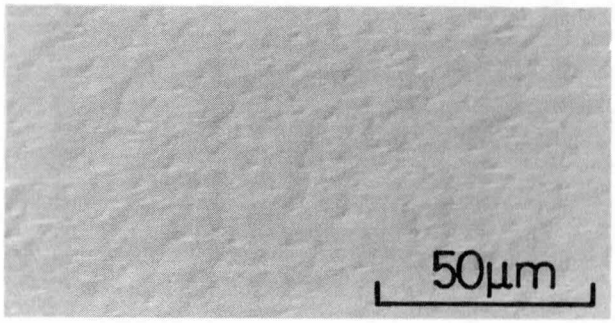

Fig.18 By the reduction of C_3H_8 flow rate during Al-doping, surface flatness was improved. Flow rate of TEA was 1.95sccm. The flow rate of C_3H_8 was reduced from 0.32 to 0.15sccm.

was heated in the range of 62-120°C. The flow rate of TEA was controlled by changing both the temperature of the vessel and the flow rate of bubbling H_2. To avoid liquefaction on the way to a reaction tube, stainless tubes between the vessels and the reaction tube were also heated. However, liquefaction was not prevented perfectly. To keep controlability of the TEA flow rate long-time evacuation was sometimes necessary. The maximum flow rate of H_2 for bubbling was 100sccm in this investigation. The combination of the low vessel temperature and the higher flow rate of bubbling H_2 is probably preferable to prevent such a problem. If bubbling is carried out by a carrier gas, the temperature of the vessel is able to be kept below 60°C. Since TMA has large enough vapor pressure at room temperature, the temperature of the vessel was maintained at 20°C and the flow rate of TMA was controlled by changing the flow rate of bubbling H_2.

Figures 17(a)-(c) show a variation of surface morphology of Al-doped layers on 2° off substrates due to the change of the TEA flow rate. Grown layers doped with TMA showed similar results. When the flow rate of TEA was 0.53sccm the surface morphology was comparable to undoped layers. As the flow rate of TEA increased, surface roughness increased and needle-like growth appeared as shown in Figs.17(b) and (c). The observed variation of the surface morphology due to doping with organic Al was similar to the variation caused by the increase of a carbon source. In the case of the sample of Fig.17(b) the flow rates of C_3H_8 and TEA were 0.32sccm and 1.95sccm, respectively. The amount of introduced carbon atoms by TEA was about 18 times larger than that by C_3H_8. TEA was considered to work as a carbon source. The flow rate of C_3H_8 was reduced to 0.15sccm. The surface flatness recovered and needle-like growth disappeared as shown in Fig.18. This variation of the surface morphology supports that TEA works as a carbon source. Further reduction of the C_3H_8 flow rate resulted in rough surfaces again. Figure 19 shows an example of the relationships between electrical properties and the flow rate of organic Al. Electrical properties were evaluated by van der

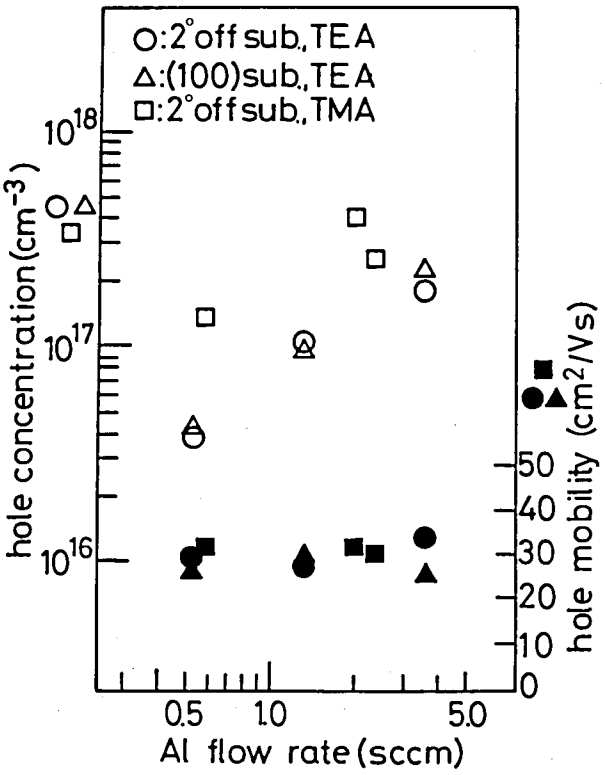

Fig.19 Hole concentration and mobility as a function of a flow rate of organic aluminum.

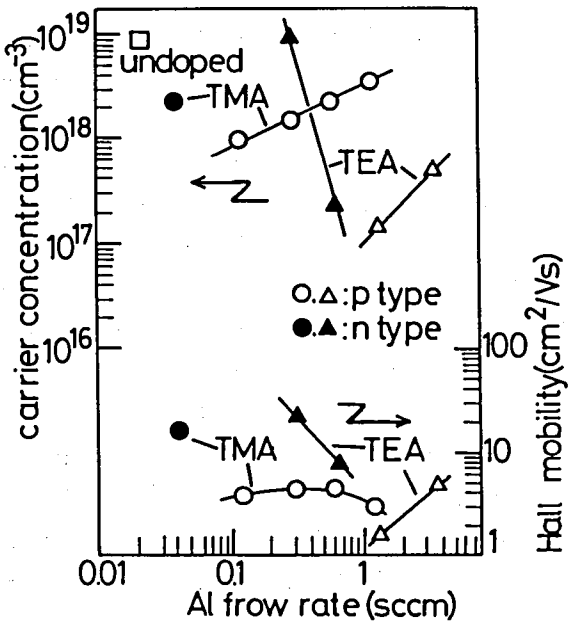

Fig.20 Carrier concentration and mobility as a function of flow rate of organic aluminum. The samples were grown under the condition of unusually high undoped carrier concentration. See text.

Pauw measurement. The grown layers were three types; i.e. grown layers on (100) and 2° off substrates doped with TEA and on 2° off substrates doped with TMA. P-type conduction was confirmed. The obtained hole concentrations were $4x10^{16}$-$6x10^{17}cm^{-3}$. The hole mobility was about $30cm^2/Vs$. When the undoped carrier concentration was very high($n \geq 10^{19}cm^{-3}$), the obtained hole concentration was also high as shown in Fig.20. The highest hole concentration of $4x10^{18}cm^{-3}$ was obtained at a TMA flow rate of 1.2sccm.

TEA-doped grown layers on (100) and 2° off substrates showed no meaningful differences in electrical properties as shown in Fig.19 different from undoped layers. The undoped layers on off substrates outwardly showed low electron mobility and low carrier concentration by van der Pauw measurement because of anisotropy. To clarify whether this result of Al-doped layers is due to the absence of anisotropy or not, Hall measurements as mentioned in Section 2-1 should be attempted. The *R* value which is nearly 1 for square and isotropic samples could not be utilized in this case. Because Al-doped layers were fragile and square samples were very difficult to prepare.

P-n junction diodes were fabricated. On n-type 2° off substrates, undoped and Al-doped layers were grown successively. Details of growth conditions are listed in Table 1. Mesa structures were formed using an Al mask by RIE(reactive ion etching) of CF_4 and O_2[16]. An example of *I-V* characteristics is shown in Fig.21. Rectification was not good. To improve characteristics an optimization of growth conditions and fabrication processes is probably necessary.

As mentioned before, organic Al simultaneously works as a dopant and a carbon source. Though the influence of organic Al could be reduced by decreasing the flow rate of C_3H_8, to improve controlability other Al-sources which contain less carbon are desirable. Nishino et al. used $AlCl_3$ as an Al source for CVD growth of 6H-SiC[15]. However, the flow rate control of $AlCl_3$ was difficult, because it is solid at room temperature and heating at temperatures above 200°C was necessary to obtain large enough

sub.: Si(100) 2° off
1st layer: undoped 6.6μm
2nd layer: TMA 0.04sccm, 1.6μm
3rd layer: TMA 0.36sccm, 0.2μm

SiH_4: 0.3sccm, C_3H_8: 0.27sccm

Table 1 Growth conditions of a p-n junction.

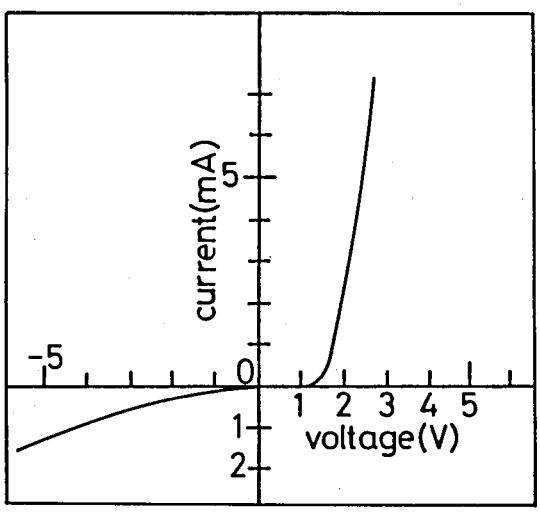

Fig.21 Current-voltage characteristics of a fabricated p-n junction diode.

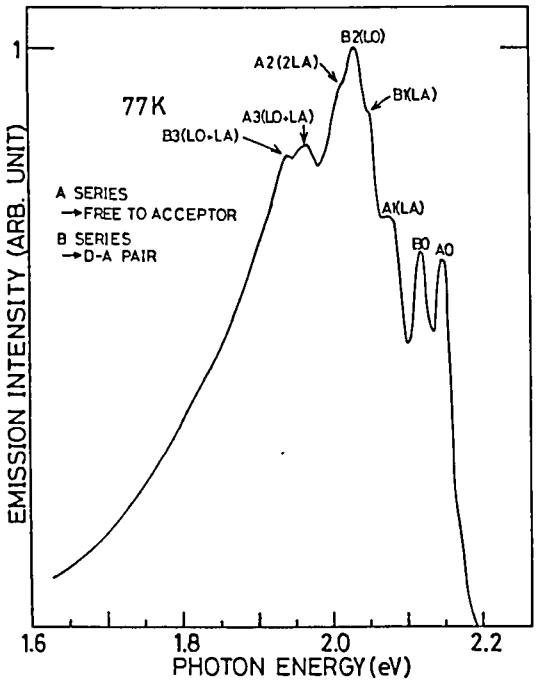

Fig.22 Typical photoluminescence spectrum of Al-doped grown layers.

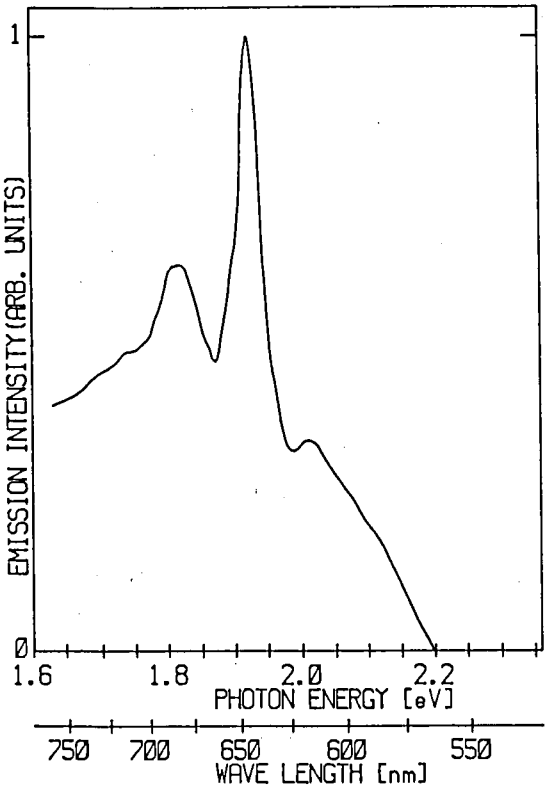

Fig.23 Photoluminescence spectrum of a undoped grown layer. Na was detected by SIMS analysis of this sample.

vapor pressure by sublimation. Moreover, $AlCl_3$ is deliquescence. Its merit is stability. Organic Al reacts with water and oxygen in flames and it is toxic. By considering these factors, $(CH_3)AlCl_2$ is interesting as a candidate of a dopant which takes the places of TEA and TMA. $(CH_3)AlCl_2$ is a white solid at room temperature and the melting and boiling points are 73°C and 152°C, respectively. The vapor pressure at 100°C is 100mmHg. This value is comparable to that of TMA at about 70°C. Its reactivity with water and oxygen is lower than TMA and TEA. Thus, it satisfies conditions necessary for new chemicals which take the places of TEA and TMA. An investigation of Al doping using $(CH_3)AlCl_2$ is expected.

4. Photoluminescence

SiC has an indirect band structure. In photoluminescence observation, light emission related to acceptors is mainly observed. In other words, to observe photoluminescence acceptor doping is sometimes necessary. In this work, Al-doping was carried out using TMA and TEA. Figure 22 shows an example of a photoluminescence spectrum of the Al-doped grown layer. A similar spectrum to Al-doped crystals prepared by a solution growth method[2] was obtained. Many peaks originated from two types of mechanisms were observed. A peak which has the highest energy and that at the second highest energy are due to free-to-bound acceptor recombination and donor-acceptor(N and Al) pair recombination, respectively. Their phonon-replicas were observed in the lower energy side. The intensity of the photoluminescence dropped as the the flow rate of organic Al increased. Doped Al or excessively supplied carbon by organic Al were considered to give rise to the drop in the intensity. There are three probable mechanisms of the drop in the intensity such as deterioration of crystallinity, generation of deep levels and change in recombination process.

Some undoped layers showed orange or red luminescence. Two

types of spectra were observed. Al was detected by the SIMS analysis of the samples which showed similar spectra to Fig.22. Some other samples showed similar spectra to Fig.23. Na was detected by the SIMS analysis for such a sample. A susceptor is one of the most likely candidates for a source of such metal impurities.

5. Summary

All undoped layers showed n-type conduction in Hall measurements. The highest electron mobility for the grown layers containing APD's on (100) substrates was $488cm^2/Vs$ with a carrier concentration of $3.18x10^{16}cm^{-3}$. Undoped carrier concentrations were usually in the range of $3x10^{16}$-$2x10^{17}cm^{-3}$. The grown layers on off substrates showed electrical anisotropy. $\mu_{\parallel}$ was about $500cm^2/Vs$ independent of off angle. $\mu_{\perp}$ decreased as the off angle became larger. Breakdown voltages of Au-SiC Schottky barriers were low compared with theoretically predicted values, and the breakdown was "soft". Improperness of surface treatment, surface roughness and crystal defects are probable origins of such breakdown problems.

To obtain p-layers B and Al were doped using B_2H_6 and organic Al, respectively. B-doped layers showed high resistive p-type conduction at room temperature. Organic Al worked simultaneously as both a dopant and a carbon source. The hole concentration was controlled in the range of $4x10^{16}$-$6x10^{17}cm^{-3}$ by changing a flow rate of organic Al. A typical hole mobility in Al-doped layers was about $30cm^2/Vs$.

References

[1] H.Kuwabara and S.Yamada, Phys. Status Solidi a 30(1975) 739.
[2] A.Suzuki, H.Matsunami and T.Tanaka, J. Electrochem. Soc. 124(1977) 241.

[3] H.Kuwabara, K.Yamanaka and S.Yamada, Phys. Status Solidi a 37(1976) K157.
[4] N.Mikoshiba, *Handoutai no Butsuri(Physics of Semiconductors)*, (Baifuukan, Tokyo, 1982), p.103, in Japanese.
[5] A.Suzuki, A.Uemoto, K.Furukawa, Y.Fujii, M.Shigeta and S.Nakajima, 48th Autumn Meeting of the Japan Society of Applied Physics, Nagoya, October, 1987, 17p-ZG-14.
[6] S.Y.Wu and R.B.Campbell, Solid State Electron. 17(1974) 683.
[7] H.Suhara, Master Thesis, Faculty of Engineering, Kyoto University, 1983.
[8] S.M.Sze, *Physics of Semiconductor Devices*, (Wiley, New York, 1981) 2nd ed., Chapter 5.
[9] S.M.Sze and G.Gibbsons, Appl. Phys. lett. 8(1966) 111.
[10] S.Yoshida, K.Sasaki, E.Sakuma, S.Misawa and S.Gonda, Appl. Phys. Lett. 46(1985) 766.
[11] G.H.Glover, J. Appl. phys. 46(1975) 4842.
[12] W. von Muench and I.Pfaffeneder, J. Appl. Phys. 48(1977) 4831.
[13] A.G.Chynoweth, W.L.Feldmann, C.A.Lee, R.A.Logan, G.L.Pearson and P.Aigrain, Phys. Rev. 118(1960) 425.
[14] A.Suzuki, private communication(1986).
[15] S.Nishino, A.Ibaraki, H.Matsunami and T.Tanaka, Jpn. J. Appl. Phys. 19(1980) L353.
[16] S.Dohmae, K.Shibahara, S.Nishino and H.Matsunami, Jpn. J. Appl. Phys. 24(1985) L873.

V. ION IMPLANTATION INTO 3C-SiC GROWN LAYERS AND APPLICATION TO MOSFET'S

1. Introduction

A selective doping technique is indispensable in fabrication of electronic devices especially for IC(integrated circuits). There are two major techniques for selective doping, namely, diffusion and ion implantation methods. Both methods are popular for a Si process. However, in the case of SiC the diffusion method is hard to apply, because the diffusion coefficients of impurities in SiC are very low. Campbel and Chang fabricated junction-gate FET's of α-SiC using a diffusion technique[1]. They reported that diffusion of Al into α-SiC required temperatures from 1800°C to 2100°C. Moreover, a special masking technique utilizing SiC was necessary. Thus, the diffusion method seems to be not practical for SiC. Ion implantation into α-SiC was attempted by many investigators[2-6]. Marsh investigated the activation of implanted impurities using various dopants[2]. Though the implantation of donor impurities such as N, P, Sb and Bi was successful, samples implanted with acceptors were high resistive even after annealing and the acceptors could not be activated. They explained that deep donor-type defects induced by the implantation prevented the activation of the implanted acceptors. Concerning 3C-SiC Kalinina et al.[7] reported a successful fabrication of p-n junction diodes by implantation of Al, however, they did not describe details of investigation. Though Kondo et al.[8] attempted hot implantation(specimens were intentionally heated during implantation) in addition to the standard implantation, the activation was unsuccessful. Edmond et al.[9] reported successful fabrication of p-n junction diodes by hot implantation of Al into undoped layers without annealing. The crystal growth methods of these two groups are similar to that of this investigation. The difference in their investigations is not clear.

In this investigation, implantation of N_2^+ and P^+ was attempted. The electrical characteristics of implanted layers were evaluated changing annealing temperatures. Planar-type p-n junction diodes were fabricated using the implantation technique.

The first successful fabrication of n-channel inversion-type MOSFET's is mentioned. The MOSFET's were fabricated by the combination of ion implantation and thermal oxidation techniques which are ordinary in the Si process.

2. Activation of implanted donors

Ion implantation of N_2^+ and P^+ was carried out into B-doped grown layers. High resistive($\rho \geqq 200\Omega$cm) B-doped layers were suitable for characterization of thin n^+ layers formed by implantation of donors. The thickness of the B-doped grown layers was about 6μm. APD-free grown layers on 2° off substrates were used. Samples were tilted at 7° during the implantation to avoid a channeling effect. The current density of an ion beam was lower than $0.25\mu A/cm^2$. Therefore, heating by the beam during the implantation was negligible[10].

The conditions of the ion implantation were listed in Table 1. The implantation was carried out by successive two steps to improve the uniformity of implanted impurities. The first implantation was high dose with high energy and the second was low dose with low energy. Figure 1 shows a calculated profile of implanted P using the projected average range and projected standard deviation in the literatures[11-13] for a total dose of $1.3\times10^{15}cm^{-2}$(condition 1 in Table 1). In the case of condition 2, the total dose was decreased to 30% of that in condition 1 with the same energy. N_2^+ implantation with a total dose of $1.95\times10^{14}cm^{-2}$(condition 3) corresponds to N^+ implantation with a dose of $3.9\times10^{14}cm^{-2}$ which is the same dose level as condition 2. The energy of the N_2^+ implantation was decided to have the nearly same impurity profile[13] as in P^+ implantation of condition 2. After the implantation samples were annealed in

No.	implanted ion	1st dose(cm^{-2}) 2nd	1st energy(eV) 2nd	total dose (cm^{-2})
1	P^+	$1x10^{15}$ $3x10^{14}$	100K 25K	$1.3x10^{15}$
2	P^+	$3x10^{14}$ $9x10^{13}$	100K 25K	$3.9x10^{14}$
3	N_2^+	$1.5x10^{14}$ $4.5x10^{13}$	100K 25K	$1.95x10^{14}$

Table 1 Conditions of ion implantation.

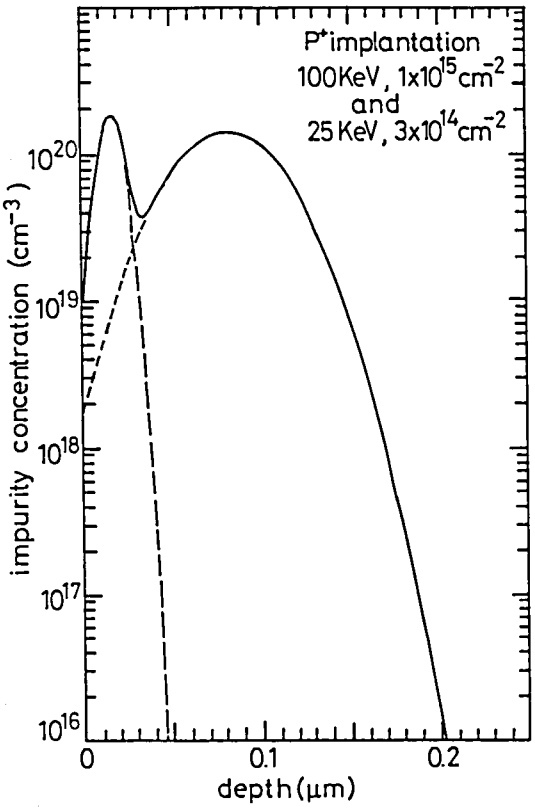

Fig.1 Calculated profile of implanted P with a total dose of $1.3x10^{15}cm^{-2}$. Details of conditions of implantaion are listed in Table 1.

Ar atmosphere for 30min. The samples were heated by RF inductive heating. By SIMS analysis the annealed specimen showed almost the same depth profile of implanted P as that without annealing by SIMS analysis.

Figure 2(a) shows a RHEED halo pattern of an as-implanted sample. The ion implantation was carried out under condition 1(P^+, total dose: $1.3\times10^{15}cm^{-2}$). The halo pattern indicates that the implanted layer was amorphous. Figure 2(b) shows a RHEED pattern of the sample after annealing at 800°C. Recrystallization to a single crystal was clearly observed. Annealing temperature was changed up to 1300°C. However, no significant difference in RHEED patterns compared with Fig.2(b) was observed. Samples implanted under condition 2(P^+, total dose: $3.9\times10^{14}cm^{-2}$) showed similar results. The implanted samples could be told from not implanted samples with naked eyes by noticing a slight difference in colors. The refractive index of the implanted layers changed by amorphization and interference took place. The difference in colors vanished by annealing.

Sheet resistance of the implanted layers was evaluated by the four-point probe method or by van der Pauw method. Si substrates of the specimens for van der Pauw measurement were removed by a mixed solution of HNO_3 and HF before the measurement to avoid errors due to current conduction through the substrates. N-type conduction was confirmed for both the P^+ and N_2^+ implanted layers by van der Pauw method. As shown in Fig.3, the sheet resistance monotonously decreased as annealing temperature increased and it reached to about $10^3\Omega/\square$ by annealing at about 1350°C.

Electrical activation rates were estimated by van der Pauw measurement. The electrical activation rate was defined as the ratio of sheet carrier concentration and total dose. The electrical activation rates were improved by raising annealing temperatures as shown in Fig.4. The P^+ implanted layer with a total dose of $3.9\times10^{14}cm^{-2}$(condition 2) gave the higher electrical activation rates than those for a total dose of $1.3\times10^{15}cm^{-2}$(condition 1). The N_2^+ implanted layers gave the

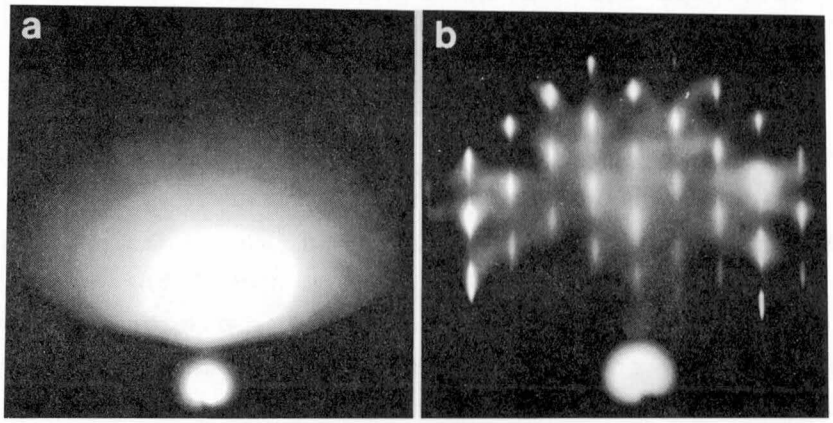

Fig.2 RHEED patterns of P^+ implanted layers. (a)Before and (b)after annealing at 800°C.

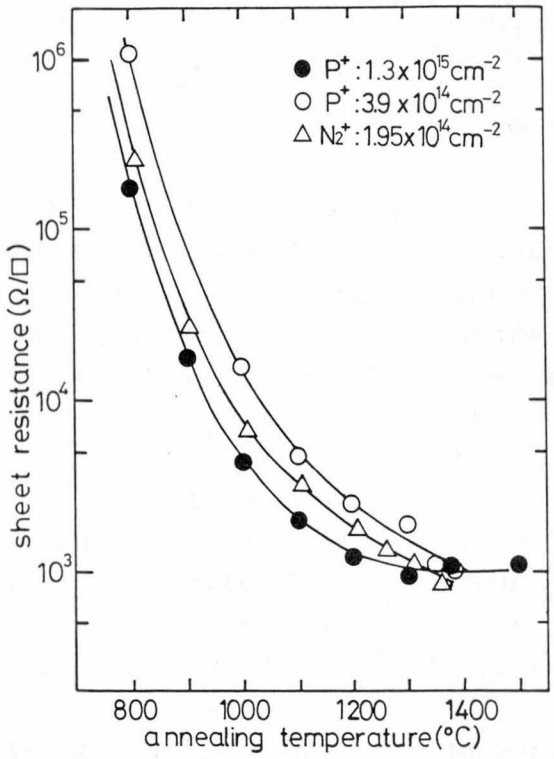

Fig.3 Sheet resistance of implanted layers as a function of annealing temperatures.

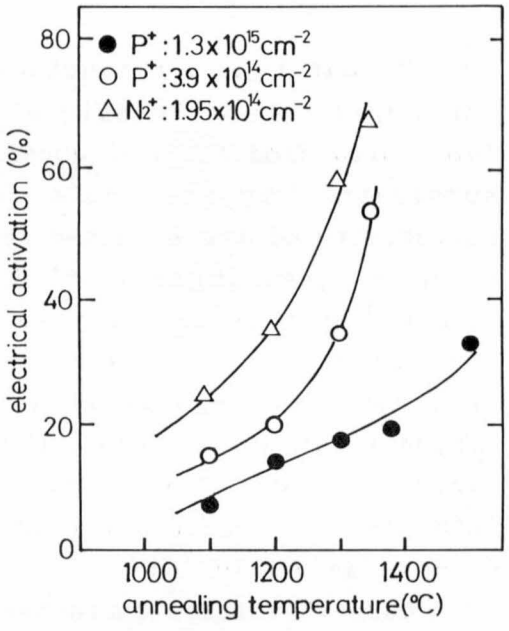

Fig.4 Electrical activation rate as a function of annealing temperatures.

higher electrical activation rates than the P^+ implanted layers, which is similar to implantation into 6H-SiC[2]. Bridge-type specimens were fabricated by the P^+ implantation to carry out the standard Hall measurement and to investigate electrical anisotropy in the implanted layers. Such specimens were fabricated by a selective implantation utilizing a deposited SiO_2 film as a mask. The implantation was carried out under condition 2. Concerning conditions 1 and 3 the standard Hall measurement was not carried out yet. The electrical activation rates obtained by the standard Hall measurement well agreed with those obtained by van der Pauw measurement. The electron mobility obtained by van der Pauw method was about $30cm^2/Vs$ in all cases. The electron mobility obtained by the standard Hall measurement showed electrical anisotropy similar to the undoped grown layers. $\mu_{\parallel}$ and $\mu_{\perp}$ were about 50 and $25cm^2/Vs$, respectively.

3. Fabrication of p-n junction diode

Planar-type p-n junction diodes were fabricated using the ion implantation technique. Figure 5 shows the structure of fabricated diodes. An Al-doped p-layer was grown on a 2° off p-Si substrate. Typical hole concentration, hole mobility and resistivity of the Al-doped layer were $3.5x10^{17}cm^{-3}$, $32cm^2/Vs$ and $0.56\Omega cm$, respectively. P^+ implantation with a total dose of $3.9x10^{14}cm^{-2}$ or N_2^+ with a total dose of $1.95x10^{14}cm^{-2}$ was carried out to obtain n-layers. Deposited SiO_2 of 500nm in thickness was used as a mask for the implantation. Annealing temperatures were 1100°C, 1200°C and 1300°C. Annealing time was fixed at 30 min. Finally ohmic contacts were formed using Al and AuGa for n-SiC and p-Si, respectively. The area of the fabricated diodes was $7.1x10^{-4}cm^2$.

Current-voltage characteristics of the P^+ and N_2^+ implanted diodes were shown in Figs.6(a) and (b), respectively. Both the P^+ and N_2^+ implanted diodes showed similar results. Rectification of the diodes annealed at 1100°C and 1200°C was superior to those

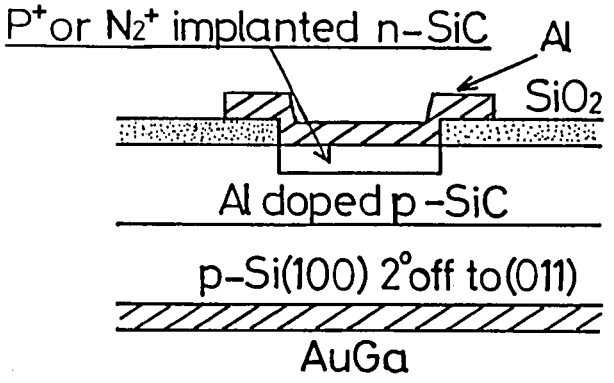

Fig.5 Schematic cross section of planar type p-n junction diodes fabricated by the ion implantation.

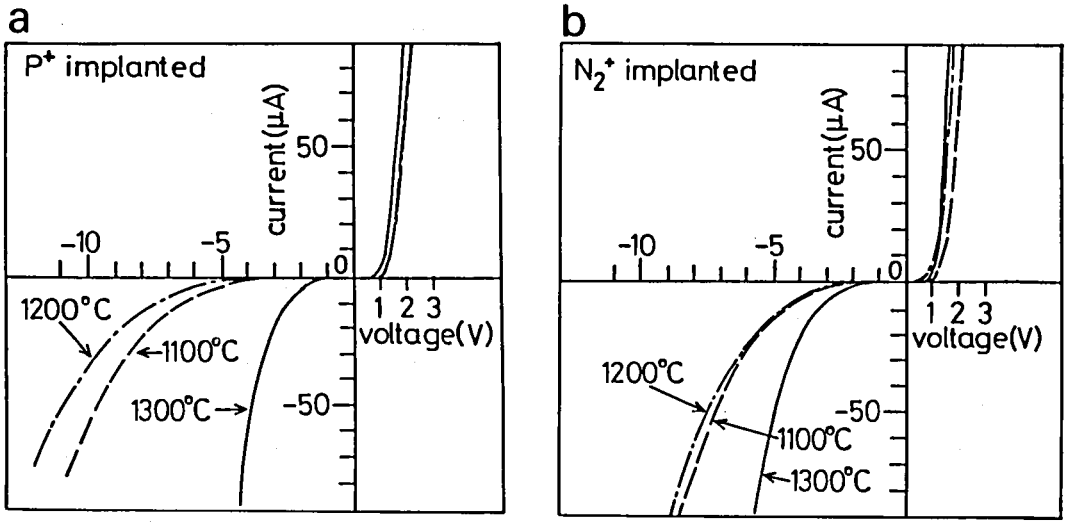

Fig.6 Current-voltage characteristics of p-n junction diodes fabricated by (a)P^+ and (b)N_2^+ implantation.

at 1300°C. As shown in Fig.4, the electrical activation rate increased abruptly by annealing at temperatures over 1300°C. And so, this annealing temperature dependence of the rectification was considered to be related to the change from an n-layer to an n^+-layer because of increase in the electrical activation rate. The best ideal diode factor of 3.8 was obtained when annealing temperature was 1100°C for both the P^+ and N_2^+ implanted diodes.

Capacitance-voltage characteristics of these diodes showed small variation in capacitance as shown in Fig.7. As annealing temperatures were raised, the capacitance and the magnitude of its variation became larger. These results mean that the diodes had p-i-n structures[14] and the thickness of the i layer became thinner as annealing temperature became higher. The N_2^+ implanted diodes showed the larger capacitance and its variation than the P^+ implanted diodes. This difference was considered to originate from the difference in electrical activation. The N_2^+ implanted layers showed the higher electrical activation rates than the P^+ implanted layers as mentioned in the previous section. Hence, the thicknesses of the i layers were thinner in the N_2^+ implanted diodes and the capacitance became larger.

4. Fabrication of MOSFET's

MOSFET's were fabricated using the ion implantation technique. A schematic cross section of the fabricated MOSFET's is shown in Fig.8. A channel layer of B-doped p-SiC with the thickness of 2μm was grown on undoped n-SiC with the thickness of 7μm. Since there is large lattice mismatch between Si and SiC, the layer with the thickness of over several microns was necessary to reduce crystal defects and to improve device characteristics by our present technique. Source and drain were formed by the ion implantation of P^+ using deposited SiO_2 with the thickness of 500nm as a mask. The implantation was carried out under the condition 1 in Table 1. Annealing after the implantation was carried out in an IR radiative heating furnace

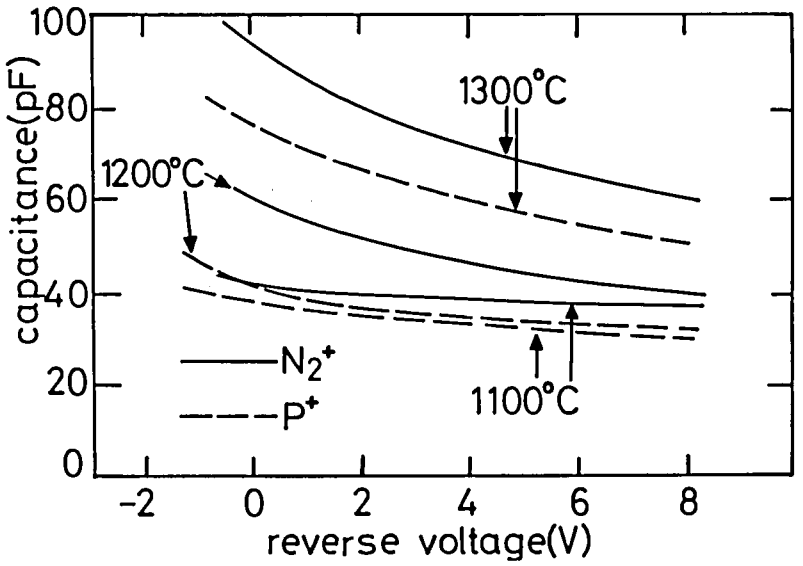

Fig.7 Capacitance-voltage characteristics of p-n junction diodes.

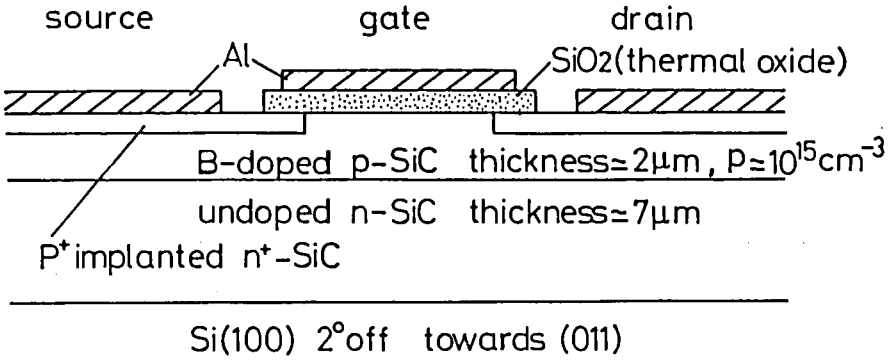

Fig.8 Schematic cross section of fabricated MOSFET's.

in Ar atmosphere at 1080°C for 1hr.

A gate insulator was formed by thermal oxidation of SiC at 1050°C using dry oxygen for 6hrs. The thermal oxide film of 3C-SiC was found to be SiO_2 and inversion was confirmed under an illuminated condition in an Al/SiO_2/n-SiC structure[15]. Typical electrical resistivity and breakdown electric field of SiO_2 formed by the thermal oxidation were $8.5\times10^{15}\Omega$cm and 2.5×10^{6}V/cm, respectively. The thickness of the gate oxide was about 60nm. The gate length and the width are 20μm and 500μm, respectively. Al was used as a gate electrode and ohmic contacts for source and drain. Alloying of the ohmic contacts was not carried out. The top view of the fabricated MOSFET is shown in Fig.9.

Current-voltage characteristics of the FET at 310K are shown in Fig.10. The sample was not illuminated. An action of inversion-type MOSFET's was achieved for the first time. Kinks in the saturation region were observed. Such kinks are known as a feature of SOI(Si-on-insulator) MOSFET's[16,17]. Since in this investigation the MOSFET's were fabricated on a high resistive B-doped p-layer, their characteristics were considered to show SOI-like features. In Al-SiO_2-SiC MOS diodes, the inversion condition was observed only under illumination, which is due to very low intrinsic carrier concentration($\simeq10$cm^{-3} at 300K) of 3C-SiC[15]. However, the MOSFET's operated without illumination. Electrons which are necessary to form an inversion layer were considered to be supplied from source.

Effective mobility of the FET was estimated using the characteristics in the linear region where drain voltage was lower than the voltage at the beginning of the kink. Ideal characteristics of MOSFET's in the linear region are given by

$$I_d=(W/L)\mu_n C_0((V_g-V_{th})V_d-V_d^2/2) \quad , \quad (1)$$

where I_d is drain current, W gate width, L gate length, μ_n electron mobility, V_g gate voltage, V_{th} threshold voltage and V_d drain voltage. Here W/L is 25 and the value of 5.75×10^{-8}F/cm^2 was used for C_0 based on an investigation of Al-SiO_2-SiC system[15]. μ_n and (V_g-V_{th}) were changed to agree with measured I_d-V_d

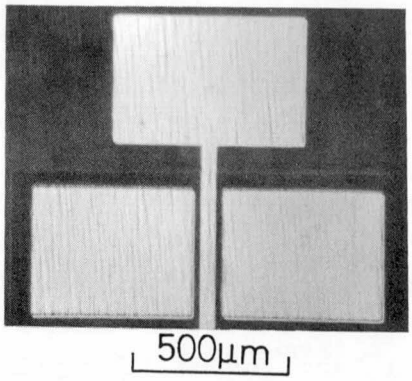

Fig. 9 Top view of a fabricated MOSFET.

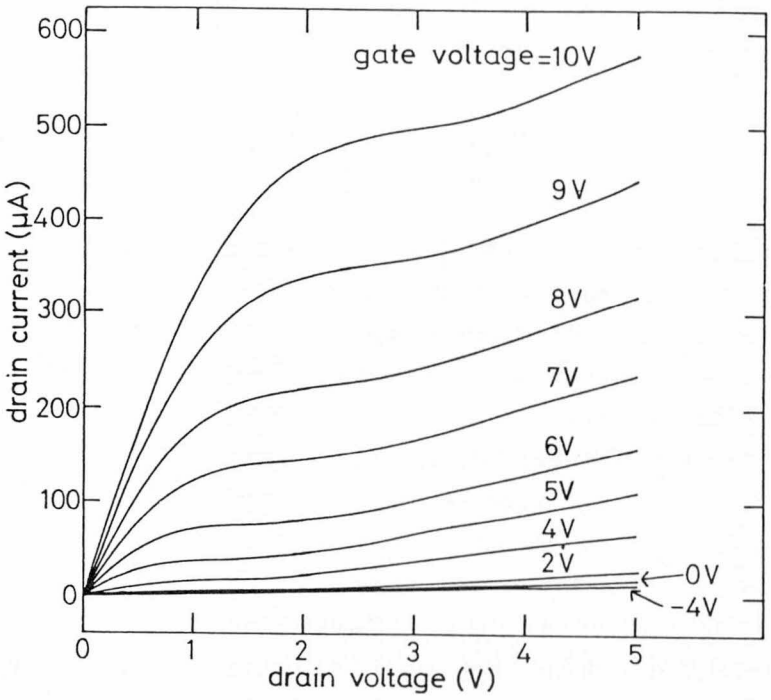

Fig. 10 Current-voltage characteristics of the MOSFET at 310K.

characteristics. The obtained effective electron mobility was about 100cm^2/Vsec.

The measurement of I_d-V_d characteristics at high temperatures was attempted. The MOSFET whose characteristics are shown in Fig.10 did not operate at temperatures above 70°C because of breakdown of gate oxide. Simultaneously fabricated MOSFET's also showed the breakdown of the gate oxide by heating up to 100°C. Such breakdown phenomena are probably attributed to contamination during fabrication. Some other MOSFET's showed variation of I_d as a function of V_g up to 440°C. However, the gate oxide became leaky after heating up to 165°C and it did not recover after cooling. The observed worsening of gate insulation was considered to attributed to a reaction of Al and SiO_2. Au gate is effective to prevent such a problem[18]. To realize practical high temperature devices of 3C-SiC a combination of peripheral materials will be an important problem.

5. Summary

Ion implantation of P^+ and N_2^+ into p-type 3C-SiC was carried out. The annealing temperature dependence of electrical properties of implanted layers was investigated up to 1400°C. Electrical activation rates of implanted impurities were improved as annealing temperature became higher. N_2^+ implanted layers showed the larger electrical activation rate than P^+ implanted layers. P-n junction diodes were fabricated using an ion implantation technique. Their capacitance-voltage characteristics indicated that they had a p-i-n structure.

Inversion-type MOSFET's of 3C-SiC were fabricated. Source and drain were formed by the ion implantation of P^+. Inversion mode operation was confirmed for the first time. Current-voltage characteristics showed kinks in the saturation region which are known as a feature of SOI MOSFET's. Effective electron mobility in the MOSFET's was estimated to be about 100cm^2/Vs. This successful fabrication of MOSFET's showed usefulness of the ion

implantation technique for device fabrication of 3C-SiC.

References

[1] R.B.Campbel and H.C.Chang, *Semiconductors and Semimetals* Vol.7 Part B, (Academic Press, New York, 1971) edited by R.K.Willardson and A.C.Beer, Chapter 9.

[2] O.J.Marsh, *Silicon Carbide-1973*, (University of South Carolina Press, Columbia, 1974) edited by R.C.Marshall, J.W.Faust, Jr. and C.E.Ryan., p.471.

[3] H.L.Dunlap and O.J.Marsh, Appl. Phys. Lett. 15(1969) 311.

[4] A.Addamiano, G.W.Anderson, J.Comas, H.L.Hughes and W.Lucke, J. Electrochem. Soc. 119(1972) 1355.

[5] V.M.Gusev, K.D.Demakov, M.G.Kosaganova, M.B.Reifman and V.G.Stolyarova, Sov. Phys. Semicond. 9(1976) 820.

[6] S.A.Belova, A.V.Vorob'ev, V.M.Gusev, K.D.Demakov, M.G.Kosaganova, N.K.Prokof'eva, M.B.Reifman, V.G.Stolyarova and V.A.Uzhegova, Sov. Phys. Semicond. 10(1976) 743.

[7] E.V.Kalinina, N.K.Prokof'eva, A.V.Suvorov, G.F.Kholuyanov and V.E.Chelnokov, Sov. Phys. Semicond. 12(1978) 1372.

[8] Y.Kondo, T.Takahashi, E.Sakuma and S.Misawa and H.Daimon, S.Yoshida and Y.Hayashi, Extended Abstr. of the 46th Autumn Meeting of the Japan Society of Applied Physics, Kyoto, October, 1985, 2p-C-11.

[9] H.Kong, H.J.Kim, J.A.Edmond, J.W.Palmour, J.Ryu, C.H.Carter, Jr., J.T.Glass and R.F.Davis, Material Society Symposia Proceedings vol.97, Anaheim, 1987(Material Research Society, Pittsburgh, 1987) p.232.

[10] H.Ryssel and I.Ruge, *Ion Implantation*, (John Wiley & Sons, Chichester, 1986), p.116.

[11] H.Ishiwara and S.Furukawa, Trans. IECE Japan 56-C(1973) 179, in Japanese.

[12] S.Furukawa, H.Matsumura and H.Ishiwara, Jpn. J. Appl. Phys. 11(1972) 134.

[13] J.E.Gibbons, W.S.Johnson and S.W.Mylroie, *Projected Range*

Statics, (Halsted Press, Stroudsburg, 1975) 2nd ed.

[14] H.Matsunami, *Handoutai-kougaku(Semiconductor Engineering)*, (Syoukoudou, Tokyo, 1983) p.139, in Japanese.

[15] K.Shibahara, S.Nishino and H.Matsunami, Jpn. J. Appl. Phys. 23(1984) L862.

[16] J.Tihanyi and H.Schleotterer, Solid-State Electron. 18(1975) 309.

[17] S.M.Sze, *Physics of Semiconductor Devices*, (John Wiley & Sons, New York, 1981) 2nd edition, Chapter 8.

[18] E.Sakuma, H.Daimon, M.Yamanaka, S.Misawa, K.Endo and S.Yoshida, Extended Abstr. of the 34th spring Meeting of the Japan Society of Applied Physics and of the related societies, Tokyo, March, 1987, 28p-W-9 and 28p-W-10.

VI. CVD GROWTH ON 6H-SiC(0001)

1. Introduction

In the former chapters 3C-SiC grown on Si was treated. In this chapter growth on 6H-SiC(0001) is the main subject. Many investigators carried out homoepitaxial growth of 6H-SiC at temperatures of about 1800°C, and applications to blue LED's[1,3] and bipolar transistors[4] were already reported. 6H-type is the most popularly obtainable polytype at high temperatures over 1800°C[5] even in the case of growth without substrates. Such high temperatures are believed to be suitable also for CVD growth. However, growth at lower temperatures reminds us of two interesting meanings. One concerns possibility of utilizing 6H-SiC(0001) as a substrate of 3C-SiC, and the other is control of polytypes of CVD grown layers.

As explained in the first chapter, structures of all polytypes of SiC are expressed by stacking sequences in the [0001] direction concerning layers of close packed atoms. 3C- and 6H- type have the stacking sequences of *ABC* and *ABCACB*, respectively. Ideally every sequence which consists of '*A*', '*B*' and '*C*' is permitted as far as the sequences does not include repetition of the same layer such as '*AA*', '*BB*' or '*CC*'. And so, ideally we can draw a structure of 3C-SiC grown on 6H-SiC with stacking sequence of *ABCABCABCACBABCACB*... In the case of growth at relatively low temperatures, 3C-type is most popularly obtained. Therefore, growth of 3C-type on 6H-substrates is expected at low temperatures.

When crystal growth begins by random nucleation, polytypes of the grown crystals are explained by the stability connected with temperatures. However, in the case of epitaxial growth, the transmission of the stacking information from substrates is considerable. Therefore, it is interesting whether the polytypes of epitaxially grown layers can be varied by controlling temperature and substrates. In this investigation, CVD growth was

carried out at temperatures in the range of 1350-1500°C, and "control of substrates" was realized by introducing off orientation.

2. CVD growth

Used substrates were all 6H-SiC(0001) Si-faces grown by Acheson method. Because naturally formed flat faces of crystals grown by Acheson method are usually (0001) Si-faces or $(000\bar{1})$ C-faces, and surface flatness of CVD and LPE grown layers on (0001) Si-faces was reported to be superior to that on $(000\bar{1})$ C-faces[6,8]. The (0001) Si-face was selected utilizing the difference in oxidation rates between these two faces[9]. Two types of substrates were prepared. One was a natural flat face and the other was a face angle-lapped with carborundum powder. Hereafter the former and the latter are called natural and lapped faces, respectively. Both faces were polished with diamond paste as finishing.

For CVD growth the same system was used as 3C-SiC on Si. Since growth temperature was higher than growth on Si, small size susceptors were used to prevent over-heating of the wall of a reaction tube. Figure 1 shows a temperature program of the CVD growth. Before the growth, etching of substrates by gaseous HCl or molten KOH was carried out. Etching temperatures by gaseous HCl and molten KOH were 1500°C and around 450°C, respectively. Source gases were SiH_4 and C_3H_8. Growth temperatures were in the range of 1350°C-1500°C. A typical growth rates was about 2μm/hr.

Figure 2 shows a typical surface morphology of the grown layers on natural faces. A mosaic pattern which consists of step-like or groove-like boundaries was observed. Such morphology was already reported[7,10,11]. Figure 3 shows a SEM photograph of pits on the surface of the grown layers etched by molten KOH. The etch pits give us the following information. Since the pits have a triangular shape, the grown layers are 3C-SiC[12-14]. The apices of the triangles of the pits point 180° opposite

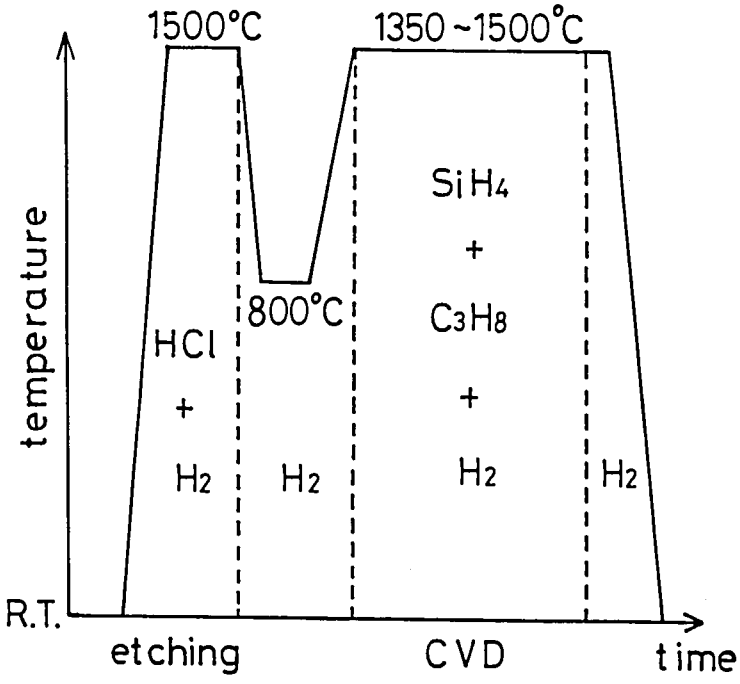

Fig.1 Temperature program of CVD growth procedure.

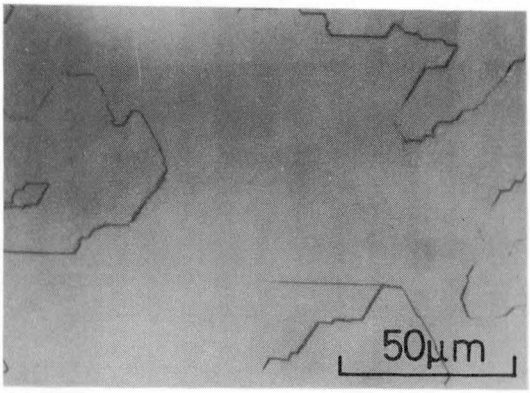

Fig.2 Nomarski microphotograph of the surface of a grown layer on a natural face. Boundarylike grooves are observed.

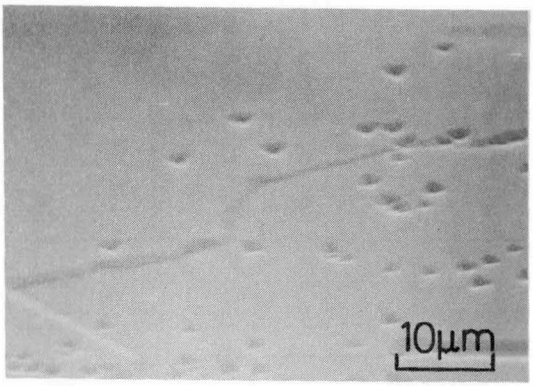

Fig.3 SEM microphotograph of the etched surface of a grown layer on a natural face. Triangular pits are observed.

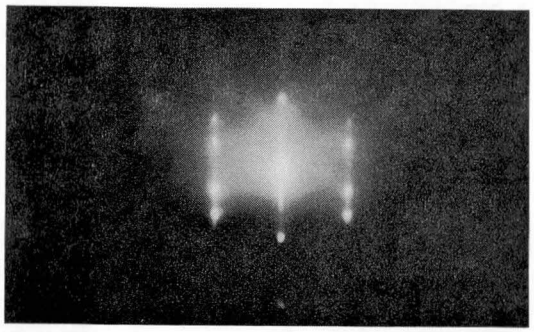

Fig.4 ⟨100⟩ (or ⟨$\bar{2}\bar{1}$10⟩) azimuth RHEED pattern of a grown layer on a natural face. 3C-SiC containing twinning was grown.

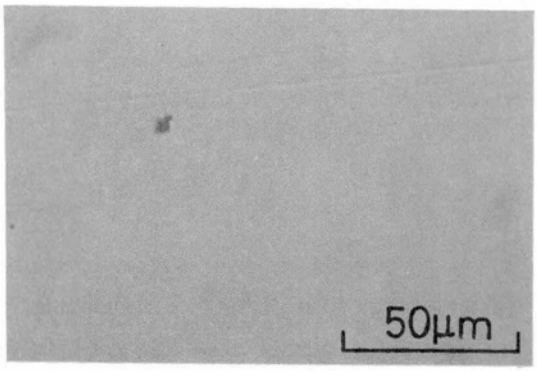

Fig.5 Nomarski microphotograph of the surface of a grown layer on a lapped face. Observed straight lines are scratches formed by polishing.

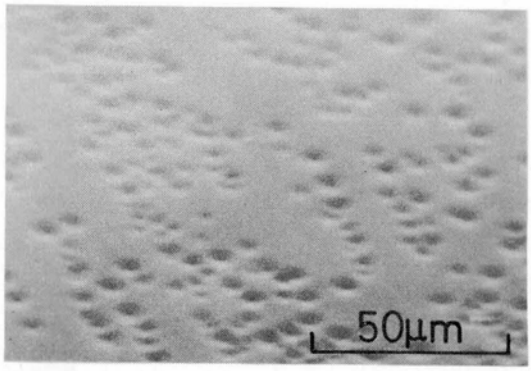

Fig.6 SEM microphotograph of the etched surface of a grown layer on a lapped face.

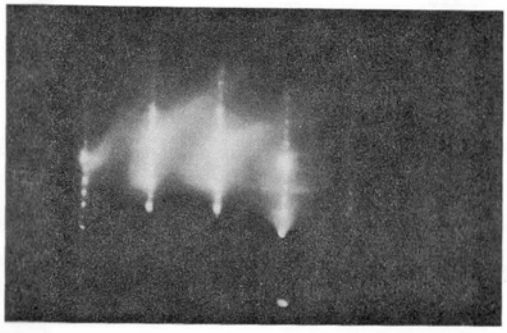

Fig.7 ⟨100⟩ (or ⟨$2\bar{1}\bar{1}0$⟩) azimuth RHEED pattern of a grown layer on a lapped face. Single crystalline 6H-SiC was grown.

directions in the neighboring regions separated by the boundaries, which means that the boundaries were twin-boundaries. In short, the grown layers on natural faces were 3C-SiC containing twinning, which was also confirmed by RHEED as shown in Fig.4. Details of interpretation of RHEED patterns are mentioned in the next section. Variation of the Si/C ratio was no help for elimination of twinning. By optimizing etching conditions, the intervals between the boundaries were slightly widened.

The (0001)Si face was lapped and polished as mentioned above to introduce off orientation. Figure 5 shows a typical surface morphology of the grown layers on lapped faces. A very smooth surface was obtained. As shown in Fig.6 pits formed by molten KOH etching had a circular shape and could not be directly utilized for identification of polytypes. No boundary-like structures were observed on the etched surface. The RHEED patterns shown in Fig.7 indicated that the grown layers were single crystalline 6H-SiC.

Single crystalline 6H-SiC was obtained on lapped faces in the range of growth temperatures from 1400°C to 1500°C. These temperatures are very low compared with an ordinary growth temperature of 1800°C for 6H-SiC. When the temperature was 1350°C, the grown layers on both natural and lapped faces were 3C-SiC containing twinning as explained below. The surface morphology of the grown layers on natural faces was similar to that grown at temperatures over 1400°C containing the boundaries. The grown layers on lapped faces showed flat surfaces as shown in Fig.8. However, RHEED patterns for the grown layers on both natural faces and lapped faces were similar to Fig.4 and indicated that the grown layers were 3C-SiC containing twinning.

There were many differences between growths at 1350°C and at 1400-1500°C in addition to the difference in polytypes of the grown layers. Figure 9 shows droplets observed on the surfaces of SiC grown at temperatures over 1400°C. The RHEED pattern of an as-grown surface with droplets showed spots due to Si. After removing the droplets with a mixed solution of HF and HNO_3, the spots due to Si in the RHEED patterns disappeared. The droplets

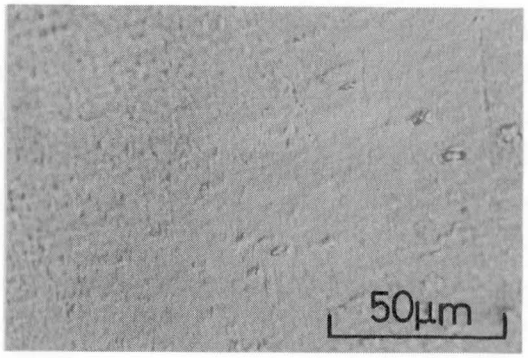

Fig.8 Nomarski microphotograph of the surface of a grown layer on a lapped face. Growth temperature was reduced to 1350°C.

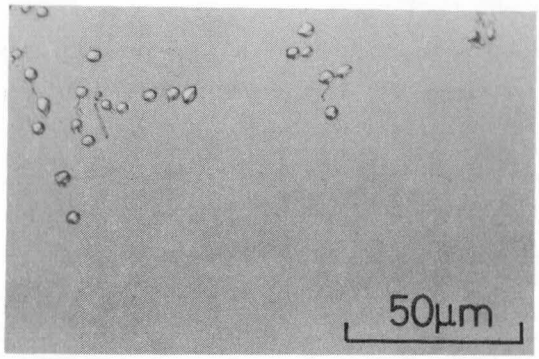

Fig.9 Si droplets observed on SiC grown at temperatures higher than the melting point of Si.

could be eliminated by decreasing the Si/C ratio. Therefore, the droplets are considered to originate from excessively supplied Si cohered as molten droplets during growth at temperatures higher than the melting point of Si. The melting point of Si is 1420°C and is higher than 1400°C. In the used system a Si wafer put on a susceptor melted over 1400°C. The difference of 20°C is an error due to temperature measuring method mentioned in Chapter 2.

Table 1 shows the relationship between the Si/C ratio and surface flatness of the grown layers on lapped faces. At 1350° the Si/C ratio should be rigidly optimized to obtain a flat surface. However, at temperatures over 1400°C a flat surface was obtained in the wide range of the Si/C ratio. These results about the droplets and the Si/C ratio are explained as follows. At temperatures over the melting point of Si, since stable Si-Si bonding cannot exist, excessively supplied Si does not prevent growth of SiC. However, at temperatures under the melting point of Si, excessively supplied Si forms crystalline Si and growth of SiC is affected similarly to the case of growth on Si mentioned in Section II-4-1. Thus, the growth mechanism at 1350°C is considered to be different from that at temperatures over the melting point of Si.

The relationship between the growth conditions and polytypes of the grown layers is shown in Table 2. The mechanism which decides polytypes of the grown layers includes two important factors of the orientation of substrates and growth temperatures. In the range of 1400°C-1500°C polytypes were varied by the orientation of substrates. Figure 10 shows the relationship between the polytypes of the grown layers and the magnitude and the direction of the off orientation. The off angle and the direction were measured using an X-ray diffractometer. When the off angle was larger than 1.5°, 6H-SiC was grown homoepitaxially. This result is explained in relation to surface steps introduced by the off orientation. We assume that fundamentally epitaxial growth takes place inheriting the stacking information of atoms nearby the surface. When the polished natural face is used, the

Si/C RATIO AND SURFACE MORPHOLOGY

Si/C \ T_s	1350°C	1400-1500°C
<0.03	---	good
0.03-0.3	---	good*
0.32	bad	good*
0.56	good	good*
0.74	bad	---

T_s: growth temperature
---: not yet tried
*: Si droplets were observed.

Table 1 Relationship between the Si/C ratio and surface morphology of grown layers.

GROWTH CONDITIONS AND POLYTYPES

sub. \ T_s	1350°C	1400-1500°C	>1800°C
natural face	3C(twin)	3C(twin)	6H*
lapped face	3C(twin)	6H	---

*: by Nishino et al.[7]
T_s: growth temperature, sub.: substrates
---: not yet tried

Table 2 Variation in polytypes of grown layers due to the change of growth temperatures and orientations of substrates.

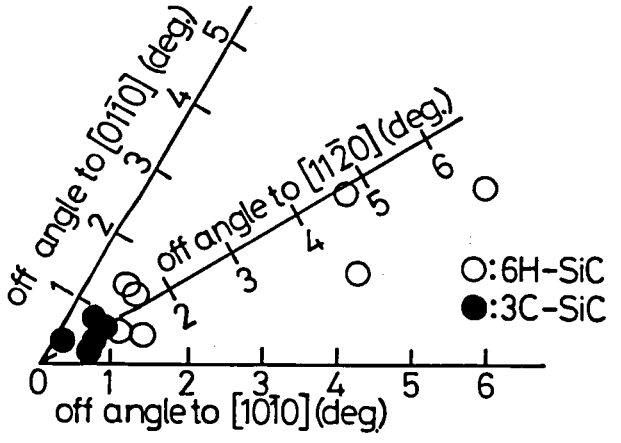

Fig.10 The relationship between polytypes of grown layers and the off orientation of substrates.

density of surface steps is very low. Therefore, growth mainly takes place on the flat surface not at the steps. Then, arrived atoms on the surface inherit the stacking information of the atoms that locate just under the surface.

Even on the natural face which has a very low offset angle from (0001), there are steps in a macroscopic view point. Hence, the surface of the 6H-SiC(0001) face can be divided into two parts. In one part the surface is occupied by the atoms belonging to *ABC* of the former half of the stacking sequence of *ABCACB*, and in the other part by the atoms belonging to *ACB* of the latter half. On the *ABC* part 3C-SiC grows in accordance with the stacking sequence of *ABC*, and on the other part in accordance with *ACB* as shown in Fig.11(a). In other words on the natural face of 6H-SiC twin crystals of 3C-SiC grow.

As the off angle becomes larger, the density of the surface steps becomes larger. Then atoms easily reach to the steps by migration. In this case, epitaxial growth takes place inheriting the stacking information around the steps as shown in Fig.11(b). Hence, 6H-SiC layers were obtained on off-oriented substrates. Even on natural faces 6H-SiC layers were obtained at 1800°C[7]. There are two mechanisms which can explain the result. One is that 6H-SiC is stable at temperatures over 1800°C. And the other is explained as follows based on the model mentioned above. At very high temperatures surface migration becomes active. Therefore, even if the density of steps is low, atoms can reach to the steps and 6H-SiC can grow epitaxially at high temperatures. Powell and Will reported epitaxial growth of 6H-SiC at very low temperatures under 1400°C on the faces perpendicular to {0001} C-faces.[13] Their investigation corresponds to growth on substrates with an off angle of 90°.

At 1350°C the introduction of off orientation did not give rise to variation in polytypes. As discussed above the growth mechanism at 1350°C is different from that at temperatures higher than the melting point of Si. And the polytype of the grown layers is probably decided in a different way.

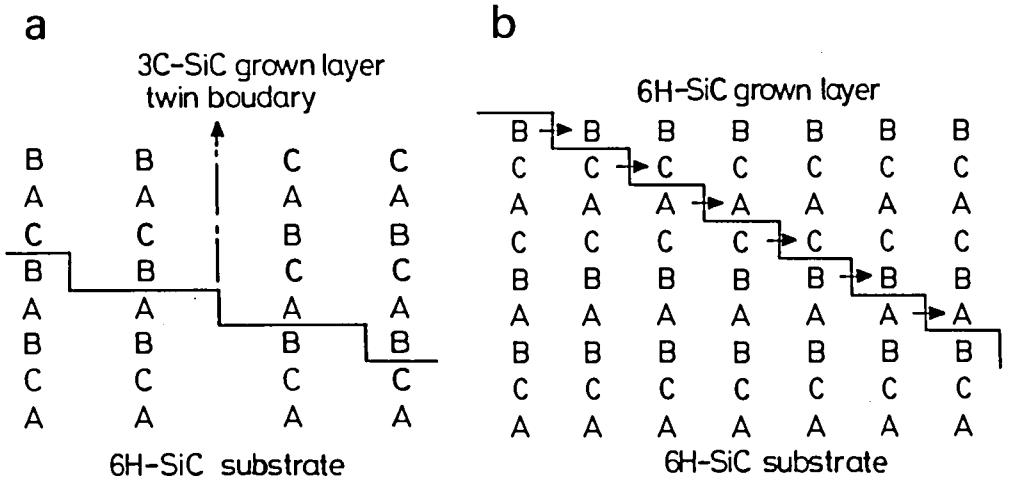

Fig.11 Model of (a) growth of twinned 3C-SiC on well oriented 6H-SiC(0001) and (b) homo-epitaxial growth on off oriented 6H-SiC(0001).

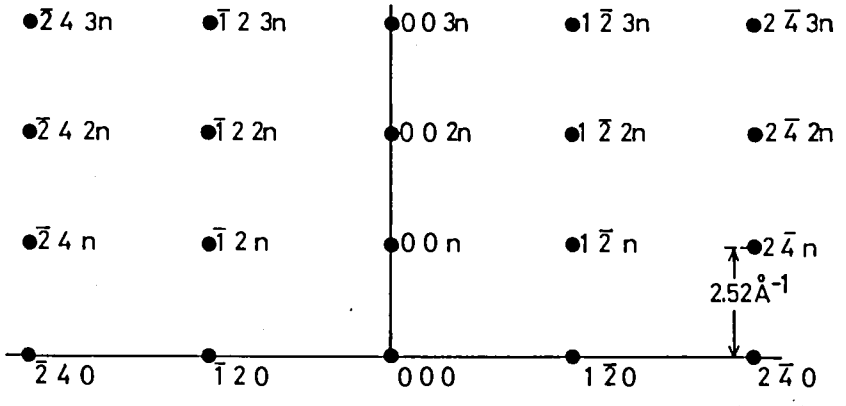

Fig.12 Theoretical <210> (or <10$\bar{1}$0>)azimuth RHEED pattern for all polytypes of SiC. Where n is a number of layers in the repeat distance.

3. Identification of polytypes

(RHEED observation)

The most fundamental method to identify the structure of crystals is a diffraction technique. The examples of identification by X-ray oscillation[15], TED(transmission electron diffraction)[11,16] and Kikuchi lines in electron diffraction patterns[17] were reported. In this work, structure identification was carried out by RHEED observation. This method is convenient for thin grown layers. Moreover, sample preparation and interpretation of results are easy.

To obtain theoretical RHEED patterns, reciprocal vectors, structural factors and double reflection should be taken into account. The detail of calculation is mentioned in an appendix. $\langle 1\bar{1}0\rangle$ and $\langle 210\rangle$*) azimuth patterns of SiC(0001) in Fig.12 are common to all polytypes. However, $\langle 100\rangle$ and $\langle 110\rangle$*) azimuth patterns are peculiar to each polytype. $\langle 100\rangle$ azimuth patterns for 3C, 6H and 15R types are shown in Figs.13(a)-(c). For hexagonal polytypes $\langle 100\rangle$ patterns are symmetrical, but those for 3C and rhombohedral polytypes are asymmetrical. When 3C-SiC contains twinning the pattern is synthesized by Fig.13(a) and its mirror image as shown in Fig.14.

*) $\langle 1\bar{1}0\rangle$ and $\langle 210\rangle$ directions correspond to $\langle 10\bar{1}0\rangle$. $\langle 100\rangle$ and $\langle 110\rangle$ directions correspond to $\langle 2\bar{1}\bar{1}0\rangle$. See an appendix for detail.

To apply this method to practical identification, spot patterns must be observed. However, surfaces of natural faces and grown layers are usually so flat that streak patterns are obtained. To obtain a spot pattern intentionally roughness should be introduced onto the surface. In this work, lapping and molten KOH etching were attempted. Figure 15 shows a $\langle 100\rangle$ azimuth pattern of a 15R-SiC (0001) substrate. The surface of the sample was lapped with carborundum. By lapping the surface was roughen and partly changed to poly-crystalline. Sometimes the surface became too rough for RHEED observation. To obtain adequate roughness was very difficult in this method. For grown layers

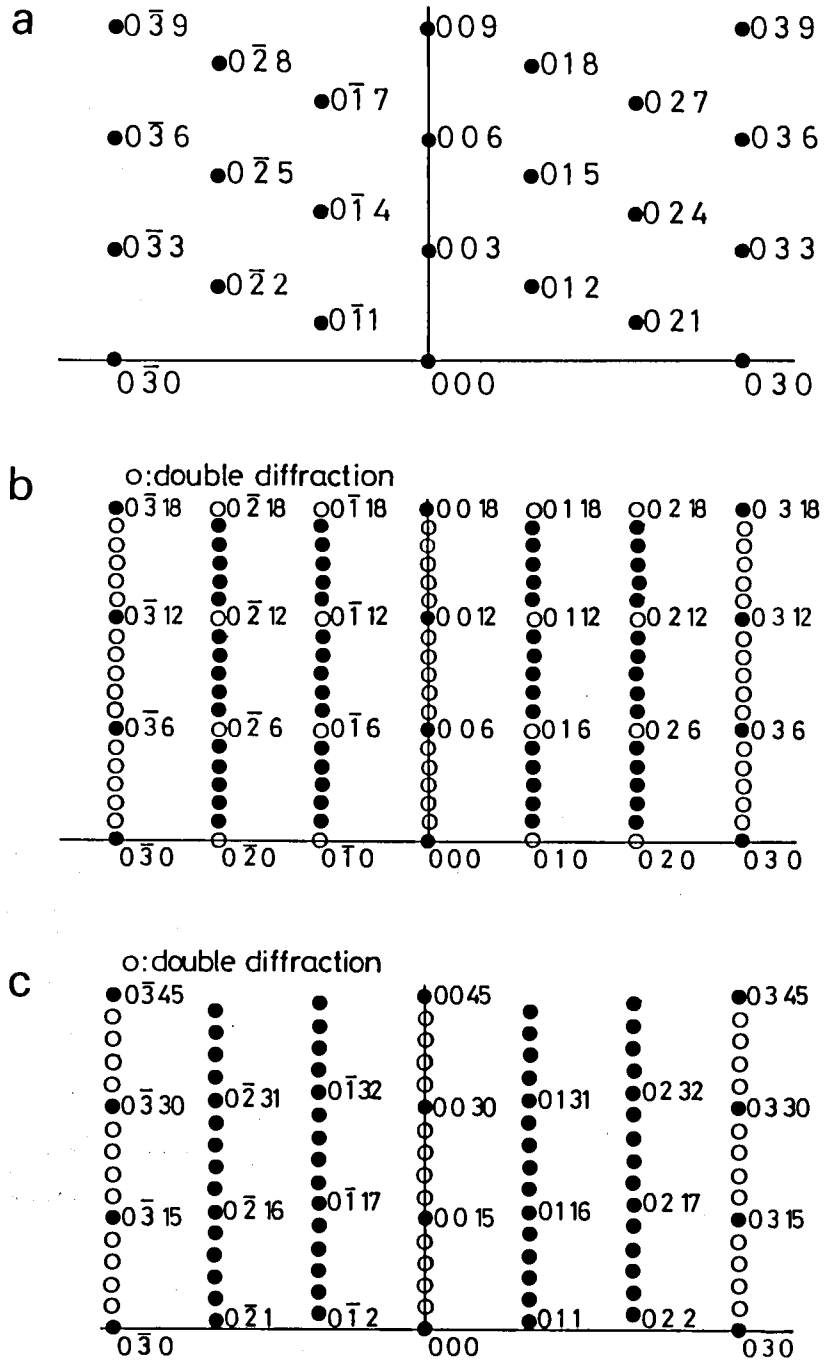

Fig.13 Theoretical <100> azimuth RHEED patterns for (a)3C-, (b)6H- and (c)15R-SiC(0001). Spots represented by white circles appear by double diffraction.

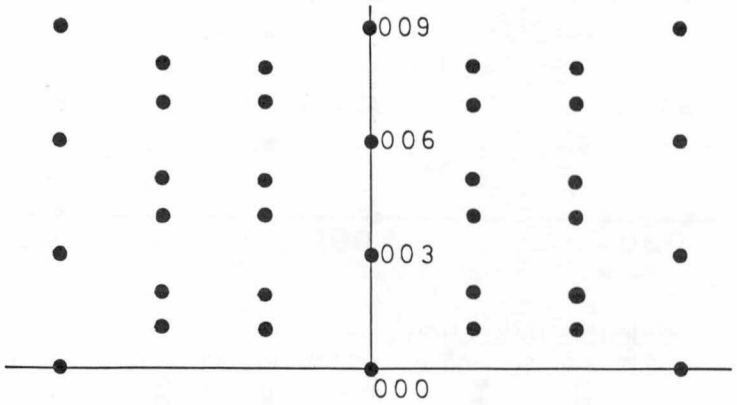

Fig.14 <100> azimuth RHEED pattern of 3C-SiC(0001) containing twining.

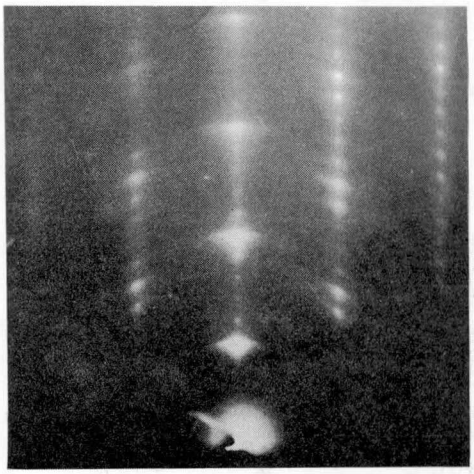

Fig.15 <010> azimuth RHEED pattern of 15R-SiC(0001). Surface of the sample was slightly lapped to obtain a spot pattern.

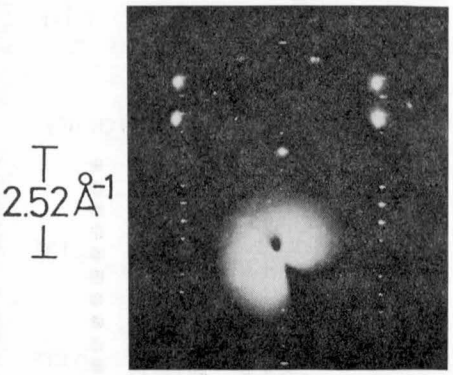

Fig.16 simultaneously obtained a RHEED pattern of a 3C-SiC grown layer and a TED pattern of a 6H-SiC substrate.

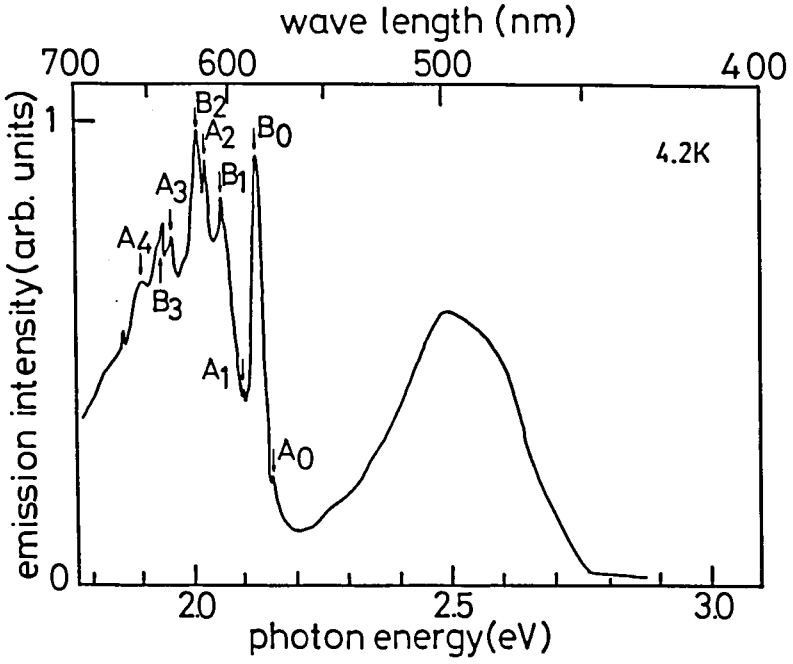

Fig.17 Photoluminescence spectrum of an Al-doped 3C-SiC grown layer. A broad peak at about 2.5eV is due to a 6H-SiC substrate.

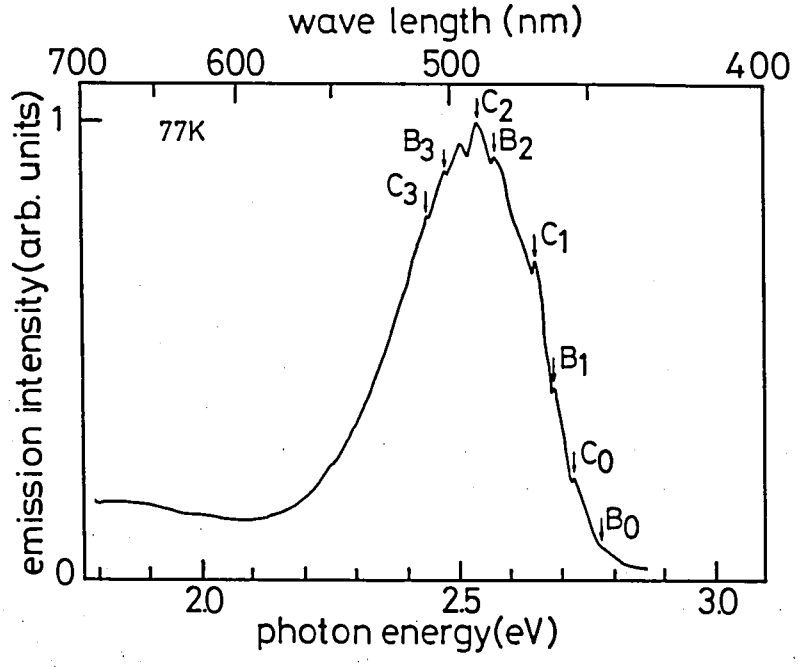

Fig.18 Photoluminescence spectrum of an Al-doped 6H-SiC grown layer.

molten KOH etching was utilized. Before etching, most samples showed streak patterns and identification of polytypes were impossible. After etching, spot patterns were obtained as shown in Figs.4 and 7. By comparing these patterns experimentally obtained with theoretical patterns shown in Figs.13 and 14, the polytypes of the grown layers were clearly identified as concluded in the previous section. When the surface of the grown layer was very rough, a spot pattern was obtained without special treatments as shown in Fig.16. In this figure a RHEED pattern of a grown layer and a TED pattern of a substrate were simultaneously obtained by exposing electron beam to the edge of the sample. Epitaxial growth of 3C-SiC containing twinning on 6H-SiC is clear in this photograph.

(Photoluminescence)

The bandgap energy and the activation energies of impurities are peculiar to each polytype. Therefore, by measuring photoluminescence spectra polytypes can be identified. Since SiC has an indirect band structure and acceptor-related light emission is mainly observed, acceptor doping is desirable to obtain bright luminescence. In this study Al-doping was carried out using TMA and TEA as mentioned in Chapter 4.

Figure 17 shows a photoluminescence spectrum of a grown layer on a natural face. One broad peak at about 2.5eV and a set of peaks under 2.2eV were observed. The broad peak was the luminescence from the substrate and the other peaks are due to the grown layer. The narrow peaks named as A_0 and B_0 were identified as free to bound-acceptor emission and donor-acceptor(N and Al) pair recombination in 3C-SiC, respectively, by comparing with reported spectra[15,18]. A_n and B_n(n is an integer) peaks were phonon replicas of A_0 and B_0, respectively.

Figure 18 shows a photoluminescence spectrum of a grown layer on a lapped face. The peaks under 2.2eV disappeared. The broad peak in Fig.17 at about 2.5eV changed to a set of narrow peaks. These peaks are due to donor-acceptor(N and Al) pair recombination in 6H-SiC. B_n and C_n series were reported to

originate from N donors occupying a hexagonallike site and a cubiclike site[19], respectively. In 6H-SiC impurities occupying different sites have different activation energies.

4. Fabrication of Schottky and p-n junction diodes

The growth temperature of 6H-SiC evaluated in this section was 1500°C. Though even at 1400°C 6H-SiC could be grown, the electrical properties of the grown layers were not yet evaluated. Figures 19(a) and (b) show current-voltage characteristics of Au-SiC Schottky diodes on a 6H-SiC grown layer and on a 3C-SiC grown layer containing twinning. Surface treatment before vacuum evaporation of Au was carried out similar to the case of 3C-SiC on Si mentioned in Chapter 4. The conduction type of undoped 6H- and 3C-type grown layers was found to be n-type by a direction of their rectification. Schottky diodes fabricated on 6H-SiC grown layers showed good rectification reproducibly. By C-V characteristics of the diodes undoped donor concentration was obtained as $2 \times 10^{16} cm^{-3}$. Rectification of the diodes on 3C-SiC grown layers was worse than that of 6H-SiC. Twin boundaries in 3C-SiC grown layers were one of the candidates for the origin of the poor rectification.

Utilizing Au-SiC Schottky barriers EBIC observation was carried out. Figures 20(a) and (b) show SEM and EBIC image photographs of 3C-SiC on natural faces. In an EBIC image boundary-like recombination centers are observed. They clearly correspond to twin boundaries observed in the SEM image as grooves. In addition to the twin boundaries recombination centers with equilateral triangular shapes are observed. Probably they are stacking faults. In the EBIC image of the 6H-SiC grown layer recombination centers with a shape of an acute triangle and random lines were observed as shown in Fig.21. Their origin was not clear. Their density widely changed due to observation points in the sample. Used substrates were grown by Acheson method to produce polishing powder and their quality was not uniform.

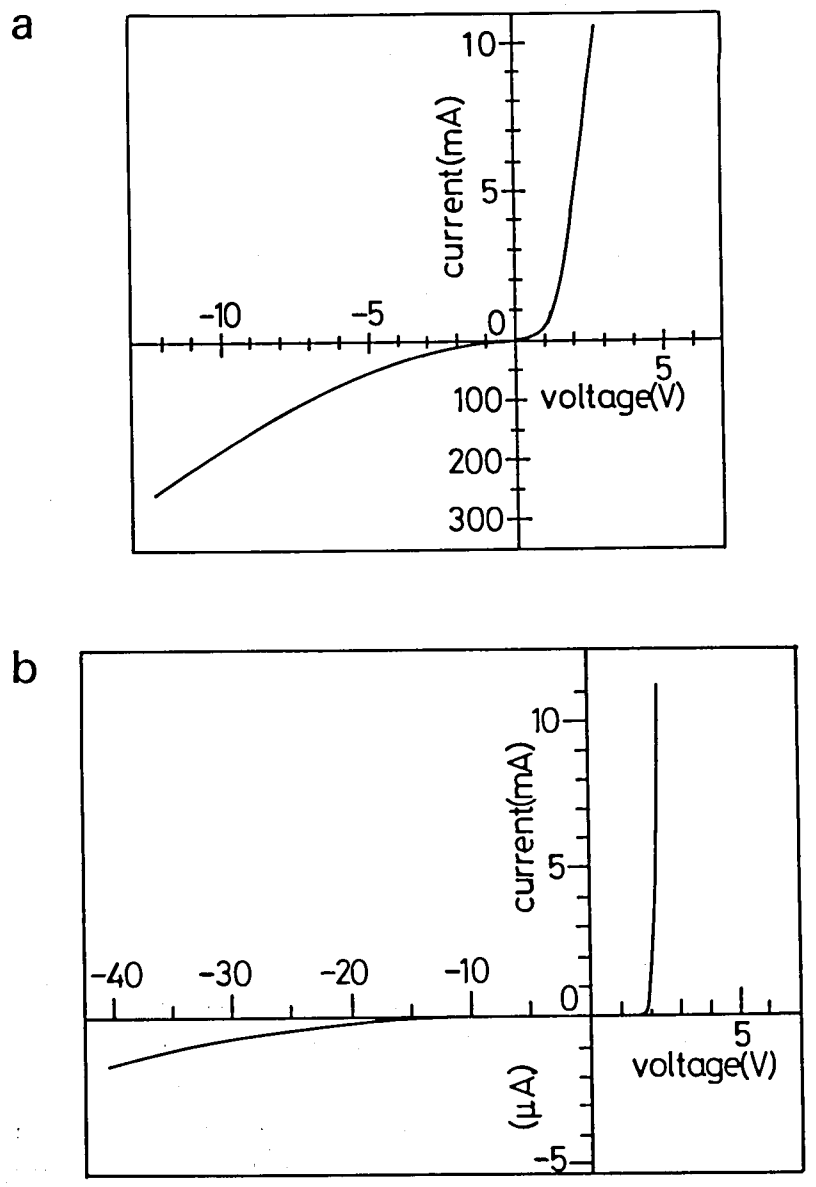

Fig.19 Current-voltage characteristics of a Au-SiC Schottky diodes on (a)6H-SiC and (b)3C-SiC grown layers.

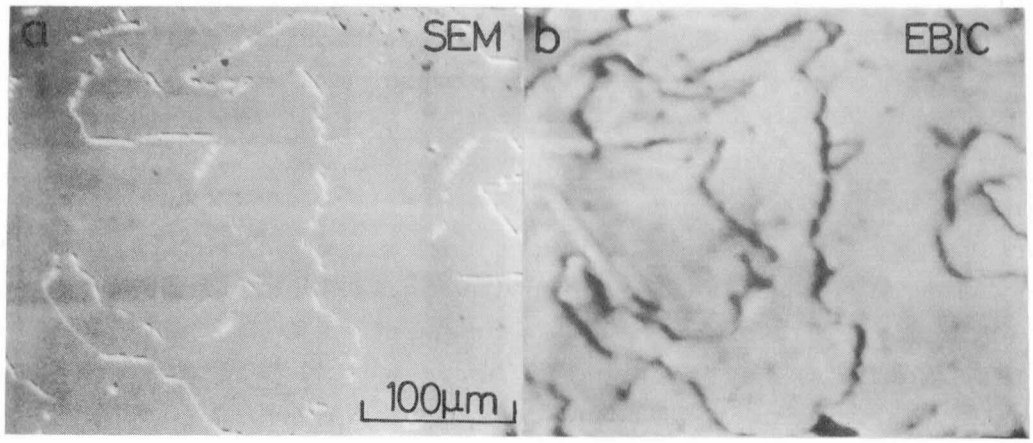

Fig.20 (a)SEM and (b)EBIC images of 3C-SiC grown layers. In EBIC image twin boundaries were observed as recombination centers.

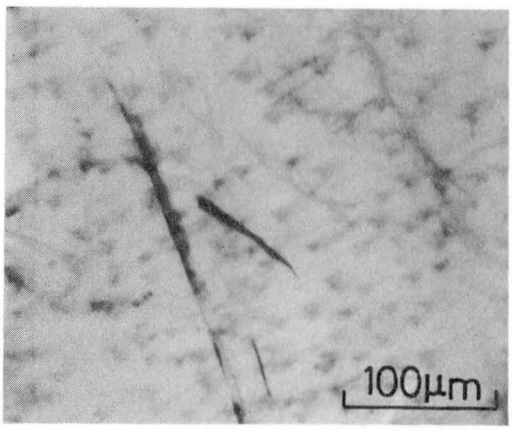

Fig.21 EBIC image of a 6H-SiC grown layer.

Therefore, the grown layers were considered to inherit the quality of the substrates.

Mesa-type p-n junction diodes were fabricated using 6H-SiC on lapped faces. To obtain p-type layers TMA or TEA was introduced by a bubbling method using H_2 during the epitaxial growth. P-type conduction with a carrier density of $4\text{-}9\times10^{17}cm^{-3}$ was confirmed by the van der Pauw method. TMA and TEA work as p-type dopants and carbon sources at the same time. Therefore, the flow rate of C_3H_8 was reduced relatively to that of SiH_4 during the growth of p-type layers. If it was not reduced, the surface of the p-type grown layers became rough. The structure of the fabricated diodes is shown in Fig.22. The undoped n-layer and Al-doped p-layer were grown consecutively. TMA was used for p-type doping. The thickness of both the n- and p-layers was about 2μm. To form mesa structures reactive ion etching(RIE)[20] was utilized with an Al mask using CF_4 and O_2 gases at 10Pa. The junction area of the fabricated diodes was $1.96\times10^{-3}cm^2$. A thermal oxide film of SiO_2 was formed at 1050°C for 6hrs to passivate the surface. Al-Si and Ni were evaporated and alloyed for p-type and n-type ohmic contacts, respectively. Figure 23 shows I-V characteristics of the fabricated p-n junction diode which showed the highest breakdown voltage of 100V. A $1/C^3$-V plotting of capacitance-voltage characteristics showed a proportional relationship(Fig.24), which means that this diode had a graded junction. However, the C-V characteristics of other diodes sometimes indicated abrupt junctions showing a proportional relationship in $1/C^2$-V plottings. The scattered C-V characteristics are probably attributed to gas-flow switching to start the growth of p-SiC on n-SiC.

Breakdown electric field was calculated using the I-V and $1/C^3$-V characteristics shown in Figs.23 and 24, respectively. Breakdown voltage(V_b) and the maximum electric field(E_m) in a graded p-n junction have the following relationship[21]

$$V_b=(4/3)E_m^{3/2}(2\varepsilon_s/aq)^{(1/2)}, \qquad (1)$$

where a is impurity gradient(cm^{-4}), ε_s semiconductor permittivity and q elementary charge. The impurity gradient can be obtained

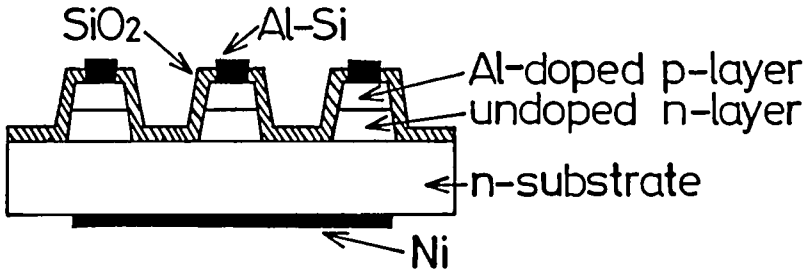

Fig.22 Schematic cross section of p-n junction mesa-diodes fabricated using 6H-SiC grown layers.

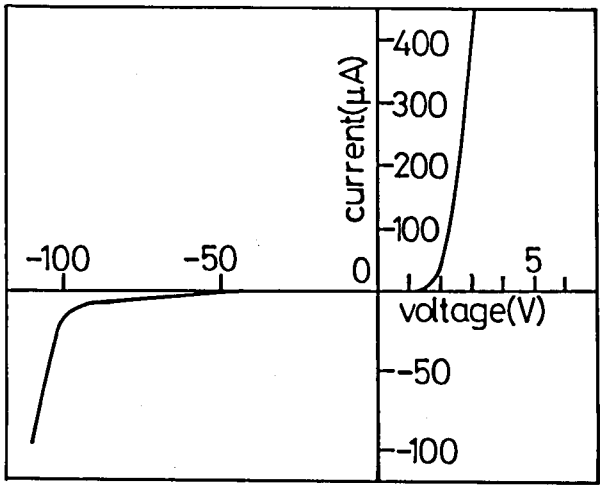

Fig.23 Current-voltage characteristics of a fabricated p-n junction diode.

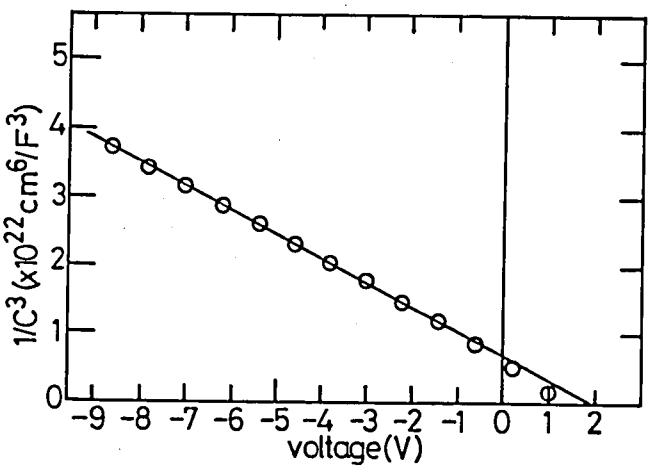

Fig.24 $1/C^3$-V plotting of capacitance-voltage characteristics of the p-n junction diode.

from the slope of the $1/C^3$-V plotting utilizing the next formula[21]

$$1/C^3=12(V_{bi}-V)/(qa\varepsilon_s{}^2) , \qquad (2)$$

where V_{bi} is built-in potential, C depletion-layer capacitance and V applied voltage. Thus the breakdown electric field was estimated to be 2.4×10^6 V/cm. von Muench et al. fabricated a onesided abrupt p-n^+ junction diode at 1800°C by CVD method and they obtained a breakdown electric field of $2\text{-}3.7\times10^6$ V/cm[22]. They compared the results with an empirical prediction by Sze and Gibbsons[23] mentioned in Chapter 4 and concluded that the experimentally obtained value of V_B(breakdown voltage) and E_m(maximum field in a junction) were larger than the prediction and the prediction cannot be applied to SiC. For graded junctions Sze and Gibbsons gave the following relationship between V_B and a[23].

$$V_B=60(E_g/1.1)^{6/5}(a/3\times10^{20})^{-2/5} \quad (V) , \qquad (3)$$

where E_g is bandgap energy. The relationship between V_B and E_m is given as eq.(1). Figures 25(a) and (b) show V_B and E_m as a function of a. Experimentally obtained V_B and E_m are plotted as circles in the figures and they are obviously larger than Sze and Gibbsons' prediction. Conclusively, in this work of preliminary trials utilizing low-temperature growth, comparable results to high-temperature grown layers were obtained.

These p-n junction diodes showed blue light-emission in the forward-biased region. Examples of electroluminescence spectra are shown in Fig.26. The diodes were driven by a pulse current of 500Hz with a duty cycle of 0.4. The wavelengths of the peaks in the spectra well agreed with those of LED's grown by liquid phase epitaxy(LPE)[24]. The peaks are attributed to three origins. The highest-energy peak at 425nm(F peak) and the peak at 455nm(E peak) are considered to be due to free-exciton recombination and Al-related localized centers, respectively. The other peaks(M peaks) are concerned with donor-acceptor(N and Al) pair recombinations.

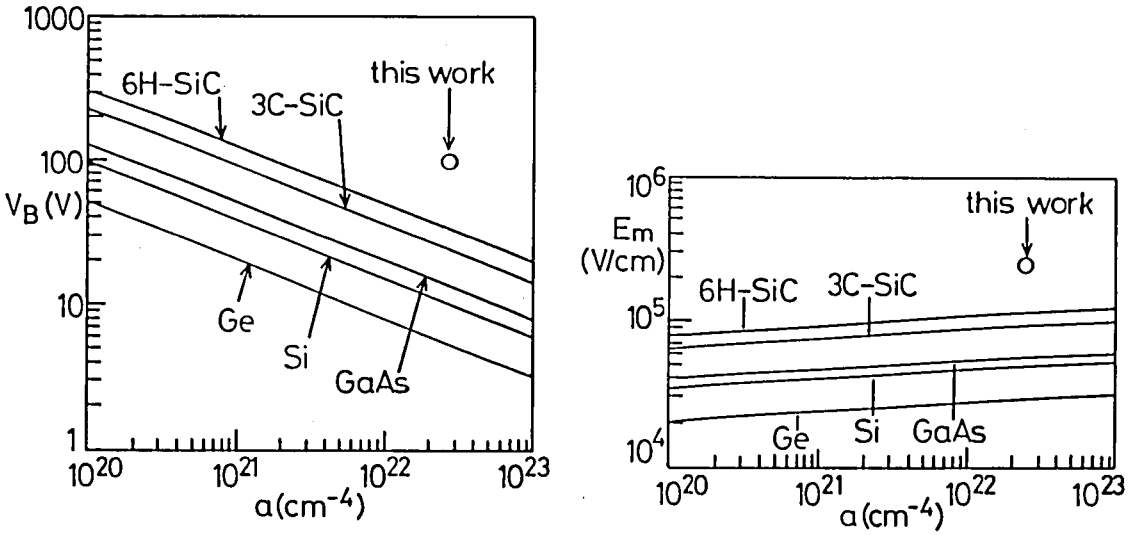

Fig.25 Predicted (a)V_B(breakdown voltage) and (b)E_m(maximum field) for graded p-n junction as a function of a(impurity gradient). Used formulas were given by Sze and Gibbsons[23]. A white circles represent results of this investigation.

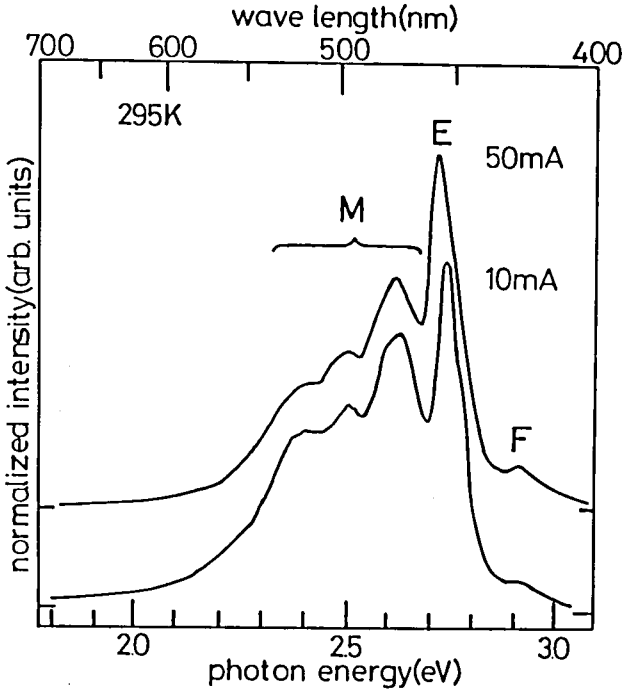

Fig.26 Electroluminescence spectra of a fabricated p-n junction diode at room temperature.

5. Summary

SiC was grown on 6H-SiC(0001)Si faces at 1350-1500°C by CVD method. Polytypes of grown layers were changed by changing growth temperatures and the orientation of substrates. In this temperature region, 3C-SiC containing twinning was obtained on a natural face. However, 6H-SiC was grown on off oriented (0001) substrates at 1400-1500°C. This temperature is 300-400°C lower than necessary growth temperature for 6H-SiC. The change in polytypes by off orientation of substrates was explained in relation to the surface step density. Polytypes of the grown layers were identified utilizing etch pits, RHEED patterns and PL spectra.

P-n junction diodes fabricated using the 6H-SiC grown layers showed good rectification. A breakdown electric field of 2.4×10^6V/cm was achieved in the p-n junction. This fact indicates that the crystallinity of 6H-SiC grown at low temperatures by introduction of off-orientation is comparable to that of grown at high temperatures.

References

[1] W.von Muench, W.Kuerzinger and I.Pfaffeneder, Solid-State Electron. 19(1976) 871.

[2] S.Nishino, A.Ibaraki, H.Matsunami and T.Tanaka, Jpn. J. Appl. Phys. 19(1980) L353.

[3] S.Yoshida, E.Sakuma, S.Misawa and S.Gonda, J. Appl. Phys. 55(1984) 169.

[4] W.von Muench and P.Hoeck, Solid-State Electron. 21(1978) 479.

[5] W.F.Knippenberg, Philips Res. Rep. 18(1963) 161.

[6] A.Suzuki, M.Ikeda, H.Matsunami and T.Tanaka, J. Electrochem. Soc. 122(1975) 1741.

[7] S.Nishino, H.Matsunami and T.Tanaka, J. Crystal Growth 45(1978) 144.

[8] A.Suzuki, M.Ikeda, N.Nagao, H.Matsunami and T.Tanaka, J.

Appl. Phys. 76(1976) 4546.
[9] A.Suzuki, H.Ashida, N.Furui, K.Mameno and H.Matsunami, Jpn. J. Appl. Phys. 21(1982) 579.
[10] V.J.Jennings, A.Sommer and H.C.Chang, J. Electrochem. Soc. 113 (1966) 728.
[11] H.S.Kong, J.T.Glass and R.F.Davis, Appl. Phys. Lett. 49 (1986) 1074.
[12] W.von Muench and I.Pfaffeneder, Thin Solid Films 31(1976) 39.
[13] J.W.Faust, Jr., *Silicon Carbide A High Temperature Semiconductor*, (Pergamon Press, Oxford, 1960) edited by J.R.O'Connor and J.Smiltens, p.403.
[14] J.W.Faust, Jr., T.Tung and H.M.Liaw, *Silicon Carbide-1973*, (Univ. south Carolina Press, Columbia, 1974) edited by R.C.Marshall, J.W.Faust, Jr. and C.E.Ryan, p.215.
[15] for example
A.Suzuki, H.Matsunami and T.Tanaka, J. Electrochem. Soc. 124(1977) 241.
[16] for example
H.Sato, S.Shinozaki, M.Yessik and J.E.Noakes, *Silicon Carbide-1973*, (Univ. South Carolina Press, Columbia, 1974) edited by R.C.Marshall, J.W.Faust, Jr. and C.E.Ryan, p.222.
[17] L.A.Zhukova, A.M.Estigneev, N.K.Prokof'eva, Yu.M.Shashkov and Yu.M.Gran, Sov. Phys. Crystallogr. 21(1976) 451.
[18] G.Zanmarchi, J. Phys. Chem. Solids 29(1968) 1727.
[19] M.Ikeda, H.Matsunami and T.Tanaka, Phys. Rev. B 22(1980) 2842.
[20] S.Dohmae, K.Shibahara, S.Nishino and H.Matsunami, Jpn. J. Appl. Phys. 24(1985) L873.
[21] S.M.Sze, *Physics of Semiconductor Devices* (Wiley, New York, 1981) 2nd ed., Chapter 2.
[22] W.von Muench and I. Pfaffeneder, J. Appl. Phys. , 48(1977) 4831.
[23] S.M.Sze and G.Gibbsons, Appl. Phys. Lett. 8(1966) 111.
[24] M.Ikeda, T.Hayakawa, S.Yamagiwa, H.Matsunami and T.Tanaka, J. Appl. Phys. 50(1979) 8215.

VII. CONCLUSIONS

In this work SiC was grown on Si and 6H-SiC substrates by CVD method. 3C-SiC was grown by a combination of carbonization and CVD growth on Si substrates. The following conclusions concerning crystal growth of 3C-SiC were obtained.

1)In RHEED observation carbonized layers on Si(100) showed a spot pattern of single crystalline 3C-SiC. However, extra spots and streaks due to crystal defects were observed, which were probably due to lattice mismatch between Si and 3C-SiC. The grown layer showed an improvement of crystallinity due to increase of the film thickness in a few characterization methods.

2) Cubic SiC was grown on Si(100), (111), (110) and (211) faces. Single crystals were obtained on (100) and (111) substrates. However, single crystal growth of SiC nonpolar surfaces such as (110) and (211) was unsuccessful, which was considered to be due to the formation of the first grown C layer by carbonization in spite that the layer should consist of both C and Si atoms.

3)The layers grown on Si(100) well oriented substrates contained antiphase domains. The origin of the antiphase domains was considered to have the close relationship with the surface step height. Growth on spherically polished (100) substrates was carried out, and introduction of off orientation towards (011) was found to be effective for elimination of antiphase domains. Antiphase-domains free layers grown on Si(100) off substrates showed electrical anisotropy.

About impurity doping and device fabrication of 3C-SiC on Si the following conclusions were obtained.

4) To obtain p-type conduction B and Al were doped during growth using B_2H_6 and organic Al, respectively. The B-doped layer showed high resistive p-type conduction. The maximum resistivity obtained was $8\times10^{3}\Omega$cm. By Al-doping the hole concentration was controlled in the range of 3×10^{16}-2×10^{17}cm^{-3}. A typical hole mobility in the Al-doped layer was 30cm^2/Vs. Too much doping by

both dopants resulted in rough surfaces. Organic Al worked as a dopant and a carbon source simultaneously.

5)Ion implantation of donors of P^+ and N_2^+ was carried out into the p-type layers. The annealing temperature dependence of electrical characteristics was investigated. Electrical activation increased monotonously as annealing temperature became higher. N_2^+ implanted layers showed larger electrical activation than P^+ implanted layers. Capacitance-voltage characteristics of the p-n junction diodes fabricated using ion implantation technique showed that the diodes had a p-i-n structure.

6)Inversion-type MOSFET's of cubic SiC were fabricated. Antiphase-domains free layers grown on Si(100) off substrates were used. A gate oxide of SiO_2 was formed by thermal oxidation. Source and drain were formed by ion implantation of P^+ into the B-doped p-layer. Inversion mode operation was confirmed for the first time. Current-voltage characteristics of the FET's showed a tendency of saturation.

By the investigation of growth on 6H-SiC, the following conclusions were obtained.

7) Crystals of SiC were grown on 6H-SiC(0001)Si faces at 1350-1500°C by CVD method. In this temperature region, 3C-SiC twin crystals were grown on a natural face. However, 6H-SiC was grown at 1400-1500°C by the introduction of off orientation into substrates. This temperature is 300-400°C lower than ordinary growth temperatures of around 1800°C. The change in polytypes by off orientation of substrates was explained in relation to the surface step density. At 1350°C twin crystals of 3C-SiC were grown both on natural faces and off substrates.

8) P-n junction diodes of 6H-SiC were fabricated at 1500°C by CVD growth. The diodes showed good rectification. A breakdown electric field of 2.4×10^6V/cm was achieved in the junction. This fact indicates that the crystallinity of 6H-SiC grown at low temperatures is comparable to that grown at high temperatures. The diodes showed blue-light emission in the forward bias region.

Finally for further investigation some suggestions are given

as follows. Layers grown on Si are considered to remain a problem of lattice mismatch. To solve the problems an innovation is necessary for the growth method. One considerable way is to utilize the grown layer as a substrate for the next growth. For the second growth method, sublimation, LPE and CVD at higher temperatures are hopeful. By sublimation method high growth rate and growth of ingots are expected. Very thick grown layers may not inherit the influence of lattice mismatch. LPE growth at equilibrium may have a possibility of the improvement of crystallinity. CVD growth at temperatures over the melting point of Si will give rise to variation in the mechanism of crystal growth, which was observed for the growth on 6H-SiC. Preliminary trials of some of these methods are already started[1,2].

Excellent results were obtained as a preliminary trial concerning homoepitaxial growth of 6H-SiC in this work. However, easily obtainable substrates are still far from satisfactory. Uniformity in shapes, sizes, impurities and crystallinity should be improved for a systematic investigation.

Reproducibility in electrical properties is not good under the present technique. Undoped carrier concentration sometimes changes unintentionally. For device application an improvement of this point is necessary. To raise the level of CVD growth technique, every part used around the gas system and the reaction tube should be reconsidered whether their qualities are adequate or not. Especially, since a susceptor, its quartz holder and a quartz reaction tube are heated during growth, they are likely to supply impurities. Their materials and how to handle them should be important problems.

References

[1] W.S.Yoo, S.Nishino and H.Matsunami, Mem. Fac. Eng. Kyoto Univ., 49(1987) 21.

[2] T.Takeuchi, private communication.

LIST OF PUBLICATION

I.Papers and Letters

(1) "Metal-Oxide-Semiconductor Characteristics of Chemical Vapor Deposited Cubic-SiC"
by K.Shibahara, S.Nishino and H.Matsunami
in Jpn. J. Appl. Phys. Part 2, vol.23(1984) pp.L862-L864.

(2) "Plasma Etching of CVD Grown Cubic SiC Single Crystals"
by S.Dohmae, K.Shibahara, S.Nishino and H.Matsunami
in Jpn. J. Appl. Phys. Part 2, vol.24(1985) pp.L873-L875.

(3) "SURFACE MORPHOLOGY OF CUBIC SiC(100) GROWN ON Si(100) BY CHEMICAL VAPOR DEPOSITION"
by K.Shibahara, S.Nishino and H.Matsunami
in J. Crystal Growth, vol.78(1986) pp.538-544.

(4) "Fabrication of Inversion-Type n-Channel MOSFET's Using Cubic-SiC on Si(100)"
by K.Shibahara, T.Saito, S.Nishino and H.Matsunami
in IEEE Electron Device Letters, vol.EDL-7(1986) pp.692-693.

(5) "Heteroepitaxial Growth of SiC on Si substrates"
by K.Shibahara, S.Nishino and H.Matsunami
in J. Jpn. Association of Crystal Growth, vol.13(1986) pp.226-232, in Japanese.

(6) "Antiphase-domain-free growth of cubic SiC on Si(100)"
by K.Shibahara, S.Nishino and H.Matsunami
in Appl. Phys. Lett. vol.50(1987) pp.1888-1890.

(7) "Fabrication of P-N Junction Diodes Using Homoepitaxially Grown 6H-SiC at Low Temperature by Chemical Vapor Deposition"
by K.Shibahara, N.Kuroda, S.Nishino and H.Matsunami
in Jpn. J. Appl. Phys. Part 2 vol.26(1987) pp.L1815-L1817.

(8) "Reflection high energy electron diffraction observation of cubic SiC on Si(100) grown by chemical vapor deposition"
by K.Shibahara, S.Nishino and H.Matsunami
To be submitted to J. Appl. Phys.

(9) "POLYTYPE CONTROL OF CVD GROWN SiC ON 6H-SiC SUBSTRATES"
by K.Shibahara, N.Kuroda, S.Nishino and H.Matsunami
To be submitted to J. Crystal Growth.

(10) "Electrical Properties of Undoped and Ion Implanted Cubic SiC Grown on Si by Chemical Vapor Deposition"
by K.Shibahara, T.Takeuchi, S.Nishino and H.matsunami
To be submitted to Jpn. J. Appl. Phys.

(11) "CVD Growth of Cubic SiC on Spherically Polished Si(111) Substrates"
by K.Shibahara, N.Kuroda, S.Nishino and H.Matsunami
To be submitted to Jpn. J. Appl. Phys. Short Note.

II.Proceedings of Conferences

(1) "Production of Single Crystalline Cubic-SiC with 2-inch Diameter by CVD and Characteristics of MOS Diodes"
by S.Nishino, K.Shibahara, S.Dohmae and H.Matsunami
in Late News Abstract of 16th 1984 International Conference on Solid State Devices and Materials, Tokyo, pp.8-9.

(2) "Inversion-type N-Channel MOSFET Using Antiphase-domain Free Cubic-SiC Grown on Si(100)"
by K.Shibahara, T.Saito, S.Nishino and H.Matsunami
in Extended Abstract of 18th 1986 International Conference on Solid State Devices and Materials, Tokyo, pp.717-718.

(3) "HETEROEPITAXIAL GROWTH OF ANTIPHASE-BOUNDARY FREE CUBIC SIC(100) SINGLE CRYSTALS ON SI(100)"
by K.Shibahara, S.Nishino and H.Matsunami

in Material Society Symposia Proceedings vol.97(1987), Anaheim, USA, pp.183-188.

(4) "INVERSION-TYPE MOS FIELD EFFECT TRANSISTORS USING CVD GROWN CUBIC SIC ON SI"
by K.Shibahara, T.Takeuchi, T.Saitoh, S.Nishino and H.Matsunami
in Material Society Symposia Proceedings vol.97(1987), Anaheim, USA, pp.247-252.

(5) "Step-Controlled VPE Growth of SiC Single Crystals at Low Temperatures"
by N.Kuroda, K.Shibahara, W.Yoo, S.Nishino and H.Matsunami
in Extended Abstract of 19th Conference on Solid State Devices and Materials, Tokyo, 1987, pp.227-230.

APPENDIX: Electron diffraction patterns

In order to obtain theoretical patterns of electron diffraction, three factors such as the reciprocal lattice, structure factor and double diffraction should be taken into account. They are explained in order below.

All polytypes of SiC can be treated using hexagonal-type primitive cells. Usually Millar-Bravais indices such as $(hkil)$ and $(hk\cdot l)$*) are used to identify lattice planes of SiC, because this notation explicitly expresses symmetrical relationships between various faces in a hexagonal lattice. However, this notation is not benefit for vector calculation. Therefore, concerning diffraction Miller indices such as (hkl) are mainly used in this thesis. Though Miller indices for a cubic lattice are more popular for 3C-SiC, here all polytypes are treated as hexagonal lattices to keep generality of discussion. Readers should take care to avoid confusion due to interminglement of these notations.

*) Here, i must be equal to $-(h+k)$[1]. Therefore, i can be omitted and substituted by a dot. It must be remembered that $(hk\cdot l)$ is equal to $(hkil)$ and not equal to (hkl).

(i) Reciprocal lattice of SiC

A primitive cell of SiC is defined by primitive vectors of $\boldsymbol{a}_1$, $\boldsymbol{a}_2$ and $\boldsymbol{a}_3$ shown in Fig.1. SiC consists of repetition of tetrahedrons shown in Fig.2. The length of edges of the tetrahedron is equal to $|\boldsymbol{a}_1|$ and $|\boldsymbol{a}_2|$ and its height is equal to $|\boldsymbol{a}_3|/n$. Therefore, $|\boldsymbol{a}_1|=|\boldsymbol{a}_2|=|\boldsymbol{a}_3|/(n\sqrt{6}/3)=a_0=3.08$Å. n is a number of layers in the repeat distance of a primitive cell in the [001] direction. The ‹001› direction is a so-called c-axis direction. $\boldsymbol{a}_1$, $\boldsymbol{a}_2$ and $\boldsymbol{a}_3$ are expressed as follows:

$$\boldsymbol{a}_1 = a_0\begin{pmatrix}\cos 30^\circ\\ \sin 30^\circ\\ 0\end{pmatrix},\quad \boldsymbol{a}_2 = a_0\begin{pmatrix}\cos 150^\circ\\ \sin 150^\circ\\ 0\end{pmatrix},\quad \boldsymbol{a}_3 = a_0\begin{pmatrix}0\\ 0\\ n\sqrt{6}/3\end{pmatrix}. \qquad (1)$$

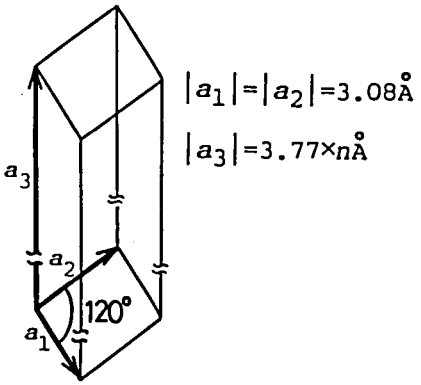

Fig.1 Primitive cell of SiC.

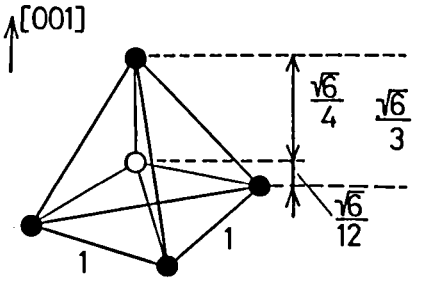

Fig.2 Tetrahedron component of SiC crystals.

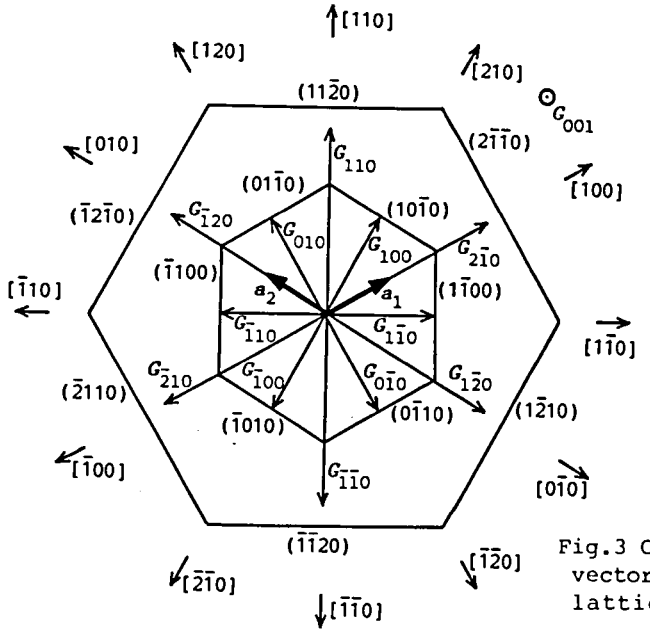

Fig.3 Orientations of reciprocal vectors, lattice directions and lattice planes.

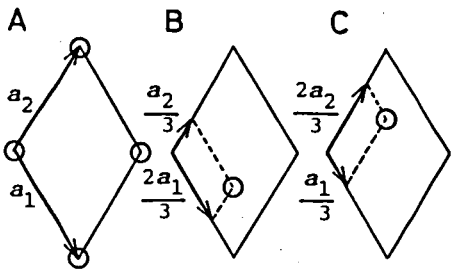

Fig.4 Positions of atoms in *A*-, *B*- and *C*-layers.

The axis vectors b_1, b_2 and b_3 of the reciprocal lattice are given as follows[2]:

$$b_1 = (2\pi/V)a_2 \times a_3 ,$$
$$b_2 = (2\pi/V)a_3 \times a_1 , \qquad (2)$$
$$b_3 = (2\pi/V)a_1 \times a_2 ,$$

where $V = a_1 \cdot a_2 \times a_3$.

Therefore, the axis vectors of the reciprocal lattice for SiC are obtained as follows:

$$b_1 = b_0 \begin{pmatrix} \cos 60^\circ \\ \sin 60^\circ \\ 0 \end{pmatrix} , \quad b_2 = b_0 \begin{pmatrix} \cos 120^\circ \\ \sin 120^\circ \\ 0 \end{pmatrix} , \quad b_3 = b_0 \begin{pmatrix} 0 \\ 0 \\ 3\sqrt{2}/4n \end{pmatrix} , \qquad (3)$$

where $b_0 = (4\pi\sqrt{3}/3)a_0$) .

In the real space the angle between a_1 and a_2 was 120°, however, in the reciprocal space the angle between b_1 and b_2 is 60°. A reciprocal lattice vector G_{hkl} is defined as follows:

$$G_{hkl} = hb_1 + kb_2 + lb_3 \quad (h,k,l: \text{integers}) . \qquad (4)$$

G_{hkl} is perpendicular to (hkl) and $2\pi/|G_{hkl}|$ is equal to lattice spacing of (hkl). Figure 3 shows relatioships concerning orientations among the reciprocal lattice vectors, lattice directions expressed by Mirror indices and lattice planes expressed by Mirror-Bravais indices. (hkl) is perpendicular to $G_{h\underline{k}\underline{l}}$ and omitted in Fig.3. (hkl) is not perpendicular to $[hkl]$. $\{2\bar{1}\bar{1}0\}$ and $\{10\bar{1}0\}$ planes are drawn by a large and small hexagons, respectively. In the case of Mirror-Bravais indices $\{2\bar{1}\bar{1}0\}$ and $\{10\bar{1}0\}$ planes are perpendicular to $\langle 2\bar{1}\bar{1}0\rangle$ and $\langle 10\bar{1}0\rangle$ directions.

(ii) Structural factor

The condition of diffraction is given as follows using the wave vector k of an incident beam($|k| = 2\pi/\lambda$, λ: wave length of the incident beam)[2]:

$$2k \cdot G_{hkl} = G^2 , \qquad (5)$$

where G is $|G_{hkl}|$. However, even if G_{hkl} satisfies this equation, sometimes diffraction cannot be observed. For example, diffraction due to Si(100) and (200) is not observed in the case of X-ray diffraction. Such phenomena are explained by the

structure factor. The structure factor S is given as [2]

$$S(G_{hkl})=\sum_j f_j \exp(-2\pi i(hx_j+ky_j+lz_j)) \ , \qquad (6)$$

$$r_j= x_j a_1 + y_j a_2 + z_j a_3 \ , \qquad (7)$$

where r_j is the vector to the center of atom j in a primitive cell and f_j atomic form factor. The atomic form factor is common to the atoms of a kind. Scattering intensity is proportional to $S\cdot S^*$. When S=0, diffraction is not observed.

The structure factor of SiC is obtained by the procedure explained below. Structures of all polytypes of SiC are identified by stacking sequences of layers in <001> direction as explained in Chapter I. For example, 3C and 6H-SiC have the staking sequences of *ABC* and *ABCACB*. The primitive cell of SiC contains n Si atoms and n C atoms. The positions of atoms in the primitive cell are expressed utilizing the stacking sequence. Locations of atoms in each layer are shown in Figs.4(a)-(c). Each Si atom locates $|a_3/4n|$ away from the nearest C atom belonging to the same layer as shown in Fig.2. When a Si atom locates at the origin and belong to A-layer the structure factor S is given for all polytypes as follows:

$$S= (f_{Si}+\exp(-2\pi i/4n) f_C)\cdot \sum_{j=0}^{n-1} \exp(-2\pi i(g_j+il/n)) \ , \qquad (8)$$

$$g_j(\text{A-layer})=0, \ g_j(\text{B-layer})=(-h+k)/3, \ g_j(\text{C-layer})=(h-k)/3 \ , \qquad (9)$$

Where f_{Si} and f_C are the atomic form factors for Si and C. $(f_{Si}+\exp(-2\pi i/4n)f_C)$ will not be zero for any G_{hkl} and the next formula can be used to obtain G_{hkl} which makes S be zero.

$$S'= \sum_{j=0}^{n-1} \exp(-2\pi i(g_j+il/n)) \ , \qquad (10)$$

For example S' of 2H-SiC whose stacking order is *AB* is explicitly expressed as follows:

$$S'_{2H}=1+\exp(-2\pi i(-h+k)/3)\cdot\exp(-\pi il) \ . \qquad (11)$$

If l is an odd number and $(-h+k)$ is a multiple of 3, S' and S will be zero.

(iii) Prediction of diffraction pattern

When G_{hkl} satisfies eq.(5) and $S'(G_{hkl})\neq 0$, diffraction is observed as a spot on a screen. In order to obtain reciprocal vectors which satisfy eq.(5), the construction due to Ewald[3] is convenient. So-called the Ewald sphere of $|k|$ in a radius which contact with the origin of reciprocal space is drawn. Reciprocal lattice points which contact with the Ewald sphere give rise to diffraction. In the case of electron diffraction, a radius of the Ewald sphere is much larger than the axis vectors of the reciprocal lattice. Therefore, nearby the origin, the Ewald sphere is approximated by a plane normal to the incident beam. The reciprocal points which contact with the plane are given using two reciprocal vectors which are not parallel to each other and perpendicular to the incident beam. A map of these reciprocal points appears as diffraction pattern on a screen.

In the case of RHEED observation of SiC(0001), G_{001} is always perpendicular to the incident azimuth. Another vector which is perpendicular to the incident azimuth is achieved by referring Fig.3. For examples, G_{010} and $G_{1\bar{2}0}$ are perpendicular to [100] and [210] azimuths, respectively. A [100] azimuth RHEED pattern of 2H-SiC(0001) is drawn as follows. G_{010} and G_{001} are perpendicular to [100] azimuth. Grid points given by $m_1G_{010}+m_2G_{001}$ (m_1,m_2: integer) represent a observable pattern. These two vectors are perpendicular to each other and $|G_{010}|/|G_{001}|=1.89$ based on eqs.(3) and (4)*). Therefore, the pattern is drawn and indices are given to each point as shown in Fig.5. In the case of RHEED observation, spots given by negative values of m_2 cannot be observed shaded by a specimen. A spot due to G_{hkl} which makes $S'(G_{hkl})$ zero is drawn by an white circle and others are drawn by solid circles. However, spots indicated by white circles are actually observed because of the double diffraction[4]. If diffraction due to $G_{h1,k1,11}$ and $G_{h2,k2,12}$ takes place, diffraction due to $G_{h1\pm h2,k1\pm k2,11\pm 12}$ also takes place even if $S(G_{h1\pm h2,k1\pm k2,11\pm 12})$ is equal to zero. Such a phenomena is called the double diffraction. For example, G_{001} in

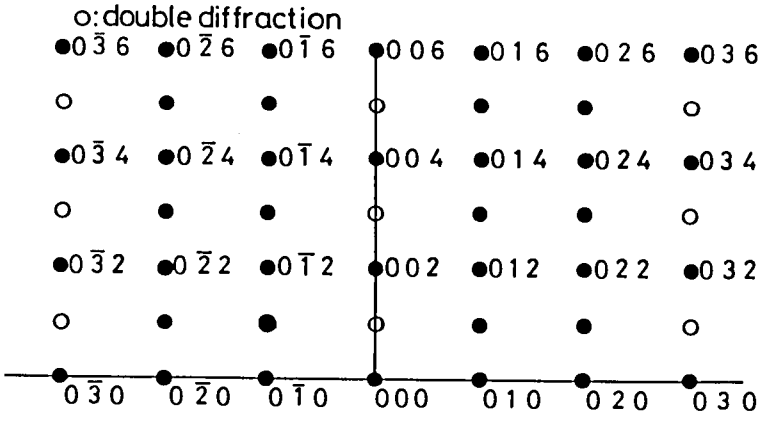

Fig.5 [100](or [2$\bar{1}\bar{1}$0]) azimuth RHEED pattern of 2H-SiC(0001).

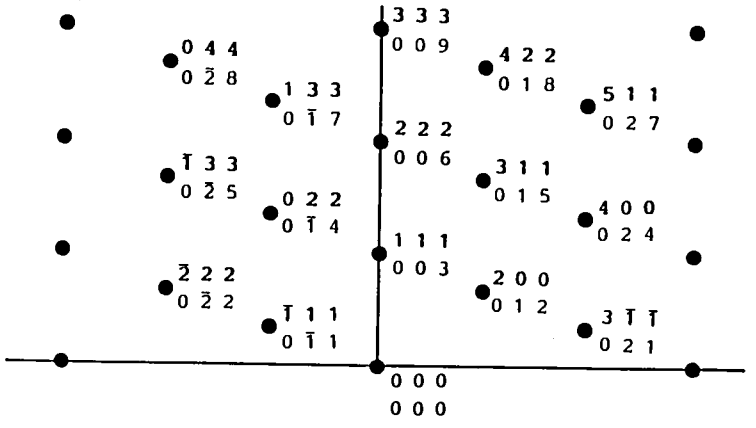

Fig.6 [100] azimuth pattern of 3C-SiC(0001). This expression is equal to "[01$\bar{1}$] azimuth pattern of 3C-SiC(111)" for cubic notation. Indicies for hexagonal and cubic notations are written in normal and bold-faced characters.

Fig.5 is synthesized by G_{100} and G_{101}.

In the discussion above, all polytypes of SiC are treated as hexagonal lattices. However, symetrical relationships peculiar to 3C-type cannot be explicitly expressed by this way. For comparison of notations for a hexagonal and a cubic lattice, A [100] azimuth pattern of 3C-SiC(0001) (or a $[01\bar{1}]$ azimuth pattern of 3C-SiC(111) in cubic notation) is shown in Fig.6. Indices are given by the both notations.

*) The lattice spacing d_{hkl} of (hkl) faces in hexagonal lattice is given by following expression.

$$d_{hkl}^{-2}=(4/3)(h^2+hk+k^2)/a+l^2/c^2 \quad (a=|a_1|=|a_2|,\ c=|a_3|)\ .$$

$|G_{hkl}|$ is also calculated utilizing this formula.

References

[1] B.D.Cullity, *Elements of X-ray Diffraction*, (Addison-Wesley, Massachusetts, 1956) Chapter 2.

[2] C.Kittel, *Introduction to Solid State Physics*, (Wiley, New York, 1986) 6th ed., Chapter 2.

[3] M.Plutton, *Surface Physics*, (Oxford Univ. Press, Oxford, 1975), Chapter 3.

[4] P.B.Hirsch, A.Howie, R.B.Nicholson, D.W.Pashley and M.J.Whelan, Electron Microscopy of Thin Crystals, (Butterworths, London, 1965), Chapter 6.